EFFECT OF POLYPROPYLENE FIBER REINFORCEMENT IN CEMENT SHEATHS EXPOSED TO CYCLIC FATIGUE LOADING

A Thesis

by

STEVEN JOHN GIESLER

Submitted to the Office of Graduate and Professional Studies of
Texas A&M University
in partial fulfillment of the requirements for the degree of

MASTER OF SCIENCE

Chair of Committee,	Jerome Schubert
Committee Members,	Sam Noynaert
	Minsu Cha
Head of Department,	Jeff Spath

August 2018

Major Subject: Petroleum Engineering

ABSTRACT

Cement slurry is pumped downhole to create cement sheaths that induce zonal isolation and maintain well integrity throughout the well's lifetime. This task is difficult to achieve due to adverse wellbore conditions and rig operations. In particular, hydraulic fracturing stimulation generates temperature- and pressure-induced stresses detrimental to the cement sheath. Recent studies have found that deviated wells, commonly drilled to access unconventional reservoirs, are three times more likely than non-deviated wells to lose zonal isolation. Due to recent increases in unconventional oil and natural gas production, this problem is relevant to the industry today.

An experiment was built to mimic wellbore conditions during hydraulic fracturing. Cement sheath samples were cured at wellbore conditions of 6,000 psi and 250^{o}F, then tested at these conditions to evaluate performance under cyclic loading. Internal casing pressure was applied to a restraining cement sheath, then cycled from the wellbore confining pressure to a positive pressure differential and back to the confining pressure. Samples endured the applied stress initially, but failed after reaching their respective fatigue limits due to cyclic fatigue. Unfortunately, equipment failure prevented the completion of tests at wellbore conditions, so a modified experiment was conducted without wellbore curing or confining pressure.

The primary research objective was to conduct cyclic fatigue tests on cement sheaths reinforced with polypropylene fibers, then compare results with cement sheaths that were not reinforced. There were two baseline slurries without fibers: one contained Class H cement plus 35% by weight of cement (bwoc) silica flour while the other contained Class H cement plus 35% bwoc silica flour plus 8% bwoc bentonite. Polypropylene fibers were added at a concentration of 0.75% by volume of batch (bvob). Fiber reinforcement doubled the fatigue life of cement sheaths without bentonite and had a negligible impact on the cement sheaths containing bentonite.

The secondary research objective was to observe crack initiation and propagation in computed tomography (CT) scans of the cement sheath before, during, and after cyclic fatigue testing. Cross-sectional scans displayed mature radial and disk cracks, however crack initiation and propagation was not clearly observed.

DEDICATION

To God who has a special plan for each of us

To my wonderful parents for their love and support

To my friends and family for their continued encouragement

To loved ones lost, but never forgotten, whom I will meet again

To my nephews, whom I love and cherish, that they may be inspired

And to my teachers from school, from NDSU, and finally from Texas A&M

for their help and guidance on this journey

ACKNOWLEDGEMENTS

I would like to thank my committee chair, Dr. Jerome Schubert, for his technical oversight and financial support. I have learned so much having him as my advisor. I also appreciate and value the guidance provided by my committee members, Dr. Sam Noynaert and Dr. Minsu Cha.

A number of other people were very important to my research. Dave Dillon, a technical lab coordinator in the Civil Engineering Department, taught me to use the Instron testing frame and Bluehill software for mechanical testing. Having worked at Halliburton, he was a terrific resource in regards to my research objectives and methodology. John Maldonado, the facilities coordinator in the Petroleum Engineering Department, provided tools and hands-on experience when I constructed my experiments. He was the person I turned to if equipment broke or something went wrong. On several occasions, he provided the means to get my experiment running again. Don Conlee, a facilities technician in the Petroleum Engineering Department, was very helpful by operating the CT scanner according to my testing schedule. Pedro Sousa, my lab-mate, provided invaluable assistance setting up the experiment's data acquisition system.

I must also acknowledge three professors from the Civil and Environmental Engineering Department at North Dakota State University, Dr. Mijia Yang, Dr. Achintya Bezbaruah, and Dr. Zhibin Lin, for their continued guidance and assistance. Without their efforts, I would not have been awarded a Graduate Research Fellowship from the National Science Foundation which provided tremendous financial support.

Thanks also goes to friends, colleagues, and fellow members of the Society of Petroleum Engineers for making my time at Texas A&M University a great experience. It is remarkable how my friend Alexander Eleiott and his dad, Allen, opened their home to me during my summer internship. I greatly appreciated their generous hospitality and guidance for a small town farm boy living in the big city. A special thanks goes to my roommate, Kevin Wylie, who consistently provided help whenever I asked him.

Finally, I wish to thank everyone in my family for their love and support. The two people who stand out the most are my parents. They offered praise during the good times and encouragement during the bad ones. I could not have finished without them.

CONTRIBUTORS AND FUNDING SOURCES

This work was supervised by a dissertation committee consisting of Dr. Jerome Schubert and Dr. Sam Noynaert of the Department of Petroleum Engineering and Dr. Minsu Cha of the Department of Civil Engineering. All work for the dissertation was completed independently by the student.

This material is based upon work supported by the National Science Foundation Graduate Research Fellowship Program under Grant No. DGE: 1746932. Any opinion, findings, and conclusions or recommendations expressed in this material are those of the author and do not necessarily reflect the views of the National Science Foundation.

Further financial support to purchase and repair equipment was provided by a Texas A&M University fellowship supplied by Dr. Schubert.

NOMENCLATURE

API	American Petroleum Institute
ASTM	American Society for Testing and Materials
BCFPD	Billion cubic feet per day
Bvob	By volume of batch
Bwoc	By weight of cement
C-S-H	Calcium silicate hydrate
C/S ratio	Lime-to-silica ratio
CT	Computed tomography
Lbf/ft^2	Pounds of force per square foot
MMBPD	Million barrels per day
NPT	National pipe thread
OBM	Oil-based mud
Ppg	Pounds per gallon
Psi	Pounds per square inch
SGS	Static gel strength
SCP	Sustained casing pressure
S-N	Stress-number of cycles
SOP	Standard operating procedure
SSD	Surface-saturated-dry
W/c ratio	Water-to-cement ratio
α- C_2SH	Alpha dicalcium silicate hydrate

TABLE OF CONTENTS

Page

LIST OF FIGURES

Page

LIST OF TABLES

Page

CHAPTER I

INTRODUCTION AND LITERATURE REVIEW

Introduction

The global energy demand rises annually due to population growth, industrialization, and as people throughout the world pursue an improved quality of life. This demand is met through the consistent development of renewable and non-renewable energy sources. Despite the efforts of many countries to decarbonize and shift towards renewable energy, oil and natural gas supplied 32 and 21 percent, respectively, of the global energy demand in 2016 (Total Energy Consumption, 2017). This is equivalent to approximately 96 million barrels per day of oil (MMBPD) and 350 billion cubic feet per day (BCFPD) of natural gas (Rapier, 2017).

Advancements in technology to drill, stimulate, and produce unconventional shale reservoirs permit such high production levels. Petroleum companies used this technology to aggressively develop several large shale plays in the United States, and now the country is a global frontrunner in oil and natural gas production. Between 2008 and 2016, national crude oil production increased from 5 to 9 MMBPD with almost half of the 2016 production from shale rock formations. Simultaneously, natural gas production increased from 6 to 47 BCFPD (U.S. Energy Information Administration, 2018). Profitable and safe production from fossil fuels depends on a variety of factors.

Background

One important factor is cement sheath integrity throughout the life of the well. Production optimization begins with a good completion, but a good completion depends on the integrity of the cement sheath. Cementing is considered a drilling process, but is generally performed by service companies instead of Exploration and Production operators. The service companies have personnel who specialize in cement slurry design, placement, and testing. New downhole tools and surface equipment are also introduced for novel applications or to improve performance.

The primary objective of cementing is to achieve zonal isolation, or create a hydraulic seal which prevents fluid flow from one underground formation to another. Steel casing is run downhole and cemented in place at casing points typically pre-determined to accommodate the drilling program or isolate underpressured zones. Bonds are formed at the cement-casing and cement-formation interfaces as the cement hydrates. Ideally, there is near-zero effective permeability through the cement sheath and strong cement-formation bonds that prevent invasion of formation fluids into the wellbore.

The secondary objectives are to protect the casing string from corrosive formation fluids and provide support from collapsing formations. In order to be effective, cement slurry is carefully designed based on a variety of factors. These factors include cement properties, cement additives, and downhole conditions.

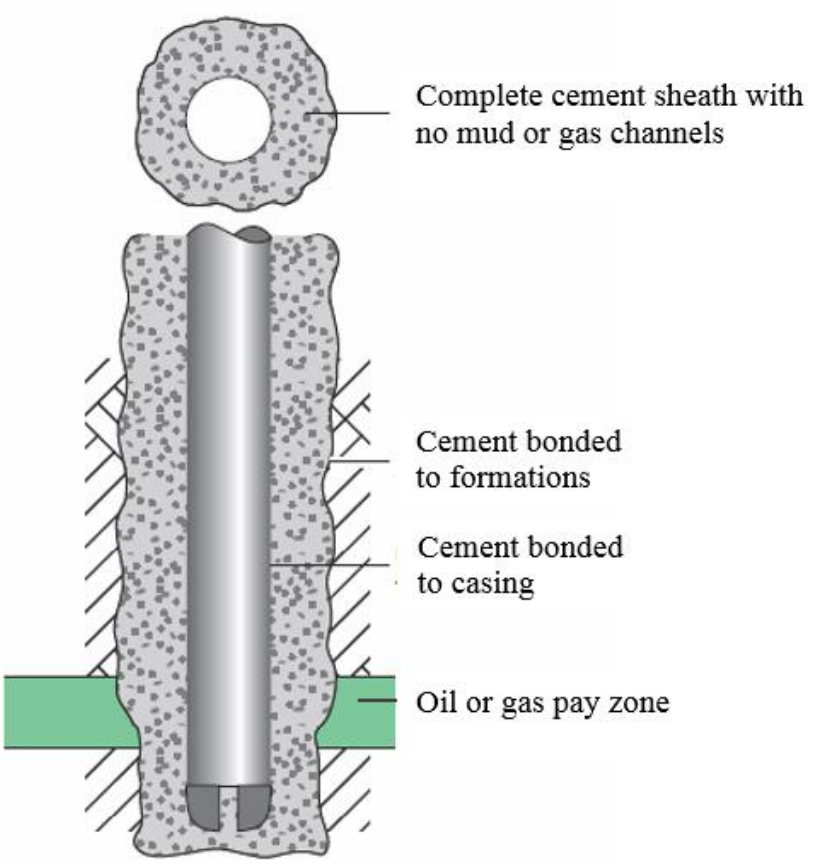

Figure 1: Objectives of primary cementing (Reprinted from Nelson & Guillot, 2006)

Well cements are prepared to contend with a wide range of temperatures and pressures. Extreme temperatures include below freezing in permafrost zones or beyond 700^{o}F in geothermal wells. Pressures may be near ambient in shallow wells to over 30,000 psi in deep wells. There are currently eight classes of American Petroleum Institute (API) Portland cement designated A through H. They are arranged according to placement depth and the predicted downhole temperature and pressure conditions. They are also grouped within classes according to their degree of sulfate resistance which includes ordinary, moderate sulfate resistance, or high sulfate resistance. Despite these distinctions, Class G and Class H are the basic well cements commonly used today (Nelson & Guillot, 2006).

Well cements are designed to contend with porous formations, corrosive fluids, and contamination from over-pressured formation fluids. All these conditions are accommodated by modifying the cement's behavior with additives which includes both mineral and chemical admixtures. There are hundreds of different additives available for well cements. One condition that is commonly faced in high temperature wells is called the strength retrogression problem.

Strength retrogression refers to how neat slurry, or a pure mixture of cement and water, deteriorates at elevated downhole temperatures. Higher temperatures naturally increase the rate of hydration and shorten the cement's induction and setting periods. However, changes also occur in the microstructure and morphology of the calcium silicate hydrate (C-S-H) phase responsible for strength and dimensional stability of the set cement. C-S-H is an excellent binding material at temperatures below 230^{o}F. Beyond 230^{o}F, the C-S-H converts to a phase called alpha dicalcium silicate hydrate (α-C_2SH). The higher density causes matrix shrinkage which undermines the set-cement integrity. It reduces the compression strength and severely increases permeability.

The problem is prevented by reducing the lime-to-silica ratio (C/S) ratio in the cement paste (Carter & Smith, 1958). Ground quartz, usually fine silica sand or silica flour at 35-40% by weight of cement (bwoc), is added to the slurry. It forms the mineral tobermorite during hydration which converts to xonotlite and gyrolite, both stable at temperatures above 230^{o}F and minimizes the deterioration of cement performance (Nelson & Guillot, 2006)

Numerous laboratory tests are conducted on the fresh and hardened properties of cement slurry prior to wellbore placement. For this experiment, slurry density, compressive strength, and the cement sheath fatigue limit are measured and described in great detail. Cement jobs are also evaluated through pressure testing and various logging methods, but these methods are not applicable here. Instead, it is important to consider how the cement sheath is placed and cured, then subjected to cyclic casing stress during continued drilling, hydraulic fracturing, and production processes which may cause or worsen cement sheath failure.

Gas Migration

Cement sheath failure implies a loss in zonal isolation and gain in effective permeability. This allows fluid migration, typically in the gas phase, and compromises well integrity. Gas migration is defined as gas entry into a cemented annulus creating permanent channels which introduce a flow path for formation fluids into the wellbore. There are three major categories called immediate, short-term, and long-term gas migration.

Immediate gas migration occurs during placement of the cement if the cement column cannot maintain overbalance pressure relative to the formation. Changes in density between the drilling fluid, pre-flush, spacer, lead slurry, and tail slurry prevent fingering and minimize drilling fluid-to-cement contamination, but one side effect is that the annular hydrostatic pressure is not constant during the cement job. Gas migration is prevented by using a computer simulator to ensure the hydrostatic pressure acting against critical zones is maintained throughout the pumping schedule. However, density fluctuations may still occur

during a cement job in the field. This causes a non-uniform column of cement to be placed in the annulus (Nelson & Guillot, 2006).

Short-term gas migration occurs after placement during the setting process. The root cause is the slow reduction of annular pressure caused by the development of static gel strength (SGS), fluid loss, and chemical shrinkage of cement during hydration. As cement hydrates, it loses the ability to transmit hydrostatic pressure. It enters a transition period where the initial SGS is about 20 lbf/100 ft^2 and behaves as neither a fluid nor a solid. Unfortunately, the gelled slurry cannot hold back high-pressure formation fluids so gas percolates into the cement column. Once a sufficient SGS is achieved, typically 500 lbf/100 ft^2 or more, the invasion of gas is stopped, but the damage is done. The contaminating gas may cause incomplete hydration, produce channels of high permeability, or prevent a good casing-cement sheath bond (Tinsley et al., 1980).

Another factor, chemical shrinkage, is important to mention because it cannot be eliminated. Chemical shrinkage naturally occurs in cement systems since the volume of the hydrated phases is less than that of the initial reactants. It contributes to secondary porosity composed of free and conducive pores and, in some cases, may initiate cracks in the cement sheath. More commonly, it reduces the annular pressure applied by the cement to provide space for gas entrance into the annulus. The space weakens or completely removes the cement sheath-formation bond and produces microannuli flow paths (Nelson & Guillot, 2006).

Long-term gas migration occurs after the cement has set and requires a permeable pathway from one zone to another. Mud channels, dehydrated filtercake, continued chemical shrinkage, free-fluid channels, and poor centralization are all potential causes, as well as many drilling and completion processes. Pressure and temperature fluctuations occur during hydraulic fracturing. The casing and its surrounding cement sheath expand and contract at different rates generating severe stress at the casing-cement sheath interface. The stress breaks the bond to motivate cement sheath failure (Bourgoyne et al., 1999).

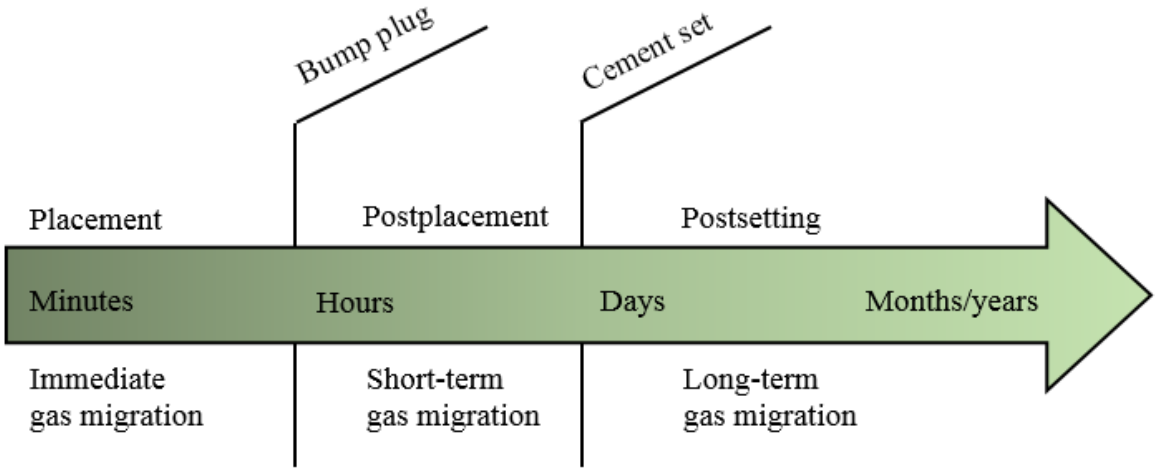

Figure 2: Categories of gas migration (Reprinted from Nelson & Guillot, 2006)

Sustained Casing Pressure

Well control is highly dependent on achieving successful cement placement and bond. The drilling operation responsible for this process is primary cementing. However, a 1995 study conducted by Westport Technology revealed that about 15% of primary cement jobs failed. One-third of these failures were attributed to gas migration or formation water flow during placement and curing of cement in the wellbore. At the time, remedial cementing services cost the oil and gas industry an estimated $450 million annually (Newman & Wojtanowicx, 2001). Although an outdated statistic, it emphasizes the economic significance of poor-quality cement jobs which plague the industry today. There are a number of recent studies that identify sustained casing pressure (SCP), an event caused by gas migration through the cement sheath.

Sustained casing pressure is defined as pressure within a casing string that persistently rebuilds when bled down. The pressure readings result from trapped formation gas in the annular space and are measured at the wellhead. SCP can be found in all, some, or none of the casing strings for any given well. The risk for failure increases as wells age. Over time, cracking, debonding, shear failure, or a combination of these conditions deteriorates the cement sheath. SCP indicates a loss in zonal isolation, whether from the cement sheath, a casing connection, or the wellhead seal. **Figure 3**, found on the next page, shows the percentage of Gulf of Mexico wells experiencing SCP in 2003. Long-term zonal isolation is not maintained for a majority of offshore wells, particularly as they age.

Figure 3: Gulf of Mexico wells with SCP (Reprinted from Nelson & Guillot, 2006)

In addition to offshore wells, SCP is also diagnosed in onshore wells. A study completed in 2009 found that 4.5% of onshore Alberta, Canada wells exhibited surface casing gas migration when tested. This statistic means leakage pathways undermined zonal isolation in about 14,200 of 315,000 wells at that time. Wells were then divided into categories to observe trends in SCP occurrence. It was discovered that certain test areas demonstrated higher rates of SCP. One test area had a 15.5% SCP occurrence rate from its 20,725 wells. Additionally, it was found that wellbore deviation plays a meaningful role in overall wellbore leakage. *Deviated wells are three times more likely than non-deviated wells to display SCP* (Watson & Bachu, 2009). This factor is important when considering oil and natural gas production from shale plays. These wells are typically drilled vertically near the surface, and then curve horizontally through the target zone to maximize wellbore contact area in the reservoir.

One of the most prolific shale basins in the United States is the Marcellus formation. In 2014, a study relevant to this topic was published. The study analyzed 41,380 conventional and unconventional wells drilled in the Pennsylvania Marcellus shale from 2000 to 2013. The objective was to ascertain statistics of casing and cement impairment with reference to Pennsylvania Department of Environmental Protection compliance reports. *It was discovered that shale gas wells are two to three times more likely to have casing or cement integrity issues compared to conventional wells*. The average impairment rate estimated for unconventional wells was 12.5% (Ingraffea et al., 2014).

These studies indicate that a significant percentage of cement sheaths, particularly in unconventional wells, do not maintain long-term zonal isolation. Cementing is a difficult operation to execute and downhole conditions readily attempt to undermine cement sheath performance. In addition to this, cyclic stresses are applied to continue drilling, perform hydraulic fracturing, and workover the well. The cement bond or matrix becomes impaired to allow gas migration. Trapped gas accumulation may cause casing collapse, unseat packers, disrupt production operations, or lead to a more severe well control problem.

Dramatic well control events, although rare, risk the safety of the rig and its crew. For this reason alone, cement sheath integrity is a very important part of well construction. Yet, there are economic and environmental considerations as well. Primary cementing services are typically about 5 percent of the total well cost. If necessary, remedial cementing is conducted for an additional 10-25% to the total well cost (Cementing Services, 2015).

There are also severe instances when blowouts occur. The most famous blowout in recent memory is Deepwater Horizon in 2010 which was caused, in part, by a failed cement job. Over three million barrels of oil leaked into the Gulf of Mexico before the British Petroleum Macondo well was finally capped. The subsequent damage, environmental clean-up, and fines were historic in proportion, but revolutionized the offshore oil and gas industry so a similar event might never happen again. Before changes are made, however, thorough research and testing is conducted to explore their potential effects.

Past Research

A number of studies have tested cement sheath failure to understand how, when, and where it occurs. Goodwin and Crook (1993) determined that cracks, which cause a loss of zonal isolation, are created by excessive increases in both internal casing pressure and surface flowing temperatures. Generally, cracks created by internal casing pressure are found near the producing region of the well while temperature-related cracks are located near the surface. The experiment tested four cement slurry designs, two of which contained 30% latex by weight of water. The results showed that ductile low-compressive-strength (500- to 1,000-psi) cements endure stress cycling better than non-ductile higher-compressive-strength cements. However, this conclusion has limits since ultrahigh-compressive-strength (> 12,000 psi) cement withstood stress cycling without cracking too.

At the same time, Jackson and Murphey (1993) ran experiments to cycle internal casing pressure. The experiments imitated casing integrity tests, commonly performed in the field after surface- and intermediate-casing cement jobs, to create a pressure differential. The tests

increase the internal casing pressure relative to the confining formation pressure. This causes the casing to exert radial stress on the restraining cement sheath. Tests were run for the experiment at five levels of pressure differential including one-, three-, five-, seven-, and nine-thousand psi. The pressure differential was applied in approximately twenty minute cycles, ten minutes at the higher pressure followed by ten minutes bleeding off to the original pressure. Upon completion of a cycle, another cycle was initiated at the next highest pressure differential or until gas migration through the cement sheath was observed. Results indicated that the hydraulic seal was lost after casing had been pressurized to the seven-thousand pressure differential and bled back to the original pressure.

Boukhelifa et al. (2004) ran similar experiments to apply radial stress to casing encompassed by a restraining cement sheath. Results showed that expanding and flexible cement designs exhibited superior performance compared to foamed or neat cement designs. More importantly, it was observed in almost all experiments that multiple loading and unloading cycles had a cumulative effect in creating cracks to increase permeability of the cement sheath. This implies that the same pressure differential can be repeatedly applied as a form of fatigue testing. A test could be developed to determine the fatigue limit of cement sheath designs at various downhole pressure and temperature conditions.

Shadravan et al. (2014) devised an evaluation method to test the long-term durability performance of cement sheaths at wellbore conditions. The testing procedure is similar to other experiments mentioned previously. Cement is mixed according to API standards, then cured around a small pressure vessel. It sets and bonds to the small vessel imitating a casing-cement sheath relationship. From there, the two are placed inside a larger pressure vessel. A constant confining pressure is applied to the cement sheath. Meanwhile, casing pressure inside the small vessel is increased to a pressure differential, held constant for some time, and then lowered back to the confining pressure level. **Figure 4** provides a visual for this procedure. Repeated pressure cycles exert radial stress due to casing expansion and eventually causes the cement sheath to crack. The number of cycles until cracking is called the fatigue limit of that cement sheath.

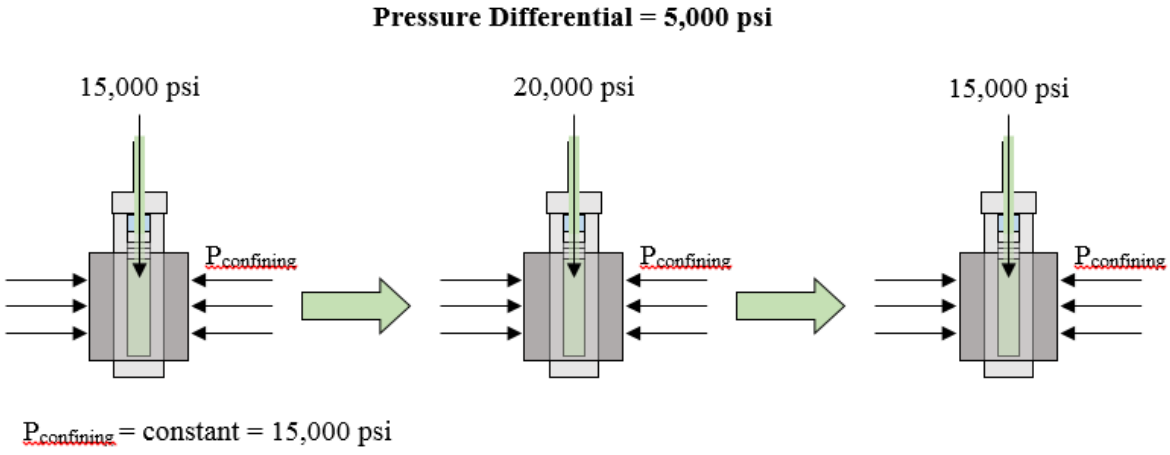

Figure 4: Cyclic pressure testing from Shadravan et al., 2015 (Copyright 2015, Society of Petroleum Engineers Inc.Copyright 2015, SPE. Reproduced with permission of SPE. Further reproduction prohibited without permission.)

The Shadravan experiment analyzes cement sheath fatigue tolerance under cyclical loading at various downhole conditions. It also allows post-testing observation to identify the mechanical damage affecting the sample. Bois et al. (2012) characterizes five types of mechanical damage that can be induced to a cement sheath during the life of the well.

Failure Type A, also called inner debonding, is shown as debonding at the casing-cement sheath interface. It occurs following contraction of the casing because the subsequent cement radial deformation is not equivalent. A gap forms and the bond is lost.

Failure Type B, also called outer debonding, is shown as debonding at the cement sheath-formation interface. It occurs following contraction of the cement sheath when the formation or outer tubular (if enclosed by a larger casing string) does not radially deform at the same rate. There is separation which removes the bond.

Failure Type C is shown as damage to the cement sheath by shear stress. It occurs when the cement sheath is located between two tubulars or between one tubular and one rigid formation. The two principal stresses are unequal creating a deviatoric state of stress that causes distortion to the cement sheath.

Failure Type D is shown as damage to the cement sheath by radial cracking. It occurs when the internal casing pressure is greater than the external confining pressure. The cement sheath experiences stress while restraining radial deformation by the casing. At failure, Hoop's stress overcomes the tensile strength causing the cement sheath to crack.

Failure Type E is shown as damage to the cement sheath by disking. It occurs when the cement sheath axially contracts because it cannot slide. The casing-cement sheath and cement sheath-formation bonds prevent its lateral movement.

Figure 5 displays these five types of damage. In the diagram, casing is colored in black, cement sheath in grey, formation in green, and failure surfaces in red.

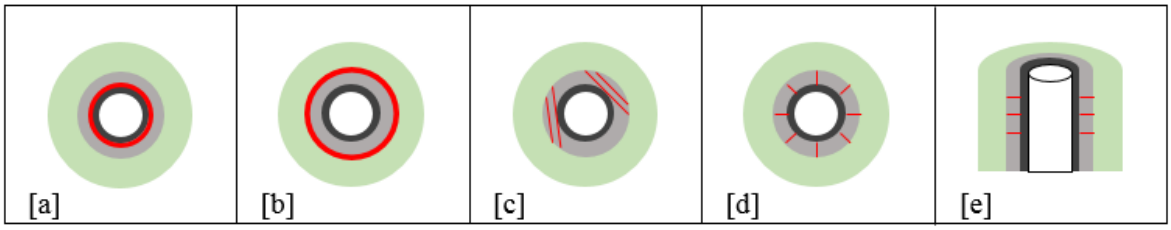

Figure 5: Cement sheath damage from Bois et al., 2012 (Copyright 2012, Society of Petroleum Engineers Inc.Copyright 2012, SPE. Reproduced with permission of SPE. Further reproduction prohibited without permission.)

It is important to note that a cement sheath can experience more than one failure type. Bois et al. (2012) identifies that the experiments conducted by Goodwin and Crook (1992), Jackson and Murphey (1993), and Boukhelifa et al. (2004) showed similar results. Equal confining and internal casing pressures are applied. The confining pressure remains constant as the casing pressure is changed. A decrease in casing pressure leads to inner debonding while an increase leads to radial cracking or shear damage, dependent on the Young's modulus of the cement and the surrounding formation. Cyclic pressure testing results in both types of damage whose effect is cumulative. The magnitude and frequency of the pressure cycles affects how quickly the cement sheath reaches its fatigue limit.

Fatigue Life

Fatigue is broadly defined as the weakening of a material due to recurring applications of stress. In relation to cement sheaths, it refers to the initiation and propagation of cracks due to cyclical stress loading. This definition can be rewritten as the equation:

$$N_f = N_i + N_p \tag{1.1}$$

where N_f is the number of cycles to failure, N_i is the number of cycles for crack initiation, and N_p is the number of cycles for crack propagation. At cycle N_f, the cement fails upon reaching its fatigue life for the given stress level.

An inverse relationship between the magnitude and frequency of cyclic stress determines the number of cycles preceding fatigue failure. It is represented using a stress-number of cycles (S-N) diagram, as shown in **Figure 6** on the next page, which plots fatigue strength against the number of cycles to failure for some material. The terms fatigue strength and fatigue life are used simultaneously to describe the S and N values at different points on the curve. As the number of cycles increases, the magnitude of the stress required to cause failure decreases. Furthermore, fatigue is divided into two classes called high- and low-cycle fatigue. High-cycle fatigue implies the cement sheath requires more than 10^3 cycles to fail. Stress levels can be greatly reduced to study this type of fatigue, however it takes more time.

The endurance limit is defined as the stress value where an infinite number of cycles will not cause fatigue failure. Low-cycle fatigue, the class studied in past cement integrity research, requires fewer than 10^3 cycles to fail. The justification for studying low-cycle fatigue is the magnitude of the stresses experienced in the field. Cement sheaths are subjected to a wide range of casing and confining pressures, so their resulting pressure differentials cause low-cycle fatigue failure (Ugwu, 2008).

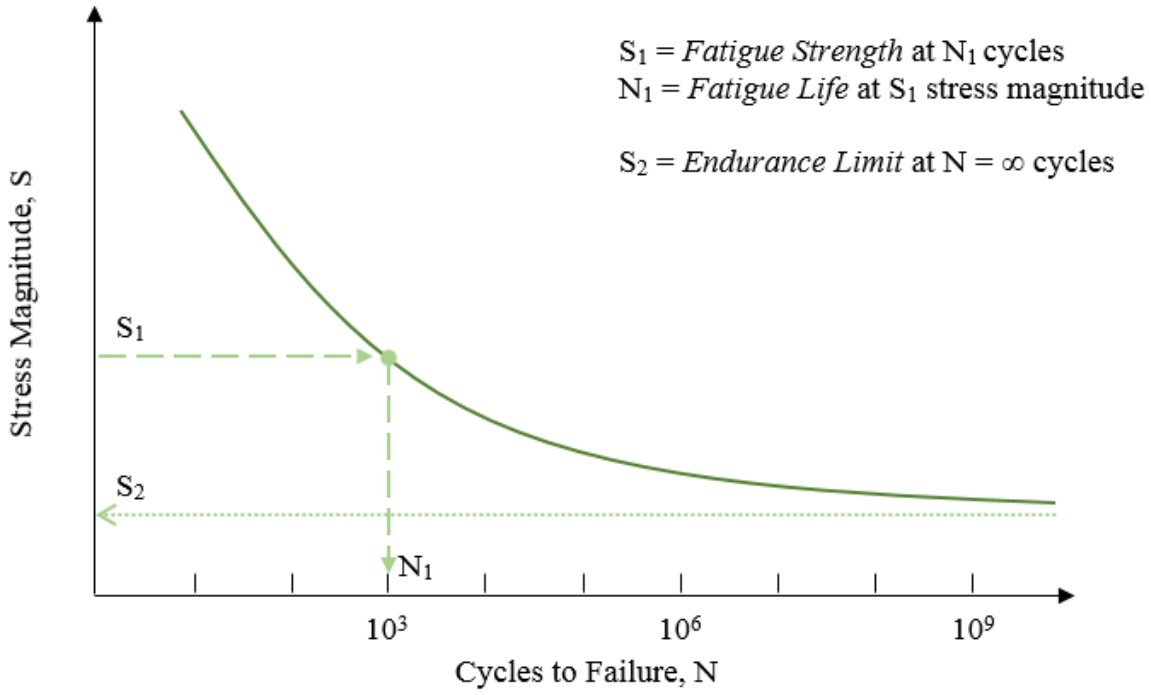

Figure 6: Common S-N diagram from materials testing

Fiber-Reinforced Cement

The tests conducted today on well cement most commonly involve placement, setting time, and fluid loss. Less emphasis seems to be placed on long term integrity or mechanical damage of the cement sheath. However, the routine occurrence of SCP in offshore and unconventional wells indicates the area requires further research. Shadravan introduced a novel method to evaluate the fatigue life of cement slurry designs at various wellbore conditions. Johns (2014) used the same method to test cement sheaths reinforced with nylon fibers. Unfortunately, equipment failure cut the experiments short but preliminary results indicated fibers would increase the fatigue life.

Fiber-reinforcement is commonly used in the construction industry to improve the hardened properties of conventional concrete. Amongst these properties are tensile strength and strain capacity, flexural and shear strength, ductility, and toughness. Furthermore, fibers are known to improve resistance to cracking caused by shrinkage, thermal fluctuations, or mechanical stress. The fibers hinder crack growth by transferring stresses across the cracks. Just as with concrete, these effects for enhanced longevity are desired in oil, gas, and geothermal wells too. Berndt and Philippacopoulos (2002) conducted research on fiber-reinforced slurry designs for geothermal wells. They found that steel fibers improved the tensile strength, increased the coefficient of thermal expansion, and had a negligible effect on permeability. Carbon fibers also improved tensile properties while glass and basalt fibers were ineffective under the tested conditions.

Many types of fibers are available for cementing applications. They can be made from steel, rock, rubber, plastic, glass, or some novel material, but their objective remains the same. They modify the elasticity of the set cement to increase both thermal and mechanical flexibility which leads to improved flexural strength and delays fatigue failure.

Kosinowski and Teodoriu (2012) experimented with cyclic loading in well cement. Results showed the brittleness of a cement sheath may reduce its ability to withstand cyclic loading conditions, especially as the well ages. Fibers are an additive which improves ductility and should combat cyclic fatigue failure throughout the well's lifetime. It is important to identify fibers that can survive wellbore conditions while improving the cement's performance.

CHAPTER II

METHODOLOGY

This chapter discusses the research objectives and experimental design used to test cement sheaths under cyclic loading conditions.

Research Objectives

A number of different cement slurry designs were mixed, cured, and tested to evaluate performance under cyclic loading at wellbore conditions. Internal casing pressure was applied to a restraining cement sheath, then cycled until the cement sheath experienced fatigue failure. The primary objective was to test cement slurry containing polypropylene fibers, then compare the results to those from a slurry without fibers. It was expected that the fiber-reinforced cement would achieve a higher fatigue limit. Additionally, computed tomography (CT) scans produced images of cement sheath cross-sections before, during, and after cyclic testing to observe crack initiation and propagation.

Experimental Design

A two-vessel system was used to generate internal casing and confining pressure. The system was enclosed in an oven so the confining pressure and temperature would imitate wellbore conditions. Cement slurry was mixed, then placed in molds to hydrate around a small pressure vessel that later applies casing pressure. After initial curing, the small pressure vessel and its encompassing cement sheath were loaded into the large pressure vessel for wellbore curing. **Figure 7**, found on the next page, provides a visual of these vessels.

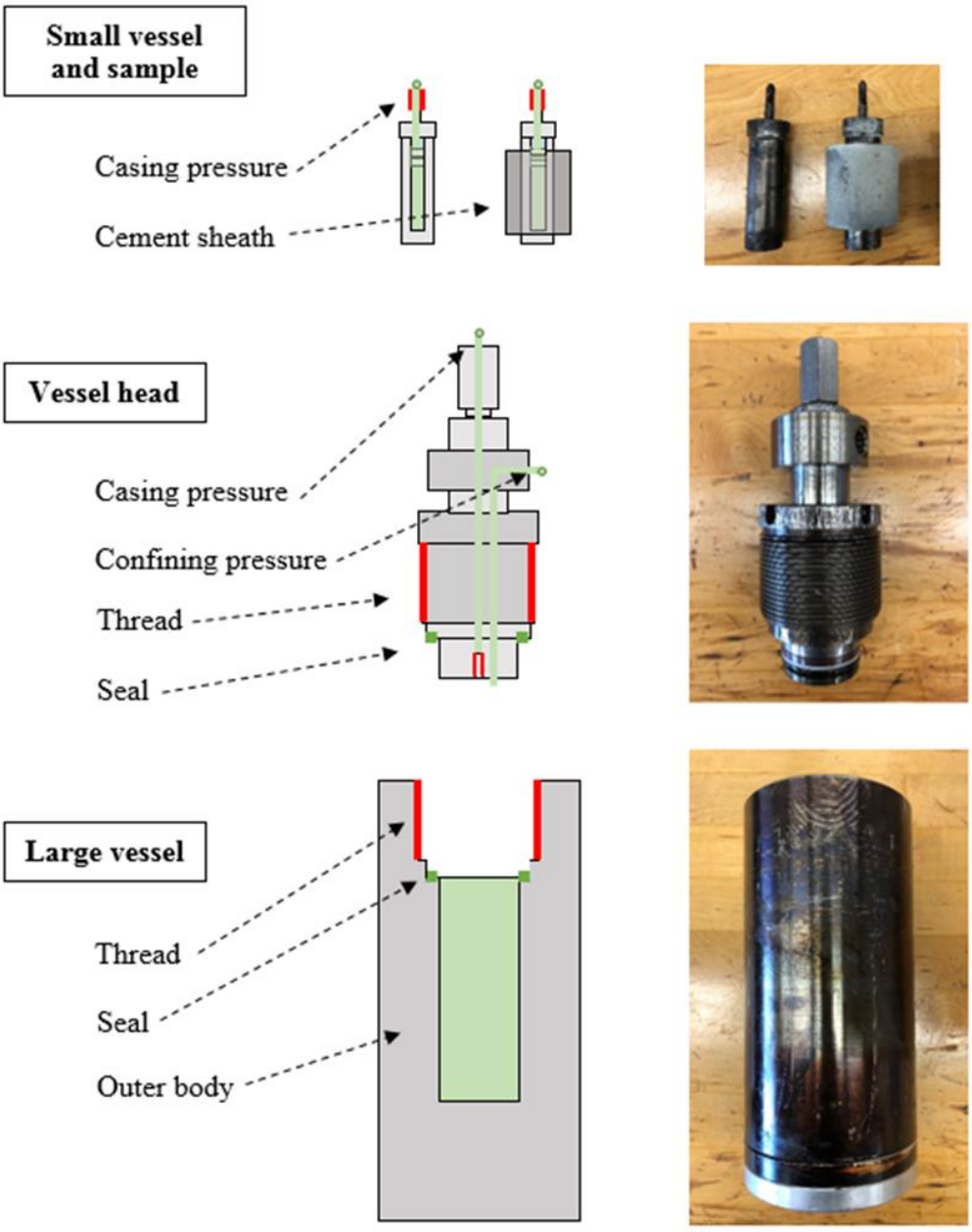

Figure 7: Schematic of pressure vessels

The testing procedure is based off the Shadravan and Johns experimental set-up. They used a Chandler Model 7600 HPHT Viscometer which applied pressure and temperature to recreate wellbore conditions. The viscometer was also programmable and had a data acquisition system to record pressure cycles, but it was repurposed for a different research project and unavailable for this study. Before running tests, the experiment was built to meet the requirements for pressure, temperature, and data logging.

The experiment was designed and constructed as shown in **Figure 8**, found on the next page. All equipment is rated to 15,000 psi or higher at 300^{o}F. In order to meet safety requirements, pressure relief valves are connected to both flow lines. They prevent equipment damage or bodily injury by bleeding off pressure that exceeds the factory setting of 12,000 psi. High pressure tubing and compression fittings provide a flow path from the pumps through the various equipment to the pressure vessel. The equipment between these two points is meant to hold pressure constant, as well as monitor and record pressure data for analysis.

The purpose for the experimental design was to construct two nearly identical flow lines, one for the casing pressure and one for the confining pressure. Two units of everything mentioned in this list were utilized and arranged as shown in **Figure 8**:

1. hydraulic hand pump
2. upstream isolation valve
3. pressure gauge
4. pressure transducer
5. pressure relief valve
6. downstream isolation valve

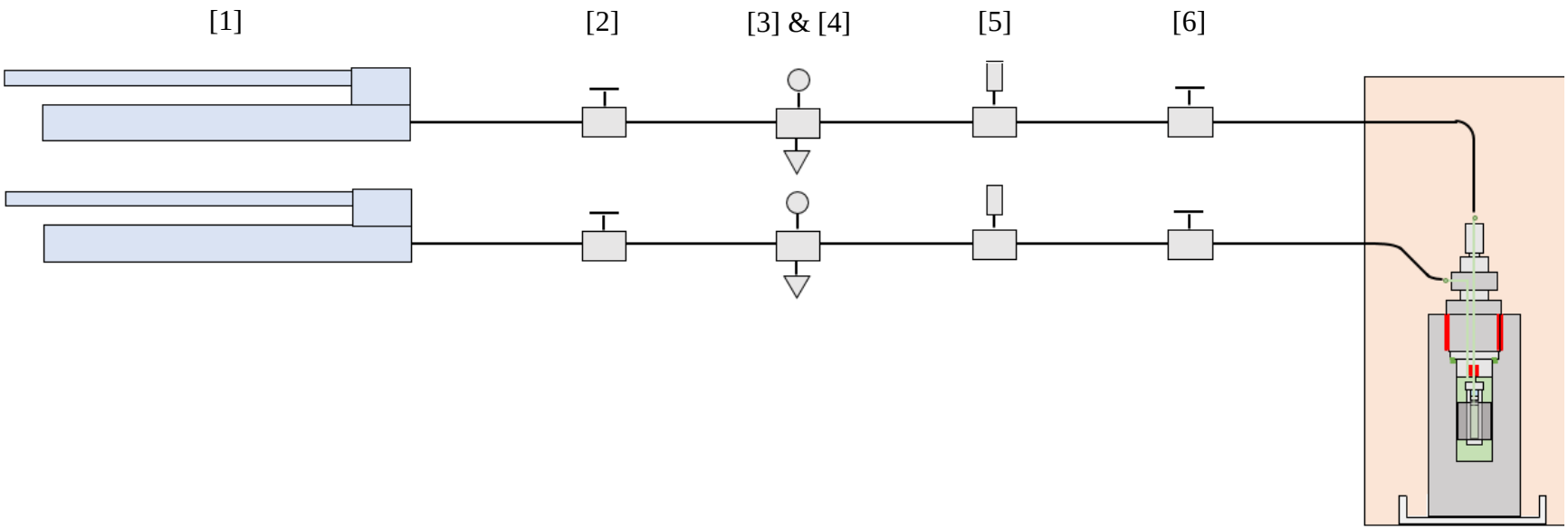

Figure 8: Theoretical experimental set-up

The samples were subjected to cyclic differential pressures of 2,000 and 4,000 psi while the confining pressure remained constant at 6,000 psi. This means the casing pressure cycled from 6,000 to 8,000 psi and 6,000 to 10,000 psi, respectively. **Figure 9** provides a visual for this procedure where ΔP equals the pressure differential. Samples were then removed from the large pressure vessel and visually inspected for cracks or debonding. If neither failure method occurred, the samples were reloaded into the large pressure vessel and subjected to more pressure cycles. The process was repeated until some severe failure method was observed, typically inner debonding, radial cracking, or disk cracking. Usually two to eight pressure cycles were applied in-between inspections. After failure occurred, it was assumed the fatigue limit of the sample was reached during the last testing period.

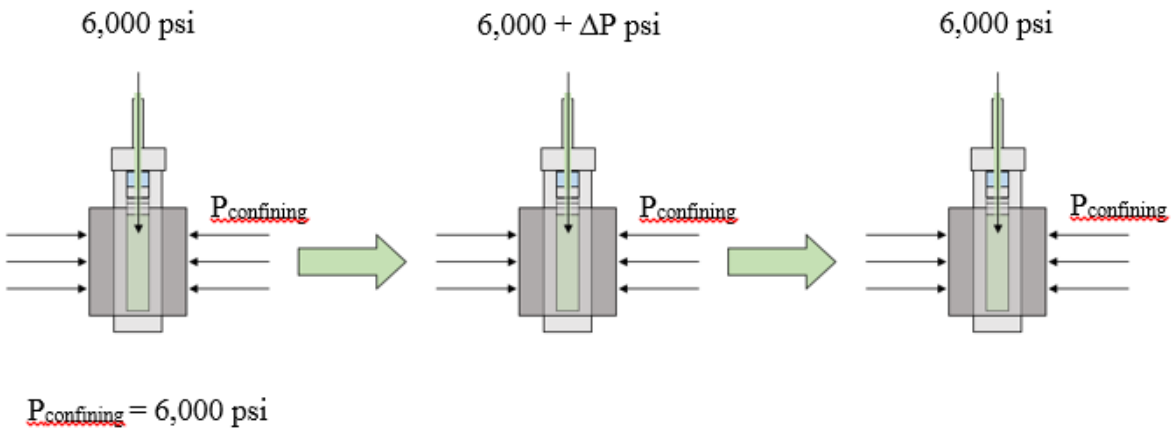

Figure 9: Cyclic loading of samples

Six samples were prepared for each slurry design. Three were tested at the 2,000 psi differential and the remaining three were tested at the 4,000 psi differential. One sample per pressure differential was CT scanned before, during, and after cyclic testing. The scans occurred during the inspection period after a round of pressure cycles.

CHAPTER III

EXPERIMENTAL PROCEDURES

This chapter presents the experimental procedures in three sections including cement sample preparation, cement sample testing, and CT image processing. The various procedures are lengthy and highly detailed, but summarized here to highlight key ideas. The more exhaustive standard operating procedures (SOP's) are found in **Appendix A**.

Cement Sample Preparation

The preparation of cement samples included mixing cement slurry, placing the mixed slurry into prepared molds, and then curing the freshly-mixed samples. There were two types of samples prepared in this experiment. The first type involved cement cured around a steel pressure vessel to imitate a cement sheath. The second type was a cement cube, two inches long on each side, to be used for compression strength testing.

Mold Preparation

The first step in this process was to prepare the two different molds:

Cement sheath – the small pressure vessel was bathed in acetone, a grease solvent, and scrubbed clean with steel wool and fine sand paper to remove any oil residue or rust. These contaminants might prevent a good cement-vessel bond. A one-half inch thick molding board with one inch diameter holes was bolted to a second retaining board using wing nuts. A small amount of silicon sealant was applied to the bottom one-half inch of the small pressure vessel. After application of the silicon, the vessel was inserted into a hole in the

molding board. Some silicone typically squeezed out of the hole and was then removed to prevent contamination with the cement slurry. PVC pipe was cut into two inch long pieces and sawed in half to provide seams for easy demolding. The two halves were taped together, centered around the small vessel, and glued onto the molding board using silicone. The mold was allowed to dry for several hours to ensure cement would not leak from the mold during the placement or curing process. **Figure 7** shows a sheath mold ready for cement placement.

Figure 10: Molding board, PVC pipe, and small vessel

Cement cubes – a three-piece cube mold was borrowed from the Civil Engineering Department to create the cement cubes. The two sidewalls were tightened together, then soundly attached to the base using a hand pliers. In order to ease disassembly and the removal of hardened cement, form release oil was applied to the interior and top surfaces. **Figure 8**, shown on the next page, presents the cube mold and a set of samples.

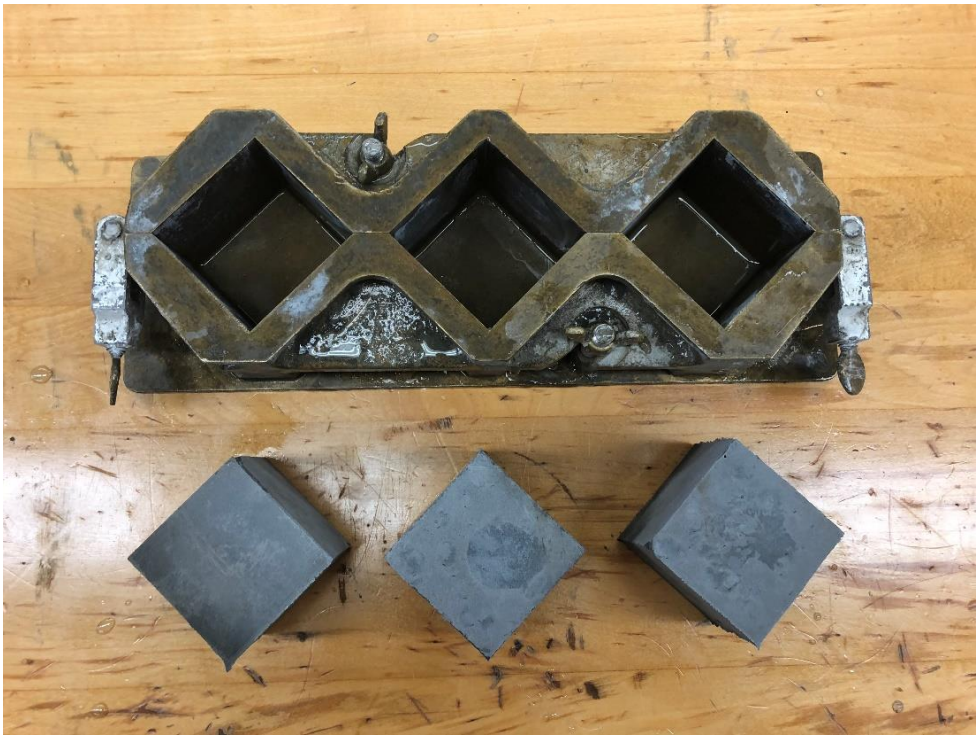

Figure 11: Cube mold and cement samples

Mixing

The second step in the cement sample preparation process involved mixing cement slurry. All procedures discussed in this section were chosen with reference to API RP 10B – Recommended Practices for Testing Well Cements.

Design – Class H cement was used as the primary bonding agent. The first slurry design was neat slurry, or a mixture of exclusively cement and water. The other four slurries included silica flour to resist strength retrogression from exposure to temperature above 230^{o}F. Additionally, the third slurry included polypropylene fibers, the fourth slurry contained bentonite, and the fifth slurry included both. The designs are listed in **Table 1**, found on the next page, with their respective test identification code.

Table 1: Slurry designs

Number	Testing ID	Basic Components
1	NS	Neat slurry
2	SF	Neat slurry + 35% bwoc silica flour
3	PP	Neat slurry + 35% bwoc silica flour + 0.75% bvob polypropylene fibers
4	BEN	Neat slurry + 35% bwoc silica flour + 8% bwoc bentonite
5	BENPP	Neat slurry + 35% bwoc silica flour + 8% bwoc bentonite + 0.75% bvob polypropylene fibers

The NS design utilized a water-cement-ratio (w/c ratio) of 0.38, as recommended by API standards for 16.4 ppg cement slurry. The addition of silica flour lowered workability so adjustments were made to increase the w/c ratio. The SF and PP designs shared a w/c ratio of 0.48. The BEN and BENPP slurries also had a 0.48 w/c ratio, but additional water was added to hydrate the bentonite additive. The API recommended practice is 5% bwoc water addition per 1% of bentonite. Consequently, the w/c ratio was increased from 0.48 to 0.88.

A density of 16.4 ppg was maintained for the NS and SF slurry designs. The PP, BEN, and BENPP designs yielded slurry with a 16.0, 14.0, and 13.7 ppg density, respectively. These densities were achieved by considering the specific gravity of the different admixtures. Silica flour, polypropylene fibers, and bentonite all have a lower specific gravity than Class H cement. The absolute volume of each additive, or the volume a solid displaces when added to water divided by its weigh, was important because the cumulative mass of the components

can be divided by their cumulative yield volume to find the theoretical slurry density. Once ready, the design was mixed for comparison with its theoretical density. A continuous process designing, mixing, and testing batches of slurry was conducted until the desired density was achieved. The scale used for measuring components in the slurry batch provided readings to the nearest 0.01 gram. For this reason, grams and millimeters (mL) were used in the design process, then converted to ppg.

Table 2: Mass of mixture components

Slurry ID	Mass of Components (g)					Batch Volume (mL)
	Water	Cement	Silica Flour	PP Fibers	Bentonite	
NS	328.58	850.53	-	-	-	600
SF	308.76	643.26	225.15	-	-	600
PP	306.19	637.90	223.27	4.98	-	600
BEN	347.15	394.50	138.08	-	31.56	600
BENPP	382.37	434.51	152.08	5.50	34.76	600

$$\textbf{\textit{Theoretical density}} = \textit{mass of slurry} \div \textit{yield volume of slurry} \quad (2.1)$$

Where:

Mass of slurry =

$$\textit{mass of cement} + \textit{mass of water} + \sum \textit{mass of admixtures} \quad (2.2)$$

Yield volume of slurry =

$$\textit{yield volume of cement} + \textit{yield volume of water} + \sum \textit{yield volume of admixtures} \quad (2.3)$$

Yield volume =

$$\textit{absolute volume} * \textit{mass of material} \quad (2.4)$$

Absolute volume =

$$\textit{1 pound of material} \div [\textit{specific gravity of material} * \textit{density of water}] \quad (2.5)$$

Batch volume selection – a batch volume of 600 millimeters or greater was chosen. It met the requirements for filling three cube molds and one cement sheath mold without excessive waste. Respectively, these volume requirements were 420 and 110 mL with a sum of 530 mL. The slurry volume was batched larger to account for density testing which requires 200 mL. Slurry from the density test was reused, but some volume was lost to the walls of the mud weight cup. Slurry was also observed to be lost during the puddling, strike-off, and placement processes. Extra volume was prepared to account for these losses.

Mixing procedure – the cement slurry was mixed using an OFITE constant speed blender control box, commercial blade-type blender, and Mettler Toledo scale accurate to ± 0.01 grams, as shown in **Figure 12** on the next page. The box controls the blade speed of the blender, but also permits the user to program the mixing speed and duration. First, dry

material additives were weighed individually, then thoroughly blended in a large container. The mix water was poured into the 1-liter capacity blender container and placed on the blender base. The blender motor was turned on high at 4,000 ± 250 rpm for 15 seconds. During the 15 second period, all dry materials were added to the mix water. Then, the container lid was attached and the blender motor was turned up to 12,000 ± 250 rpm for an additional 35 seconds of mixing. Once this period was over, it was often observed that a layer of dry material would float on top of the cement batch. A spatula or similar instrument was used for hand mixing until the batch reached a satisfactory uniform composition.

Figure 12: Cement mixing equipment

Placement

The third step in the cement sample preparation process was placing cement slurry into the prepared molds. Placement is important to reducing the entrapped air content and forming a favorable cement slurry consistency. Otherwise, air pockets are prevalent and heavier particles in the blend settle to the bottom of the mold. Good placement techniques also prepare cement samples with the desired dimensions and smooth testing surfaces.

The procedure was identical for the cement sheath and cube molds. Mold release agent was lightly applied to all interior surfaces of the mold to ease removal. Cement slurry was added to the mold in two layers, each puddled and vibrated to remove air bubbles and ensure a good consistency. The top of the cube molds were struck off to provide a flat surface. **Figure 13**, found on the next page, shows one mold that was well-prepared using the aforementioned methods versus two other molds that were not well-prepared.

Throughout the placement process, cement slurry was continuously hand mixed in the blending container. It is also important to mention the order for pouring cement into the molds. The first layer of all cube molds was poured first, then the first layer of the cement sheath mold. A second layer was added to one cube mold, then the cement sheath mold, and finally the remaining two cube molds. The intricate order, combined with continuous hand mixing, provides a good distribution of different parts of the slurry batch into the molds.

Figure 13: Cement placement into cube mold

Curing

The fourth and final step in the cement sample preparation process was curing the cement samples. One condition was surface curing which implies the sample was placed underwater at atmospheric pressure and 120^{o}F, as shown in **Figure 14** on the next page**.** Two temperature probes were used to monitor temperature at all times. The curing water was drained and replaced as needed, usually two times per week. Also, a small amount of lime was added to the curing water to prevent calcium carbonate from leaching out of the samples. The other condition was wellbore curing, and it entailed loading the sample into the large pressure vessel at 6,000 psi, confining and casing pressure set equal, and 250^{o}F.

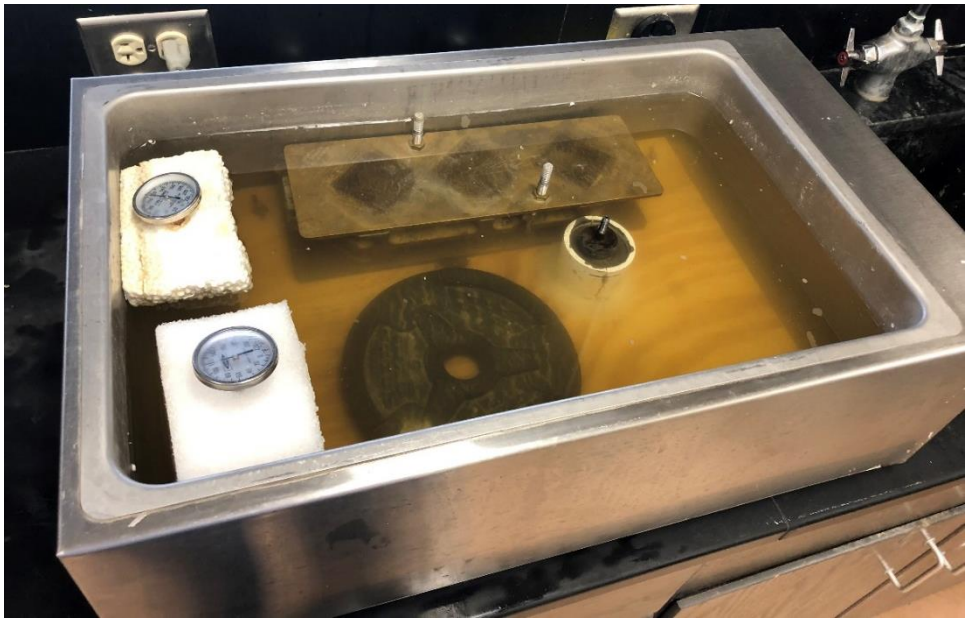

Figure 14: Surface curing conditions

The cement cubes were cured exclusively at surface conditions for 24 hours. They were cured inside the cube mold with a lid to minimize pooling which made the cement surface very uneven. The cement sheath samples were cured at surface conditions for 12 hours, 6 hours inside the PVC mold then 6 hours without the mold. A razor blade and flathead screwdriver were used to remove the mold. Then, the sample was loaded into the large pressure vessel. The vessel was placed inside the oven, set to 250^{o}F, and connected to the pressure lines, as shown in **Figure 15** on the next page. Casing and confining pressure were raised together in 400 psi steps until 6,000 psi was reached. Further directions for the loading process are found in *Cement Sample Testing* and **Appendix A**.

Figure 15: Large vessel arrangement inside the oven

Once the pressure was achieved, the process of reaching thermal equilibrium was initiated. Hydraulic fluid would expand with the rising temperature and increase the pressure in the flow lines. The pressure was relieved every 15 minutes for 2 ½ hours. By that time, the change in pressure was typically insignificant. The upstream isolation valves were closed and the system was allowed to finish curing undisturbed. Wellbore curing lasted 14 hours and included the time to reach thermal equilibrium. This means the cement sheath sampled was cured for a total of 26 hours.

Cement Sample Testing

Tests conducted on well cements are typically divided into two categories. One category involves fresh properties while the other involves hardened properties. In this experiment, the density of freshly mixed cement slurry was measured for quality control. Compression strength and cyclic fatigue were also tested, but involved hardened cement samples.

Density

After mixing cement slurry and prior to its placement, the fresh density was measured using a mud balance. The mud balance was placed on a flat level surface with the cup in surface-saturated-dry (SSD) condition, as shown in **Figure 16** on the next page. This condition implies the material surfaces are dry, but the interparticle voids are saturated with water. Fresh slurry was poured into the cup from the blender container. Once full, the lid was placed on the cup and twisted shut to expel excess cement slurry through a hole in the cup's lid. The cup and its attached arm were cleaned with a paper towel and placed on the balance, then the rider was moved along the arm until the two sides balanced out, as shown in **Figure 17** on the next page. The rider arm had a scale of values to indicate the slurry density to the nearest 0.1 ppg. Measured density was required to be ± 0.1 ppg from the theoretical density.

Once tested, the slurry was poured from the cup back into the blender container and thoroughly mixed. The measured density was then compared with the acceptable range. If the slurry passed the density test, it was placed into the molds. If it failed, the density was measured a second time. A second failed density test meant the batch failed specifications and the entire batch was discarded.

Figure 16: Mud balance and cement slurry for density testing

Figure 17: Slurry cup balanced with rider arm

Compressive Strength

Compression tests were conducted on the 2 x 2 x 2” cement cube samples after 24 hours of surface curing. Samples were removed from the curing bath and immediately transported to the testing area. It is important that samples were saturated when tested, as recommended by API standards. A swivel plate was placed onto the bottom cross of the Instron testing frame, as shown in **Figure 18**. The sample was placed sideways onto the swivel plate so its top surface would point forward. The top platen was quickly lowered to touch the sample, then more slowly lowered to preload the sample with 50 lbf. A computer program ran the actual test using parameters entered by the user. Once the sample broke, the top platen was raised to relieve the load.

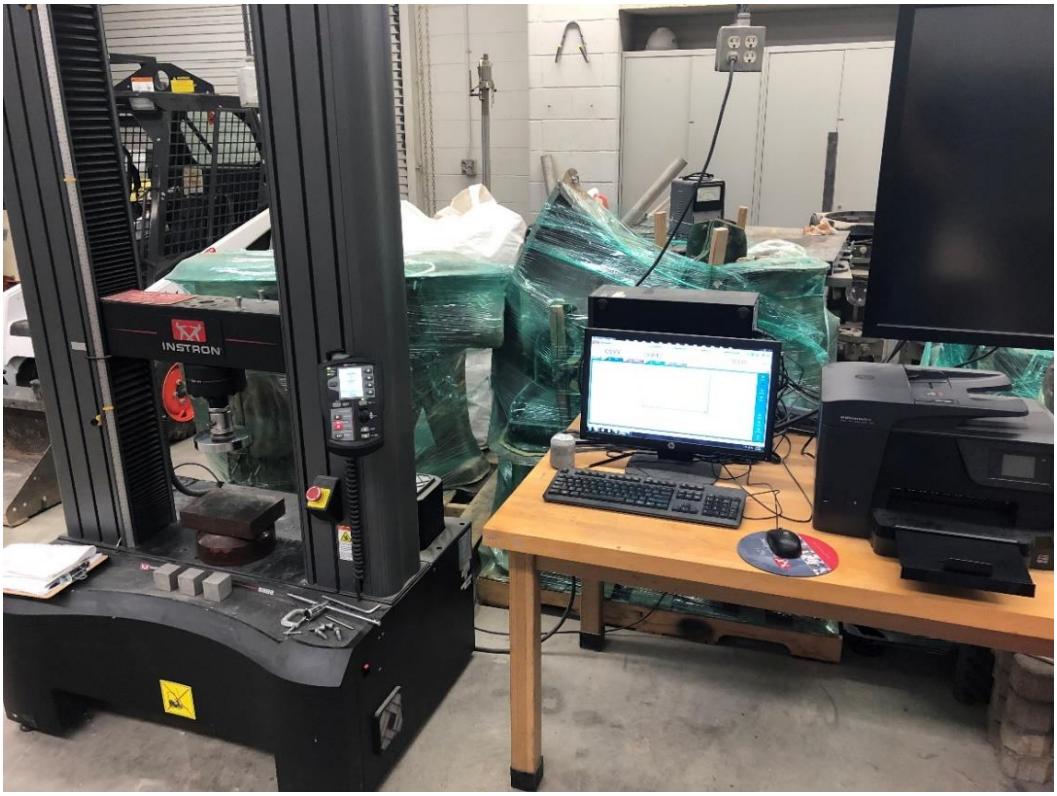

Figure 18: Compressive strength testing area

The testing procedure was repeated for all cubes in the set to generate load vs. time curves, as shown in **Figure 19**. A computer program called Bluehill would automatically find the global maximum load on each curve, then divide the load by the sample's area to calculate the compressive strength of the sample. Values were recorded to the nearest 10 psi.

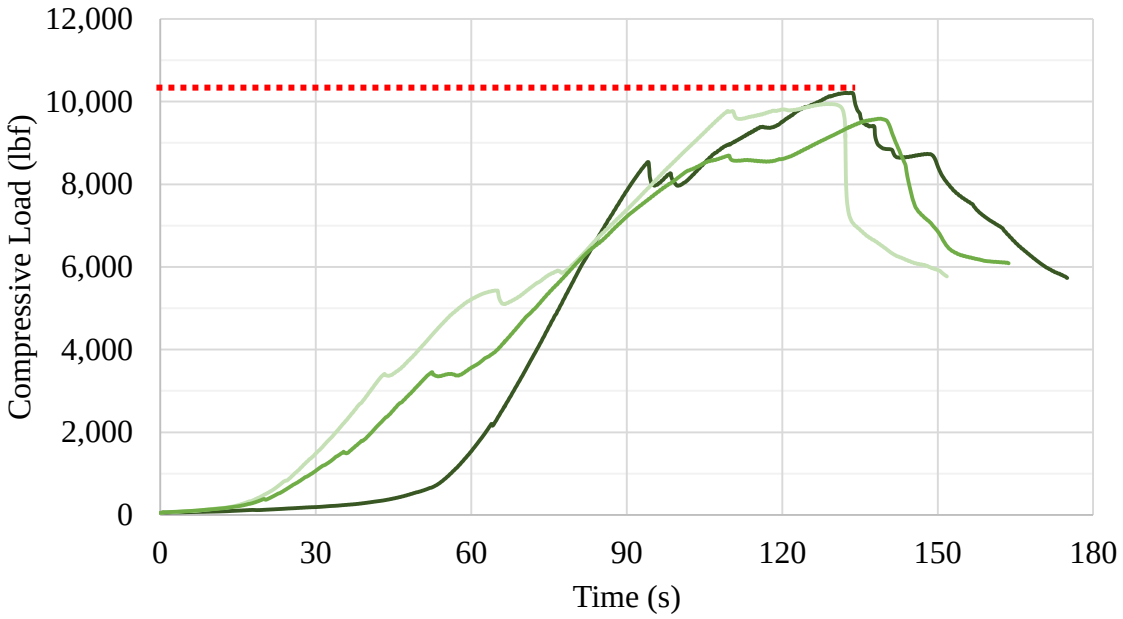

Figure 19: Load vs. time curves with an indicated global maximum

Bluehill also controlled the testing frame to execute the test. Unfortunately, API-recommended testing parameters could not be fully applied. The API standards require applying 4,000 lbf per minute for samples with an expected strength of 500 psi or less. For samples with strength expected to be greater than 500 psi, a 16,000 lbf per minute rate should be applied. The Bluehill program could not apply loads of force per minute, as shown in **Figure 20** on the next page. There was trouble with calculating the proportional gain factor of the cement sample.

This factor controls how the extension rate is applied to achieve the required force rate. Several attempts were made to calculate the proportional gain factor for neat slurry cube samples, but the calculated value was inconsistent between each sample. There was concern that damage might occur to the testing frame due to vibration at heavy loading. For this reason, it was decided to use an extension rate instead of a force rate. A rate of 0.035 inches per minute was applied.

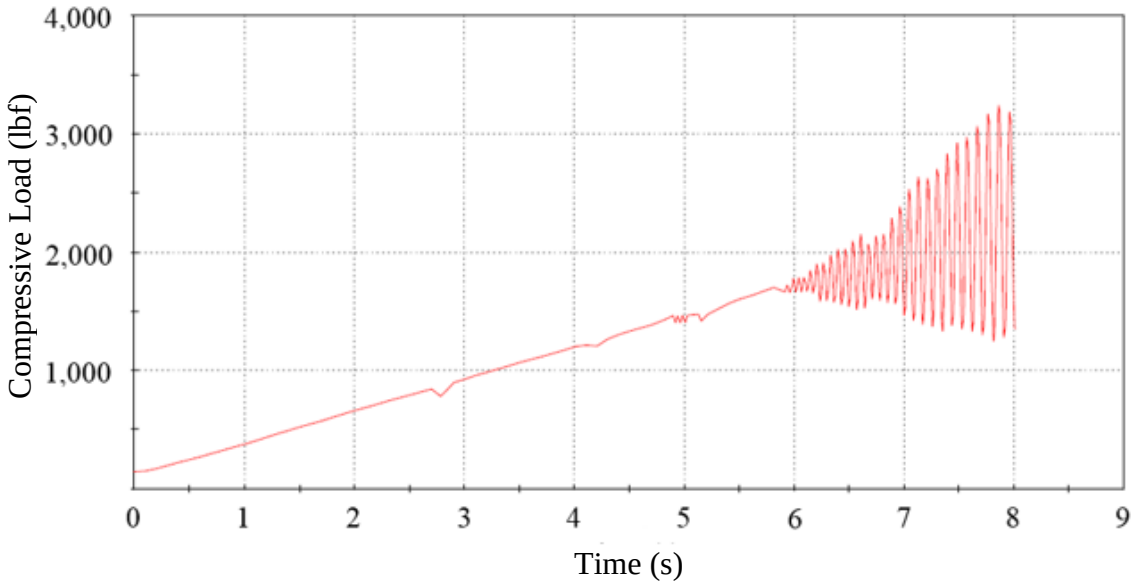

Figure 20: Vibration caused by force rate loading

Cyclic Fatigue

Cement sheath samples, as shown in **Figure 21**, were cured at surface conditions for 12 hours, then an additional 14 hours at wellbore conditions. Wellbore conditions included a pressure of 6,000 psi and temperature of 250^{o}F. Once curing was complete, the sample was removed from the large pressure vessel and inspected for failure. A number of neat slurry samples displayed post-curing failure due to strength retrogression. To resolve this problem, 35% bwoc silica flour was added to the other slurry designs. If the sample failed following the curing period, the test was concluded, but more commonly the sample was prepared for fatigue testing.

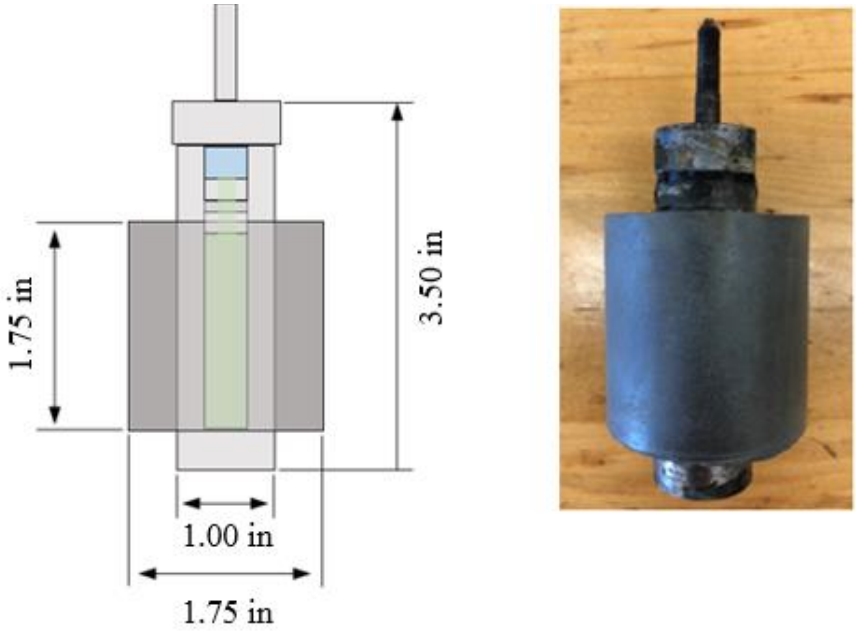

Figure 21: Approximate dimensions of the cement sheath

The sample was reloaded into the large pressure vessel, and the entire arrangement was set back into the oven at 250^{o}F. The casing and confining pressure flow lines were attached to the vessel head. Then, pressure was applied simultaneously in both flow lines in equal step increases of 400 psi to reach 6,000 psi. If the pressure remained constant in both flow lines, there were no leaks which meant the sample was ready for testing. If a rapid drop in pressure was observed, steps were taken to locate and fix the leak.

The data acquisition system, shown in **Figure 22**, recorded pressure data from transducers connected to the flow lines at a rate of 10 samples per second. The data was recorded on a range of 0 – 10 volts, so the transducers were calibrated to their respective pressure gauges. The calibration process generated equations to convert the output voltage data to psi.

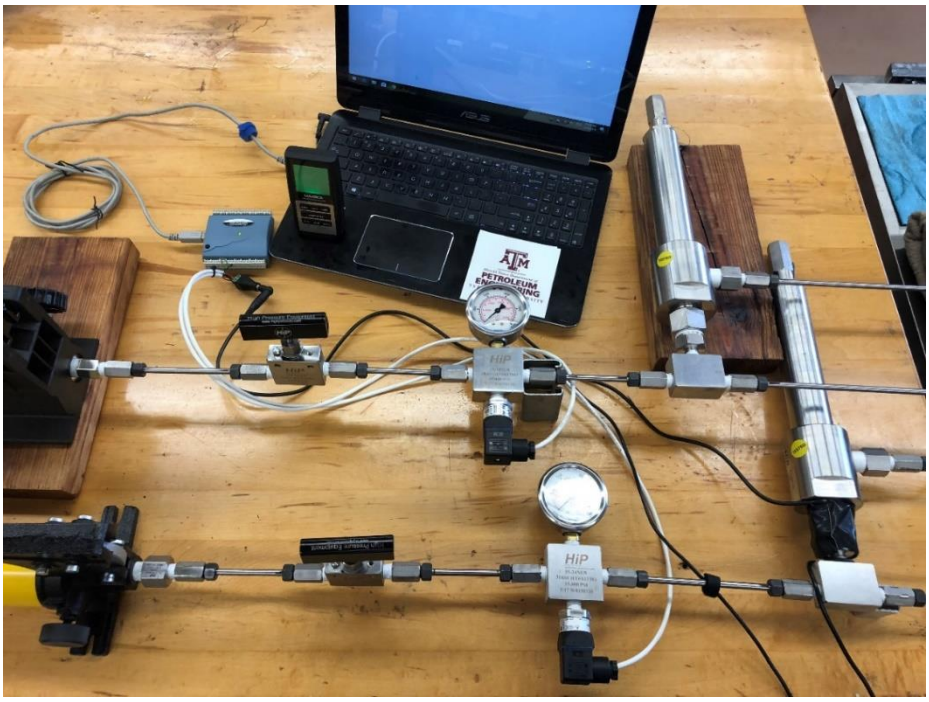

Figure 22: As-built experimental set-up

The cyclic fatigue test was started by initiating the program to record pressure data. After two minutes of equal confining and casing pressure at 6,000 psi, the casing pressure was raised by the desired pressure differential to 8,000 or 10,000 psi. Two minutes later, the casing pressure would be reduced back to the confining pressure held constant at 6,000 psi. Then, the process was repeated for two minutes on followed by two minutes off. Each period of four minutes was considered one pressure cycle.

After a predetermined number of pressure cycles, the test was stopped to remove the cement sheath sample. The sample was checked for cracks or debonding failure, as shown in **Figure 23**. If the sample had failed by severe debonding, the test was immediately stopped. Otherwise, the test continued with more pressure cycles until the sample did fail in this manner. Later, the test's voltage data was exported into a spreadsheet and converted to psi.

Figure 23: Radial cracking (left) vs. debonding (right)

Figure 24 and **Figure 25**, found on the next page, present pressure data obtained from two cyclic tests. The gray line represents the confining pressure held constant at 6,000 psi. The green line represents the casing pressure which changes with time. The figure indicates that the test was paused after eight cycles to check for failure in the sample. The sample had not failed, so it was reloaded into the large pressure vessel for eight more pressure cycles. As shown below, the pressure differential was applied and relieved quickly. There were attempts to slow the rate of pressure change, but it was difficult to achieve consistently.

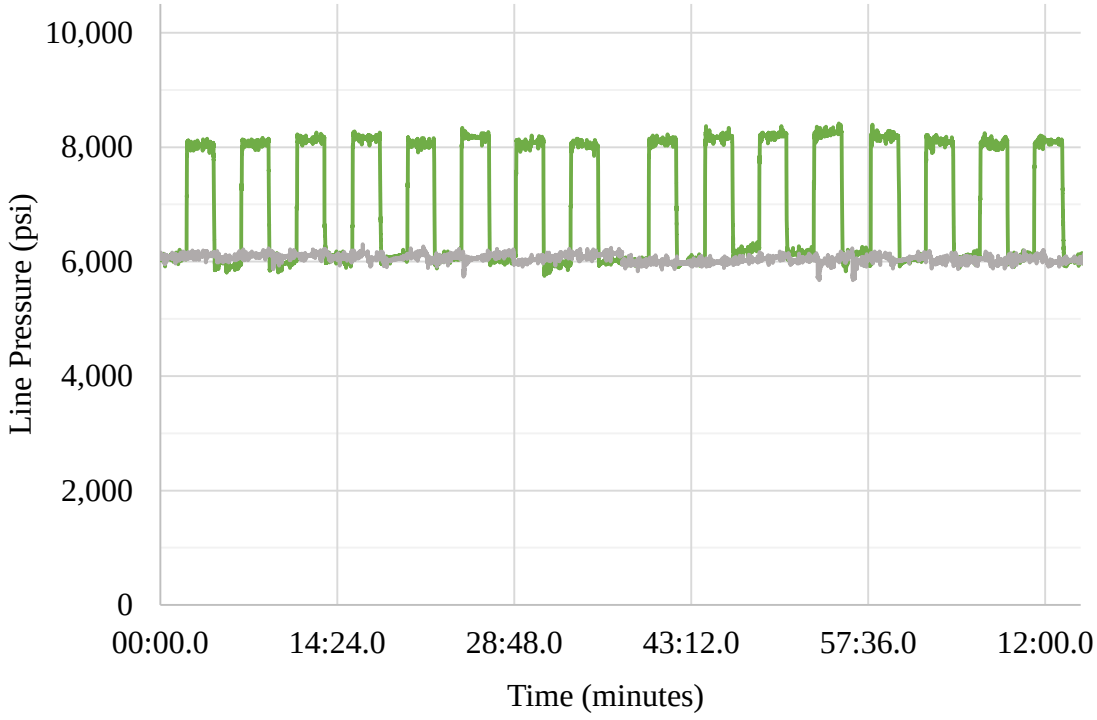

Figure 24: Pressure data recording at 2,000 psi differential

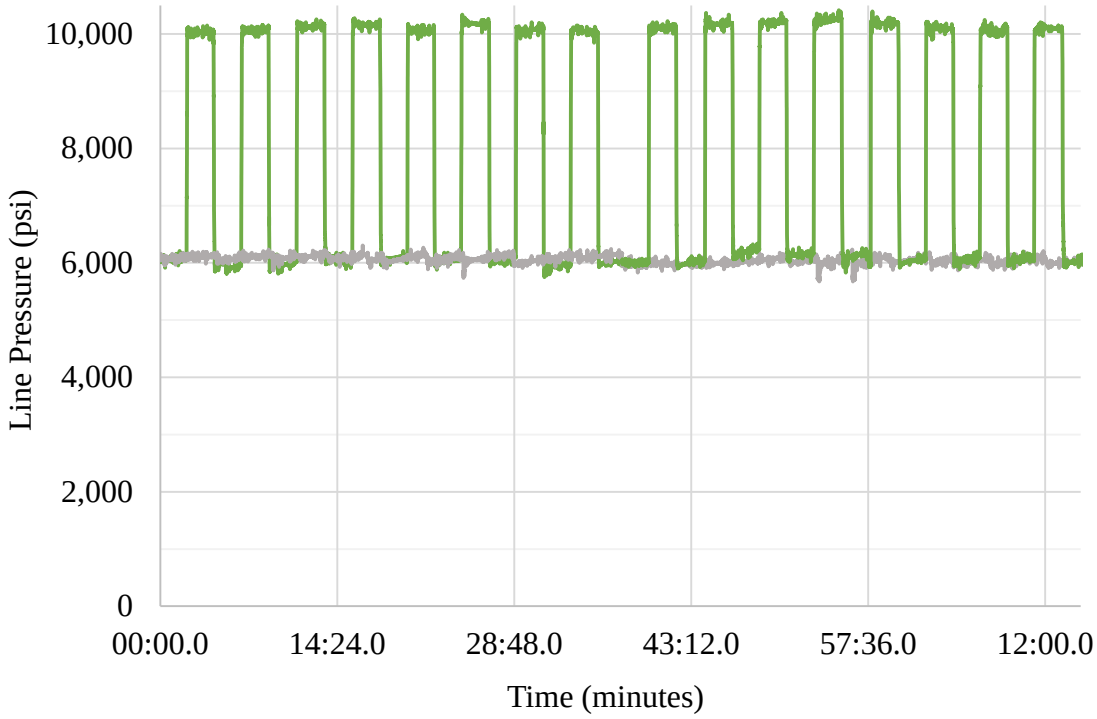

Figure 25: Pressure data recording at 4,000 psi differential

CT Image Processing

Cement sheath samples were scanned using a computed tomography (CT) scanner to observe crack initiation and propagation during the cyclic pressure tests. The scanner works by firing a narrow X-ray beam into the sample from many different angles. A computer then creates cross-sectional images from the retrieved data. The images are slices that can be organized into a 3-D image or 2-D image sequence. **Figure 26** presents the piece of equipment that scanned the samples.

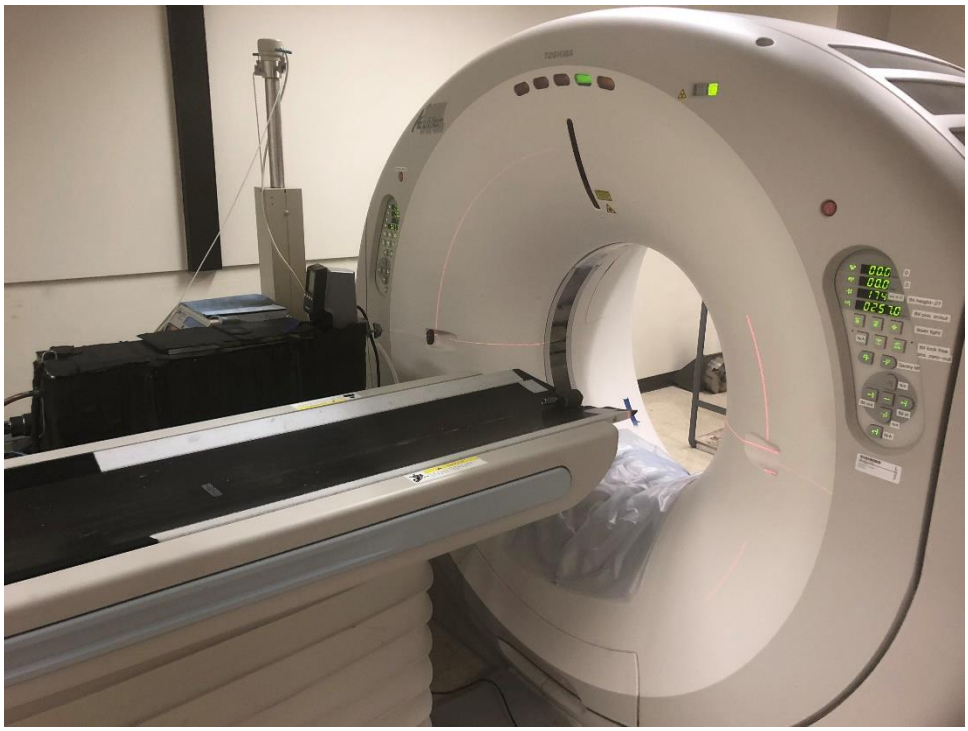

Figure 26: Department-owned CT scanner

In order to save time, not all samples were scanned. The primary objective was to determine if images could be produced that showed cracks within the cement sheath sample. Samples were scanned following the curing process before the cyclic test started, then in-between rounds of cyclic fatigue, and finally once the sample had failed.

Samples were placed on the scanning table in the same manner, the top pointing to the left, for consistent reference during analysis. An image processing program, ImageJ, was used to organize the image sequences. **Figure 27** shows two views of a cement sheath sample. The left image displays an overall plan view, the right image is a single cross section within the image sequence. More cross sections are presented in the results chapter that indicate radial and disk cracks.

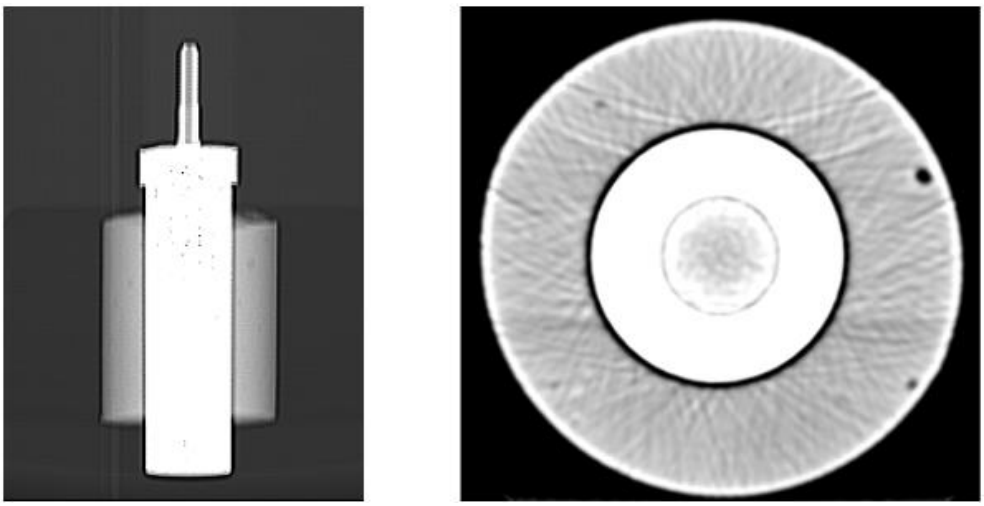

Figure 27: Plan view and cross section of cement sheath sample

CHAPTER IV

RESULTS

Density

The density of each cement slurry batch was tested after mixing to ensure it met design specifications. If the batch failed two consecutive density tests, it was discarded. **Table 3** shows the acceptable range for the different slurry designs. All cube and cement sheath samples were produced from batches that passed the density specification. The cement slurries were well-designed and mixed beforehand as trial runs, so failing the density test was a rare occurrence.

Table 3: Density specifications

Slurry ID	Theoretical Density (ppg)	Acceptable Density Range (ppg)
NS	16.4	16.3 – 16.5
SF	16.4	16.3 – 16.5
PP	16.0	15.9 – 16.1
BEN	14.0	13.9 – 14.1
BENPP	13.7	13.6 – 13.8

Compressive Strength

This section contains the results from compressive strength testing. In general, there were two types of failure observed, as shown in **Figure 28**. High compressive strength cubes failed catastrophically with a single large crack while the lower compressive strength cubes failed gradually in an hourglass shape. This behavior is attributed to the relative level of ductility from one slurry design to another.

Figure 28: Brittle failure (left) vs. ductile failure (right) of cement cubes

Two or three cubes were tested per batch of cement slurry. **Table 4** and **Figure 29**, both found on the next page, show the average compressive strength for the slurry designs overall. Results indicate that the NS and SF slurries performed the best in compression, or yielded at the highest compressive strength, and exhibited brittle failure. The slurries PP, BEN, and BENPP were weaker in compressive strength and displayed ductile failure. The results from each batch were combined to produce **Figures 30 - 34**, found on the following pages. Light green bars represent individual sample strength while the dark green bar shows the average strength of the batch. Load vs. time curves for every sample can be found in **Appendix B**.

Table 4: Compressive strength organized by slurry design

Slurry ID	Compressive Strength (psi)
NS	2,500
SF	1,920
PP	1,500
BEN	370
BENPP	460

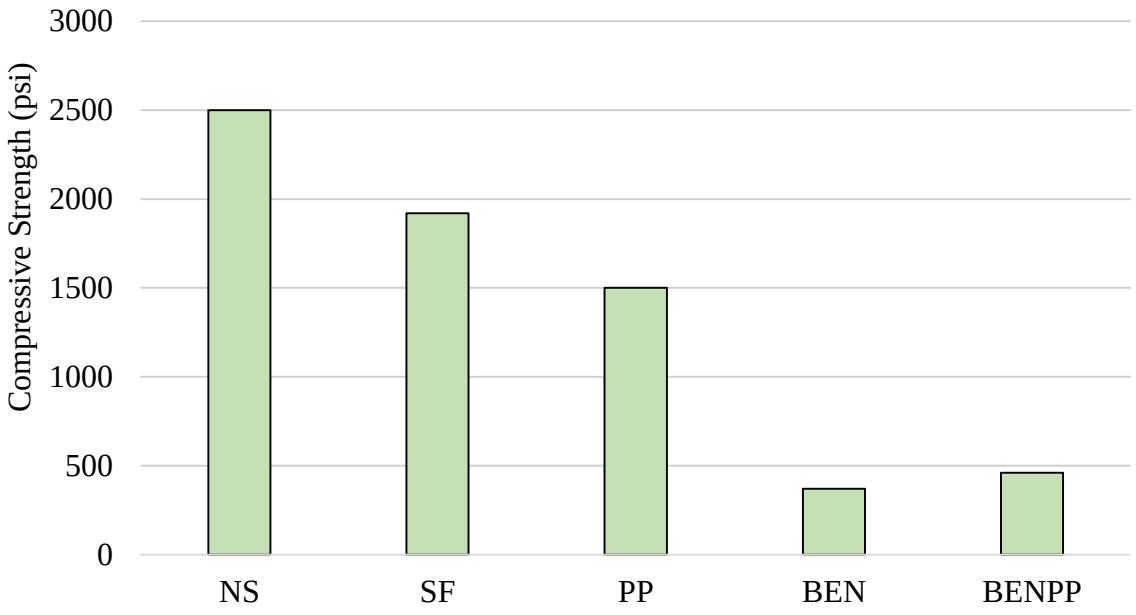

Figure 29: Compressive strength organized by slurry design

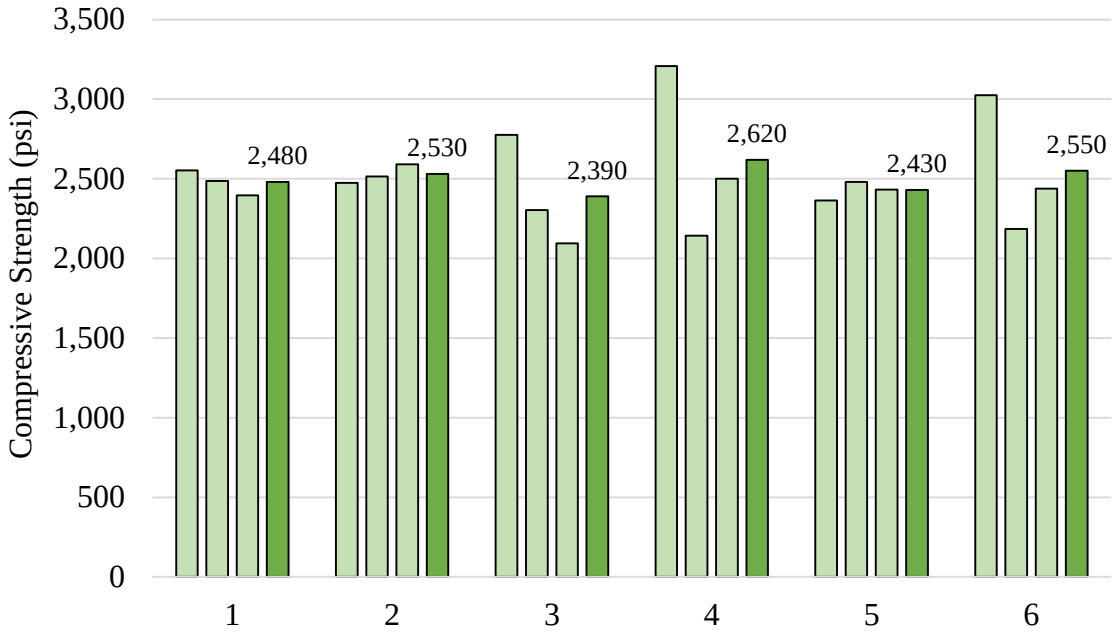

Figure 30: Compressive strength organized by batch for NS

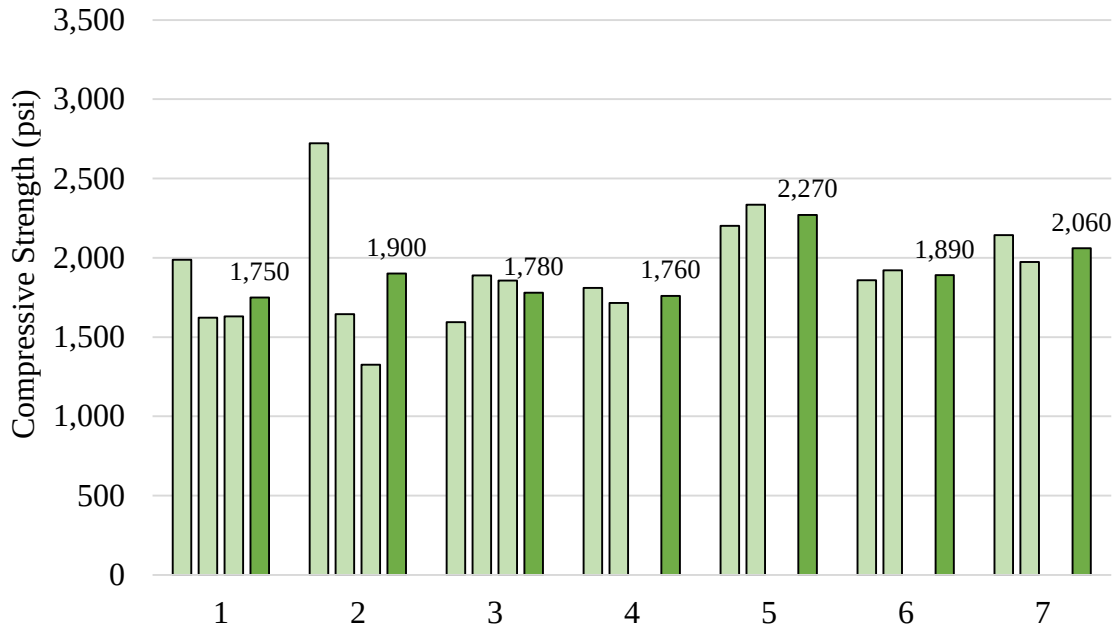

Figure 31: Compressive strength organized by batch for SF

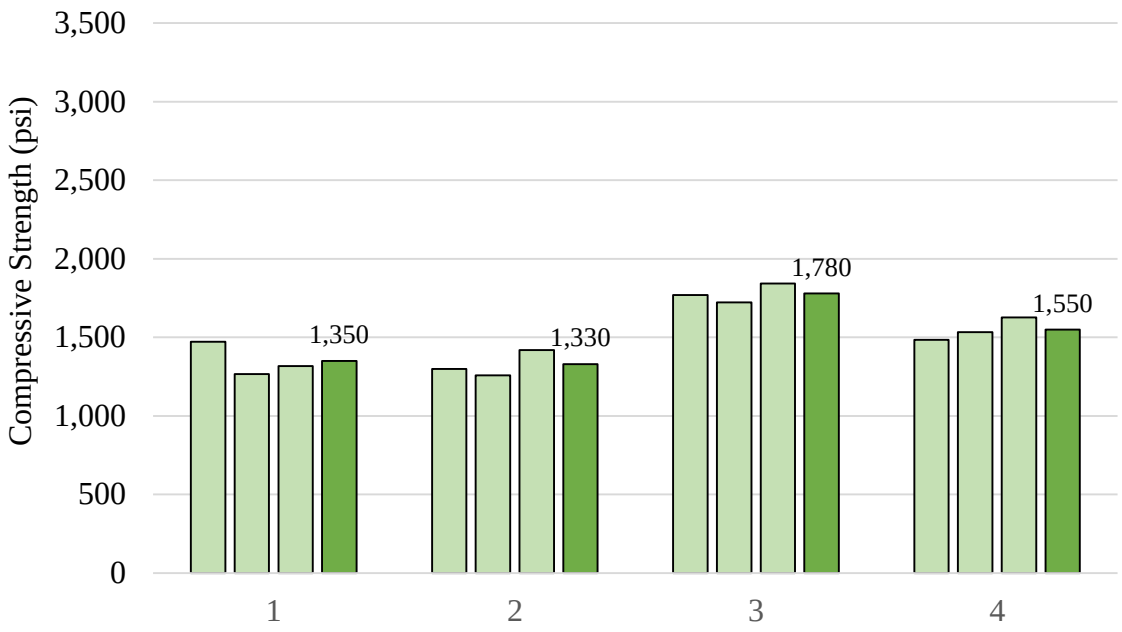

Figure 32: Compressive strength organized by batch for PP

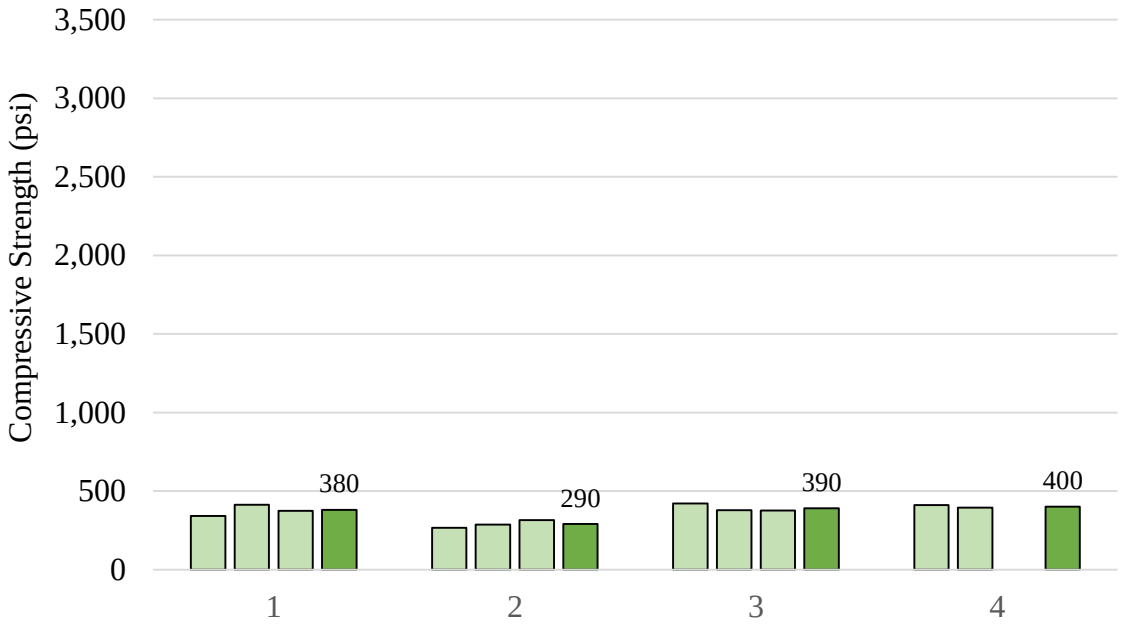

Figure 33: Compressive strength organized by batch for BEN

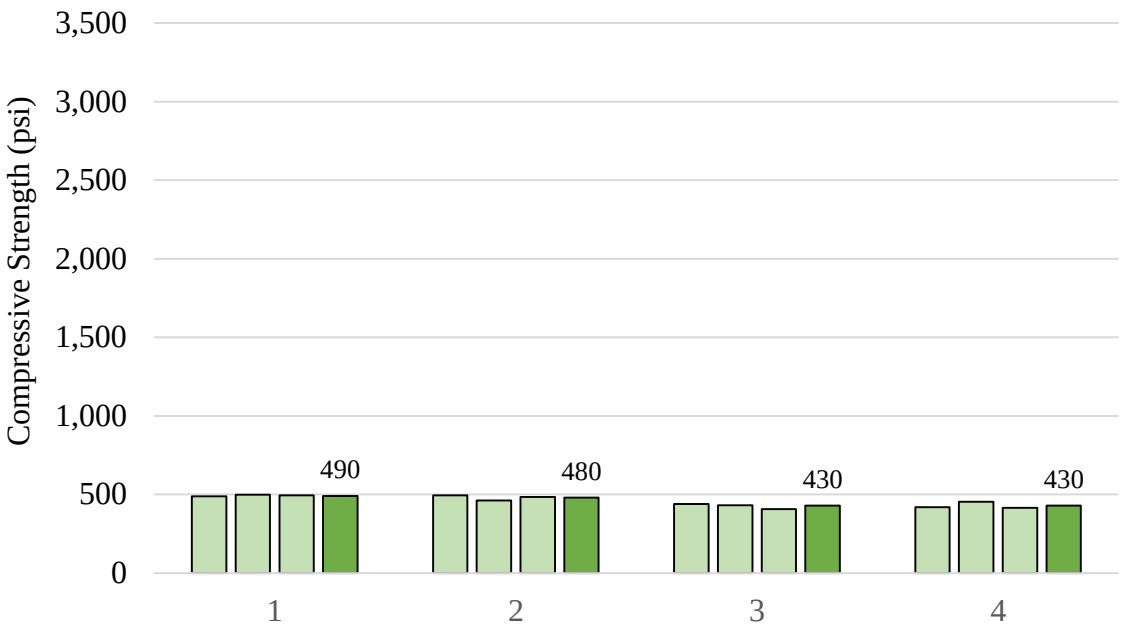

Figure 34: Compressive strength organized by batch for BENPP

Cyclic Fatigue – Wellbore Conditions

Cement sheath samples underwent cyclic fatigue loading at wellbore conditions. Results from those tests are presented in this section. Samples exhibited three types of failure including radial cracks, disk cracks, and debonding from the small pressure vessel, as shown in **Figure 35**. The methods of failure were termed minor or severe according to the level of propagation which is shown in **Figure 36**.

Figure 35: Types of failure – radial crack (left), disk crack (center), debonding (right)

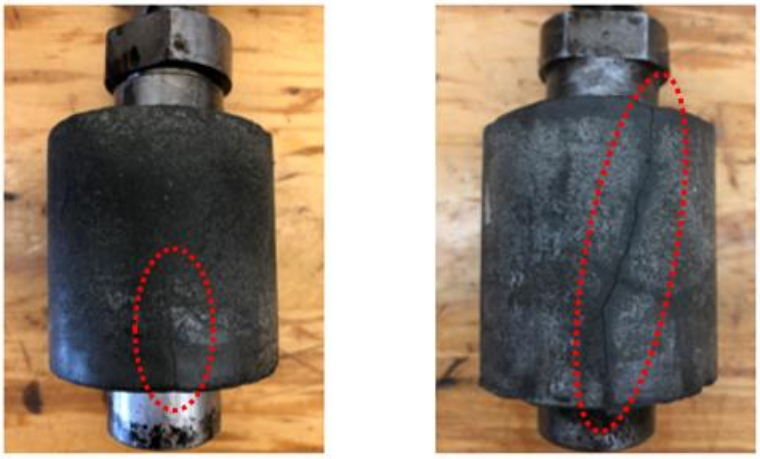

Figure 36: Radial cracks – minor (left) vs. severe radial (right)

Pressure fluctuations, temperature changes, or a combination of the two generate radial cracks. The conditions cause the internal casing pressure to exceed the external confining pressure. More importantly, the restraining cement sheath is damaged in the process. In this experiment, a radial crack was considered minor if its length was less than 0.5 inches, or about 1/3 of the cement sheath length, and severe if greater than 0.5 inches.

Disking failure was observed, but it was very rare. The failure method is generally caused by the contraction of the cement sheath when it cannot slide in the wellbore. The casing-cement sheath and cement sheath-formation bonds prevent its lateral movement. Without a cement-formation bound, disking failure was not expected in this experiment.

Debonding of the cement sheath from the small pressure vessel was the most important type of failure. The cyclic fatigue test almost always continued until severe debonding was observed. The failure method was diagnosed by holding the small pressure vessel in one hand, the cement sheath sample in the other hand, and applying a very slight torque. If the cement sheath did not rotate, it had not debonded. If the cement sheath rotated slightly, it was called minor debonding. Finally, if the cement sheath could easily slide off the small pressure vessel, it was considered severe debonding.

The number of cycles to failure was recorded using the data acquisition system. Pressure data for every sample can be found in **Appendix B**. However, **Figure 37** and **Figure 38**, found on the next page, show the concept behind the pressure data. The gray line represents the constant confining pressure while the green lines symbolize rounds of pressure cycles.

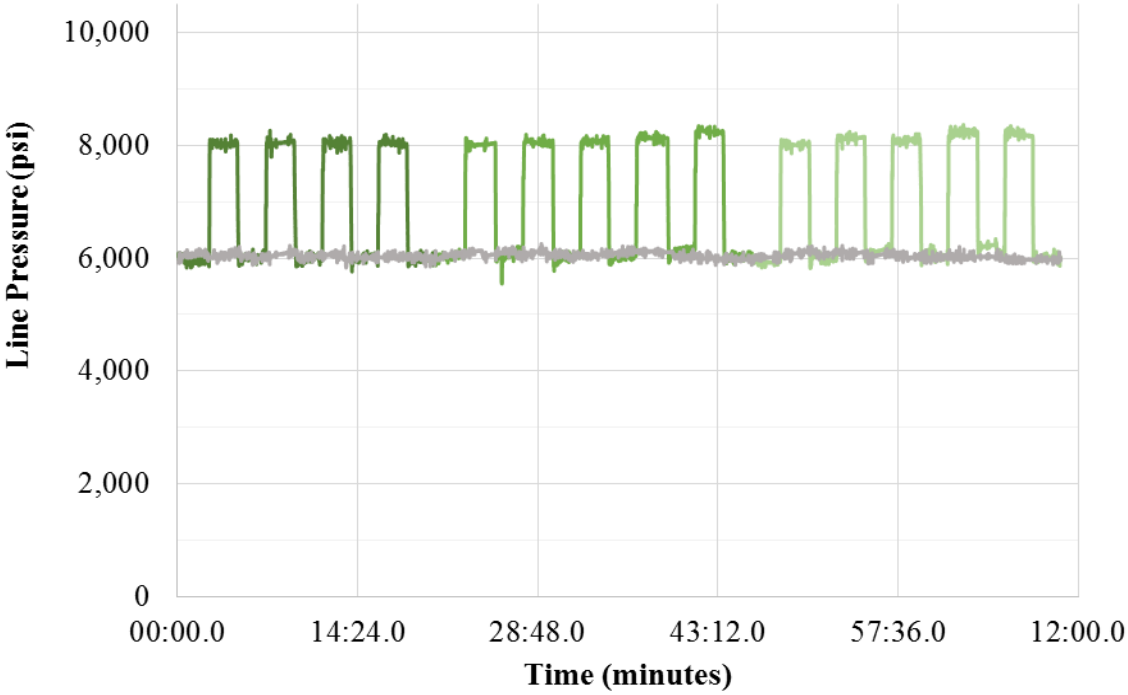

Figure 37: Pressure cycles for NS 2-3

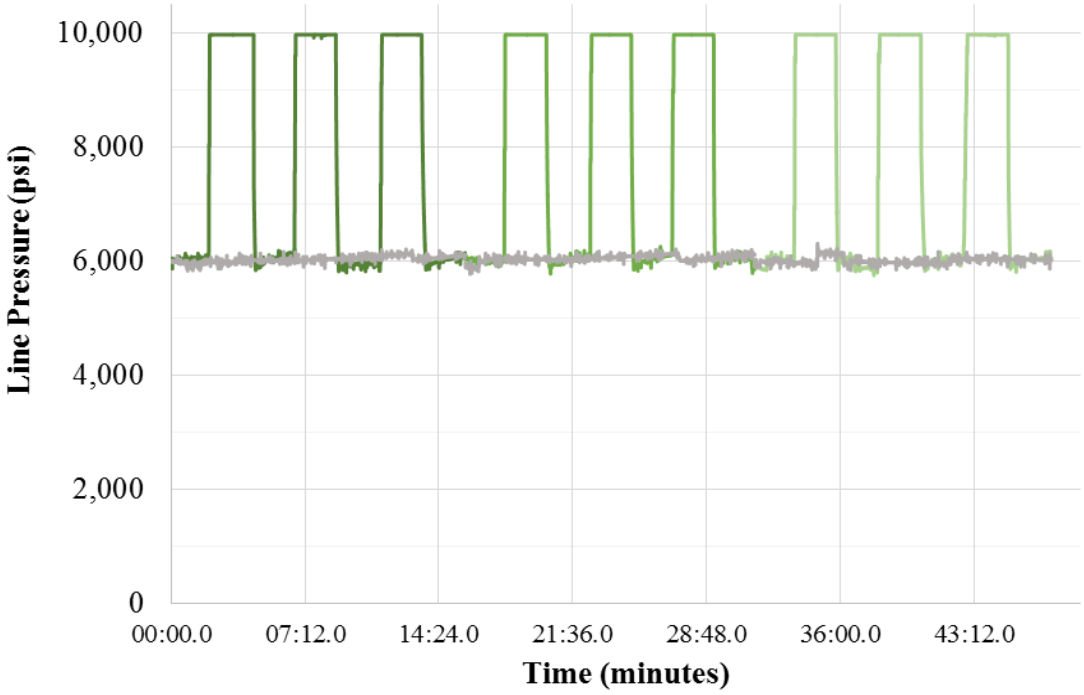

Figure 38: Pressure cycles for NS 4-2

Six samples were tested for the NS slurry design, three at 2,000 psi pressure differential and three at 4,000 psi pressure differential. The sample ID is based off of this system. The first number represents the pressure differential. The second number indicates the sample within the group of three. The third sample from each group was scanned with the CT scanner.

Table 5: Cyclic fatigue results for NS slurry

Slurry ID	Sample ID	Cycles to Failure	Failure Type/Observations
NS	2-1	0	• Did not survive curing process • One severe radial crack, severe debonding
	2-2	8	• 1 minor radial crack at 3 cycles • 1 minor radial crack at 5 cycles • 3 minor radial cracks, severe debonding at 8 cycles
	2-3	14	• No changes at 4 cycles • 1 minor radial crack, 1 minor disk crack at 9 cycles • 1 minor radial crack, 1 minor disk crack, severe debonding at 14 cycles
NS	4-1	3	• 1 severe radial crack, 2 minor disk cracks at 0 cycles • 1 severe radial crack, 2 minor disk cracks, severe debonding at 3 cycles
	4-2	9	• 2 minor radial cracks at 0 cycles • 2 minor radial cracks at 3 cycles • 1 severe radial crack, 1 minor radial crack at 6 cycles • 1 severe radial crack, severe debonding at 9 cycles
	4-3	4	• 1 minor radial crack at 0 cycles • 2 minor radial cracks, severe debonding at 4 cycles

Figure 39 presents a way to observe the pressure cycles until fatigue failure. The vertical lines on the bar chart show checkpoints to pause the test and check for cement sheath failure. As expected, the higher pressure differential generally reduced the number of cycles. Also, without the addition of silica flour, all NS samples experienced strength retrogression during the curing process. Evidence was provided upon removal of the samples from the large pressure. Cracks had already formed in the cement sheath matrix and white foam, expected to be calcium hydroxide phases, was expelled from the cracks, as shown in **Figure 40** on the next page. One sample, NS 2-1, did not survive the curing process and was not tested.

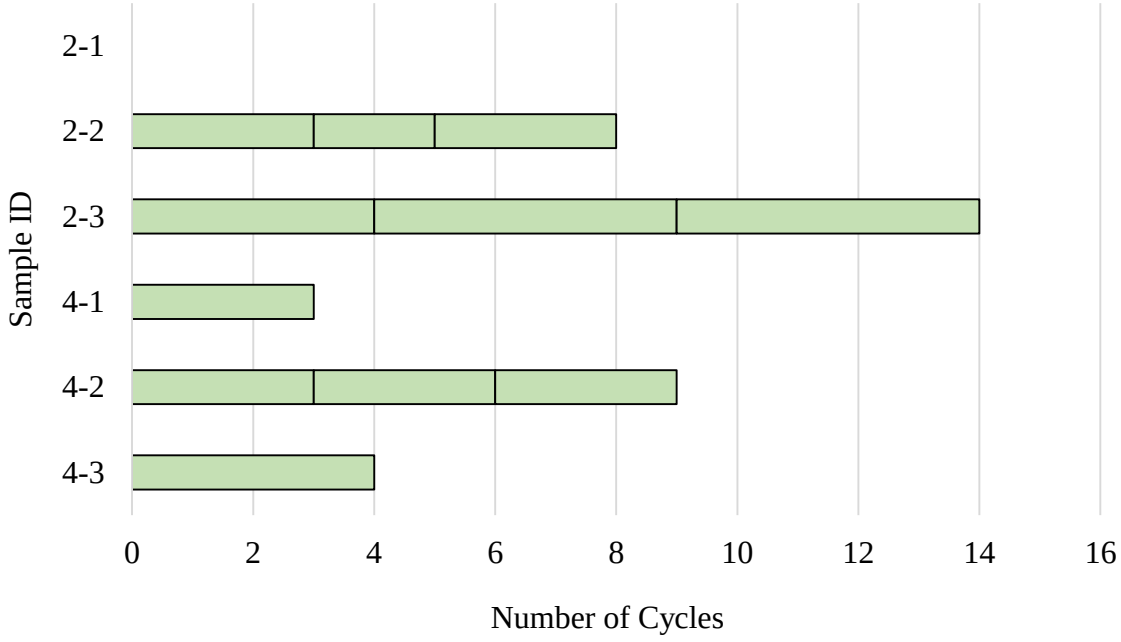

Figure 39: Bar chart for NS slurry

Figure 40: NS samples after wellbore curing

Unfortunately, equipment failure occurred after the wellbore curing period for SF 2-2. The failure stopped cyclic fatigue tests at wellbore conditions, and it is further discussed in the next section. A single sample was tested for the SF slurry design, as shown in **Table 6**. No cyclic fatigue tests were conducted on the other three slurries, PP, BEN, or BENPP, following these procedures at wellbore conditions.

Table 6: Cyclic fatigue results for SF slurry

Slurry ID	Sample ID	Cycles to Failure	Failure Type/Observations
SF	2-1	24	• 1 minor disk crack at 8 cycles • 1 minor disk crack, 1 minor radial crack at 16 cycles • 1 severe disk crack, 2 minor radial cracks, severe debonding at 24 cycles

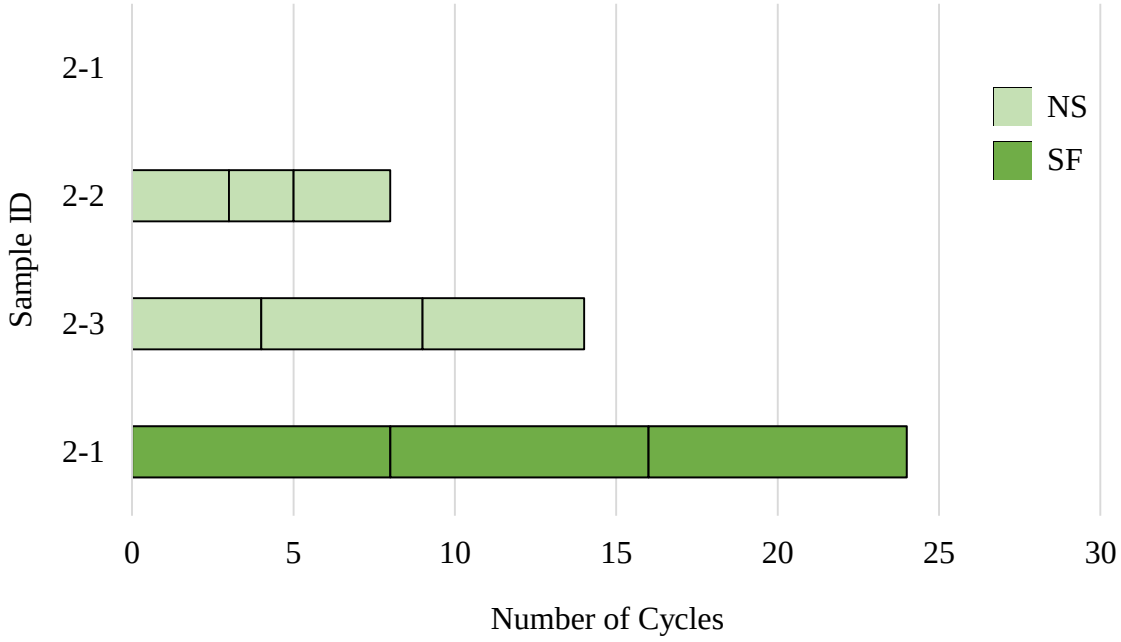

Figure 41: Bar chart to compare NS to SF slurry

Only one cyclic fatigue test on a SF slurry sample was completed to compare against results from the NS slurry. The test is singular and isolated, however it indicates that the cement sheath performance was improved with the addition of silica flour. The number of cycles increased from 8 – 14 to 24, as shown in **Figure 41.** The light green represents the NS slurry while the dark green shows the SF slurry at 2,000 psi differential.

Equipment Failure

One morning after curing the SF 2-2 sample at wellbore conditions, the vessel cap could not be removed from the large pressure vessel. It was rotated about half-way out, but stopped as shown in **Figure 42.** Torque was applied to force rotation forward, then backward, then forward again. However, the cap was stuck and needed to be machined out. It was taken to Hydraulic Works, Inc., a nearby metalworking machine shop. They successfully machined the cap out, but it was destroyed in the process, as shown in **Figure 43** on the next page. A new cap was manufactured from 4140 HT steel and the threads in the large pressure vessel were cut to 82 mm x 3mm pitch. Additionally, a spirolox ring was machined into the vessel head to improve the head's removal process.

Figure 42: Pressure cap stuck in large pressure vessel

Figure 43: Pressure cap without its threads after being machined out

An investigation was conducted at Hydraulic Works, Inc. to determine the root cause of the equipment failure. Several ideas were produced, but the best theory was the last 4-5 rows of threads in the large pressure vessel, closest to the top of the outer body, experienced some form of mechanical damage. These were the only damaged threads in the large pressure vessel after the cap was machined out. The theory is that prior to failure, the pressure cap screwed into the large pressure vessel just fine, but during removal the cap's threads jumped and cross-threaded with the large pressure vessel's threads near its top. Then, the cap could not be turned forward or backward. It is recommended to apply an anti-seize lubricant on the threads for future testing. However, the researcher must take care not to overtorque the cap into the large pressure vessel, or it will be extremely difficult to remove.

Parameter Investigation

The equipment took several weeks to repair. During this time, tests were conducted to determine what parameters lead to cement sheath failure. The primary considerations were pressure cycles, temperature cycles, and confining pressure. The only slurry design tested in this investigation was SF samples. The reason is that SF samples were easier to mix consistently compared to the PP, BEN, or BENPP designs. Also, SF samples were preferred to NS samples due to their resistance of heat retrogression. It should be noted that samples underwent surface curing in 120^{o}F water for 26 hours prior to testing.

The first test involved two SF cement sheath samples connected to the flow lines. There was 0 psi confining pressure, constant temperature at 72^{o}F, and the samples were not immersed in hydraulic oil. They were exposed to cyclic casing pressure differentials of 2,000 and 10,000 psi. Neither sample exhibited signs of cracking or debonding after 50 pressure cycles.

Without the large pressure vessel, confining pressure could not be held constant at 6,000 psi. Instead, Sch. 40 PVC pipe was used to apply confining pressure according to its burst rating of 1,000 psi for 2 inch diameter pipe, as shown in **Figure 44** on the next page. Confining pressure was considered 1,000 psi, temperature constant at 72^{o}F, and the samples were not immersed in hydraulic oil. The two SF cement sheath samples were exposed to cyclic casing pressure differentials of 4,000 and 8,000 psi. Neither sample exhibited signs of cracking or debonding after 50 pressure cycles.

Figure 44: Sch. 40 PVC pipe confining pressure

Next, Sch. 80 PVC pipe was used to apply confining pressure. Its burst rating is 1,400 psi for 2.5 inch diameter pipe, somewhat higher than the Sch. 40 PVC pipe. Confining pressure was considered 1,400 psi, temperature constant at 72^{o}F, and the samples were not immersed in hydraulic oil. The two SF cement sheath samples were exposed to cyclic casing pressure differentials of 4,000 and 8,000 psi. Neither sample exhibited signs of cracking or debonding after 50 pressure cycles.

It was then decided to reduce the density of the cement from 16.4 ppg to 14.0 ppg by increasing the w/c ratio. The lower density cement was considerably weaker in compressive strength, therefore samples were expected to break more readily. 0 psi confining pressure was applied at 72^{o}F without immersion in hydraulic oil. The two SF samples were exposed to cyclic casing pressure differentials of 4,000 and 8,000 psi. Neither sample exhibited signs of cracking or debonding after 50 pressure cycles.

The process was repeated with 14.0 ppg SF samples and Sch. 80 PVC pipe. Confining pressure was considered 1,400 psi, temperature constant at 72^{o}F, and the samples were not immersed in hydraulic oil. The two SF cement sheath samples were exposed to cyclic casing pressure differentials of 8,000 and 10,000 psi. Neither sample exhibited signs of cracking or debonding after 50 pressure cycles.

At this time, it was realized that cement sheath samples would not break without the influence of temperature cycles. Two SF cement samples were prepared and placed in metal containers holding 72^{o}F hydraulic oil. The containers were placed in the oven and slowly heated to 250^{o}F over the next 90 minutes. Then, 20 minutes temperature cycles were applied, as shown in **Figure 45**. Each cycle included 10 minutes at 250^{o}F in the oven and 10 minutes in a bucket of water at 72^{o}F. The process was repeated every 20 minutes for 13 cycles, or about 4 hours. Both samples developed 1 severe radial crack, but did not debond.

Figure 45: Samples immersed in oil and water for temperature cycles

The final set of samples was exposed to temperature and pressure cycles simultaneously. Two SF cement sheath samples were prepared and placed in metal containers holding 72^{o}F hydraulic oil. The containers were placed in the oven and heated to 250^{o}F over the next 90 minutes. The samples were connected to the flow lines, as shown in **Figure 46**, and 5 pressure cycles were applied at pressure differentials of 4,000 and 8,000 psi. Afterwards, the samples were detached from the flow lines and placed in 72^{o}F water for 10 minutes. Once 10 minutes had passed, the samples were inspected for failure and reattached to the flow lines in the 250^{o}F hydraulic oil containers. After 10 minutes in the hot oil, the samples were exposed to pressure cycles again. Each round of 5 pressure cycles and 1 temperature cycle was called a super cycle, or S-cycle. The sample exposed to 4,000 psi differential failed after 3 S-cycles. The sample at 8,000 psi differential failed after 1 S-cycle. These results lead to the development of a new series of tests without confining pressure.

Figure 46: Samples connected to flow lines for S-cycles

Confining pressure, pressure differential, slurry density, and temperature cycles were the parameters modified between tests detailed in this section. The objective was to determine which parameters led to cyclic fatigue failure of the cement sheaths. Results, summarized in **Table 7**, indicate that temperature cycles were essential to this failure. Each batch of failed samples experienced temperature cycles, however it was not enough to only cycle temperature. The samples developed a radial crack, but did not debond. The combination of temperature and pressure cycles generated radial cracks and lead to severe debonding.

Table 7: Results of the parameter investigation

Confining Pressure (psi)	Pressure Differential (psi)	Density (ppg)	Temperature Cycles (Y or N)	Failure Observed (Y or N)
0	2,000	16.4	N	N
0	10,000	16.4	N	N
1,000	4,000	16.4	N	N
1,000	8,000	16.4	N	N
1,400	4,000	16.4	N	N
1,400	8,000	16.4	N	N
0	4,000	14.0	N	N
0	8,000	14.0	N	N
1,400	8,000	14.0	N	N
1,400	10,000	14.0	N	N
0	0	16.4	Y	Y
0	4,000	16.4	Y	Y
0	8,000	16.4	Y	Y

Modified Cyclic Fatigue

A new series of tests was conducted following the parameter investigation. All samples were cured underwater at 120^{o}F for 26 hours, then prepared for simultaneous temperature and pressure cycles. In each round of tests, two cement sheath samples were placed in separate metal containers holding 72^{o}F hydraulic oil. The containers were then placed in the oven and heated to 250^{o}F while the two samples were connected to their respective flow lines. There was 0 psi confining pressure.

The samples were exposed to 5 pressure cycles with a pressure differential of 9,000 psi. Each pressure cycle involved pressuring the flow line up to 9,000 psi for two minutes, then relieving the pressure to 0 psi for two minutes. Afterward 5 cycles, the samples were detached from the flow lines and placed in 72^{o}F water for 10 minutes. Once this time had passed, the samples were individually inspected for failure.

If the sample had experienced severe debonding, the test was considered complete. If not, the sample was reattached to its flow line within the 250^{o}F hydraulic oil container. After 10 minutes in the hot oil, the samples were exposed to pressure cycles again. Each round of 5 pressure cycles and 1 temperature cycle was called a super cycle, or S-cycle. The S-cycles were applied consistently for every sample tested. This means the 5 pressure to 1 temperature cycle ratio did not change, even if the sample had minor debonding and appeared on the verge of failure.

The number of cycles to failure was recorded using the data acquisition system. Pressure data for every sample can be found in **Appendix B**, however **Figure 47** shows the general concept behind the pressure data. Confining pressure was constant at 0 psi and was disregarded for these tests while the green line symbolizes pressure cycles. In the figure below, the sample was exposed to 3 S-cycles. This implies failure occurred after 15 pressure cycles and 3 temperature cycles were applied.

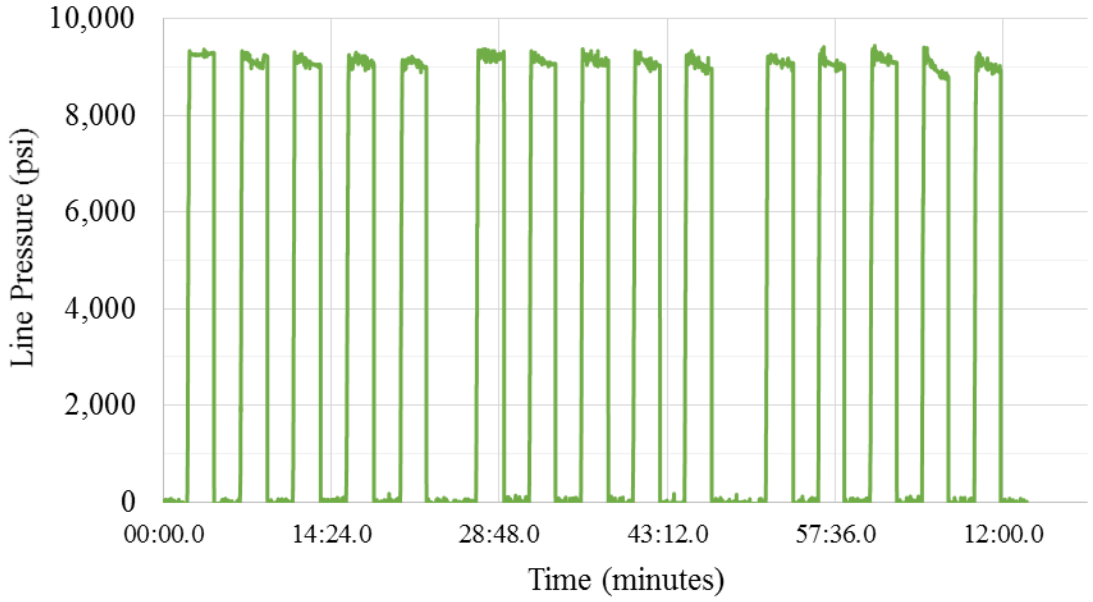

Figure 47: Modified cyclic fatigue pressure cycles

The NS slurry acted as a baseline slurry design which means the other four slurries were based off its mixture proportions. Due to strength retrogression caused by high temperature, the NS cement sheath samples performed poorly after wellbore curing. However, strength retrogression was not experienced here. The samples underwent surface curing and performed much better in cyclic fatigue.

Four samples were tested for the NS slurry design, all at 9,000 psi pressure differential. They first exhibited radial cracks after 2 S-cycles. Two samples failed after 3 S-cycles, the other two failed after 4 S-cycles. Results from the tests are shown in **Table 8** and **Figure 48**, found on the next page. The vertical lines on the bar chart represent the end of pressure cycles and initiation of a temperature cycle. It was also a checkpoint to look for cement sheath failure. **Figure 49**, found on the next page, shows the difference in pressure cycles at wellbore conditions versus the modified conditions.

Table 8: Modified cyclic fatigue results for NS slurry

Slurry ID	Sample ID	Cycles to Failure	Failure Type/Observations
NS	9-1	3S	• No changes at 1S • 1 severe radial crack, minor debonding at 2S • 1 large radial crack, severe debonding at 3S
	9-2	3S	• No changes at 1S • 1 minor radial crack at 2S • 2 minor radial cracks, severe debonding at 3S
	9-3	4S	• No changes at 1S • 1 severe radial crack, 2 minor radial cracks at 2S • 1 severe radial crack, 2 minor radial cracks, minor debonding at 3S • 1 severe radial crack, 2 minor radial cracks, severe debonding at 4S
	9-4	4S	• No changes at 1S • 1 severe radial crack at 2S • 1 severe radial crack, minor debonding at 3S • 1 severe radial crack, 1 minor radial crack, severe debonding at 4S

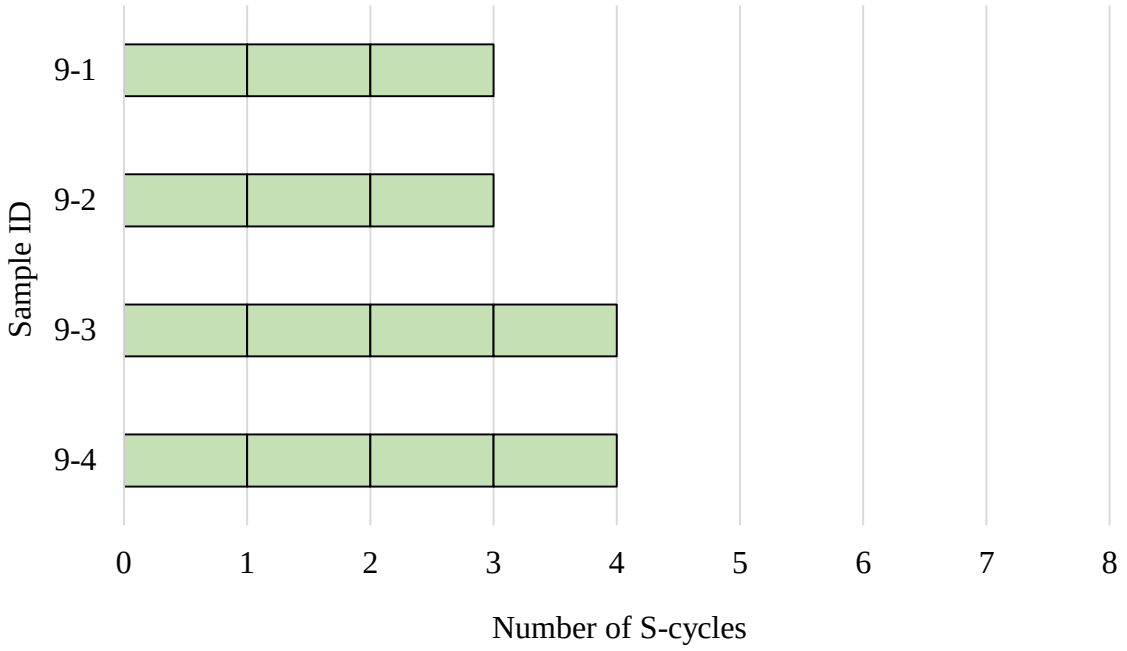

Figure 48: Bar chart for NS slurry

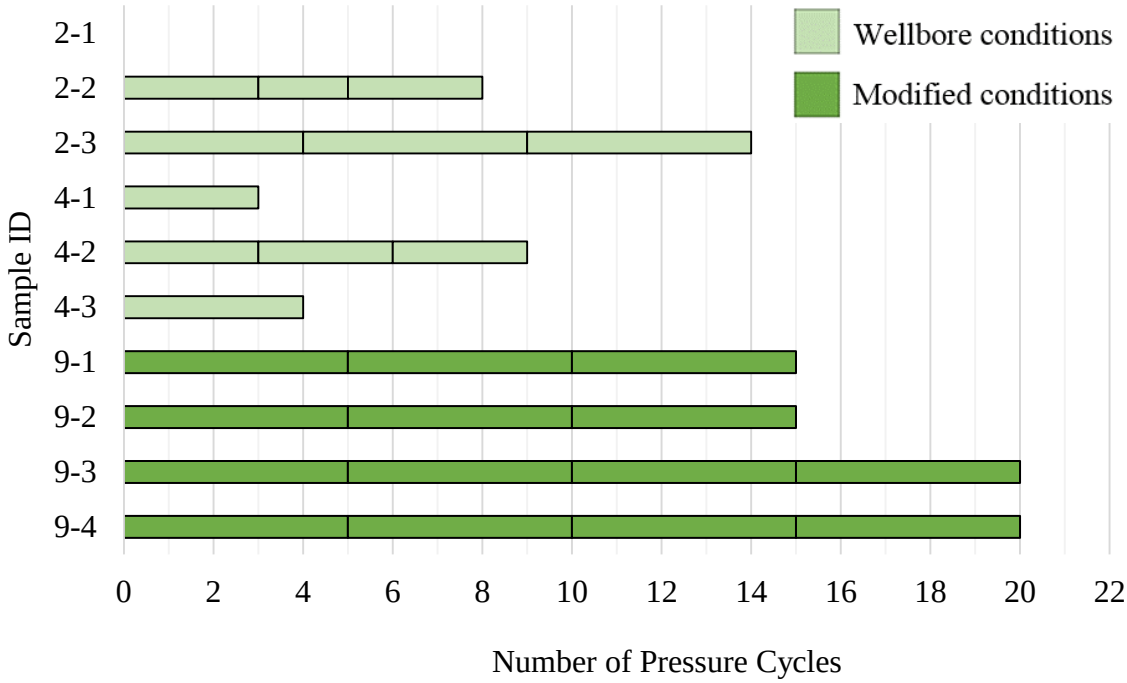

Figure 49: Bar chart for NS slurry at different confining conditions

Four samples were tested for the SF slurry design, all at 9,000 psi pressure differential. They typically first exhibited radial cracks after the first S-cycle. One sample failed after 1 S-cycle, one sample after 2 S-cycles, and the other two samples after 3 S-cycles. It was observed that three of the four samples failed severely in planes, as shown in **Figure 50**. Typically, the samples failed this way in the containers while still attached to the flow lines. The pieces were then removed at the end of the S-cycle.

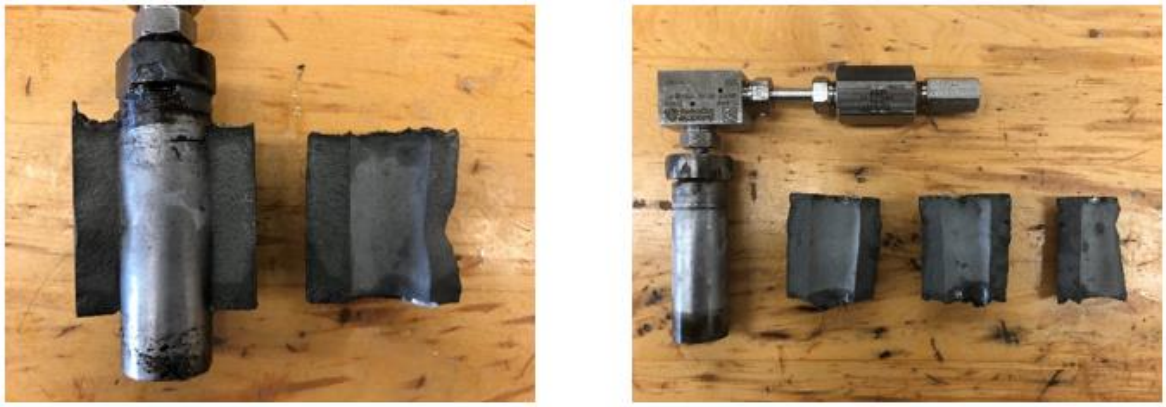

Figure 50: 1 plane, 2 point failure (left) and 2 plane, 3 point failure (right)

Results from the tests are shown in **Table 9** and **Figure 51**, found on the following pages. The vertical lines on the bar chart represent the end of pressure cycles and initiation of a temperature cycle. It was also a checkpoint to look for cement sheath failure. **Figure 52**, found on page 74, shows the difference in pressure cycles at wellbore conditions versus the modified conditions.

Table 9: Modified cyclic fatigue results for SF slurry

Slurry ID	Sample ID	Cycles to Failure	Failure Type/Observations
SF	9-1	1S	• 2 severe radial cracks, severe debonding at 1S • Severe failure (1 plane, 2 points)
	9-2	3S	• 1 severe radial crack at 1S • 1 severe radial crack, minor debonding at 2S • 1 severe radial crack, severe debonding at 3S
	9-3	3S	• 1 minor radial crack at 1S • 2 severe radial cracks at 2S • 2 severe radial cracks, severe debonding at 3S • Severe failure (1 plane, 2 points)
	9-4	2S	• No changes at 1S • 3 severe radial cracks, severe debonding at 2S • Severe failure (2 planes, 3 points)

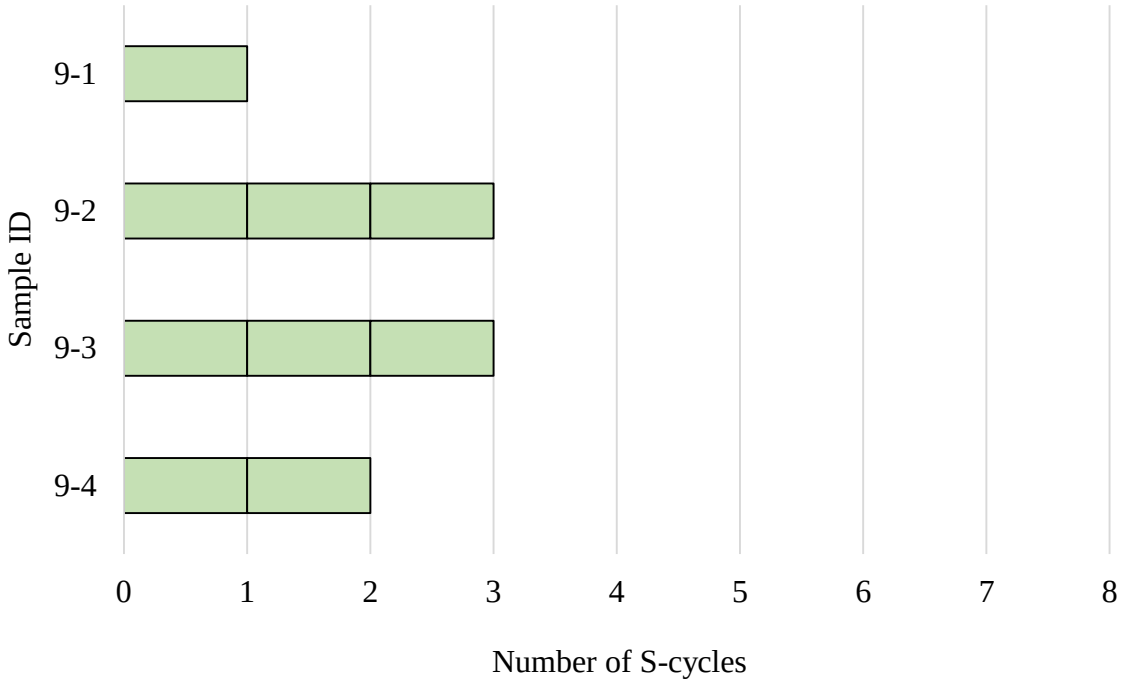

Figure 51: Bar chart for SF slurry

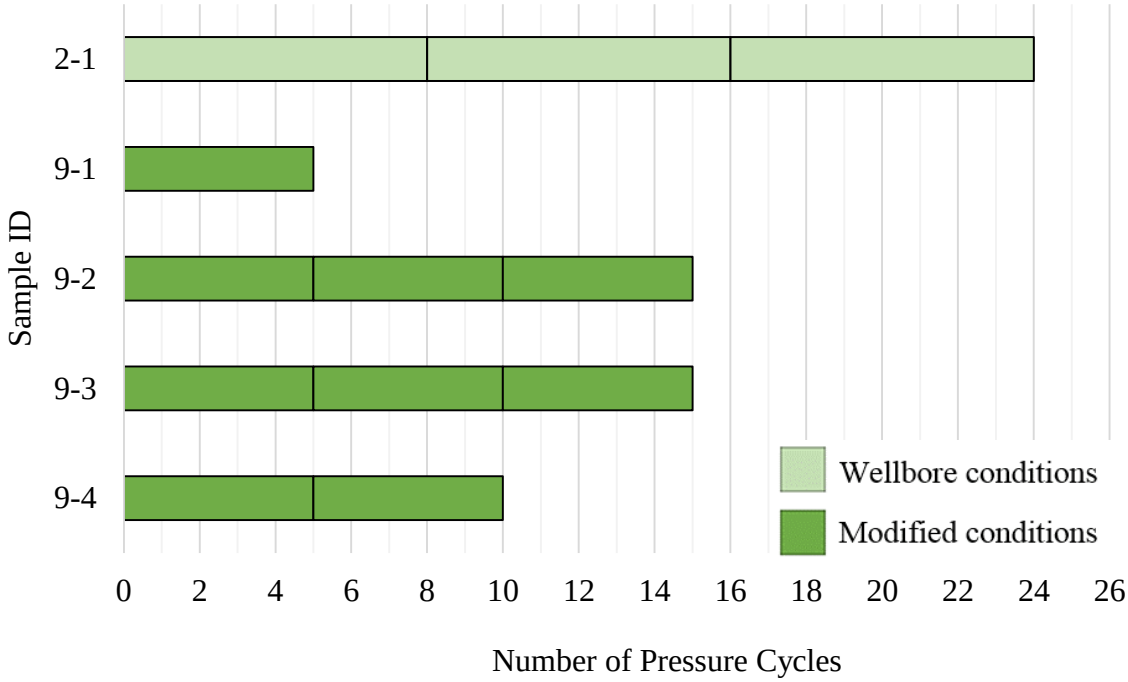

Figure 52: Bar chart for SF slurry at different confining conditions

Four samples were tested for the PP slurry design, all at 9,000 psi pressure differential. They typically first exhibited radial cracks after the second S-cycle. One sample failed after 5 S-cycles and the other three failed after 6 S-cycles. Results from the tests are shown in **Table 10** and **Figure 54**, found on the following pages. The vertical lines on the bar chart represent the end of pressure cycles and initiation of a temperature cycle. It was also a checkpoint to look for cement sheath failure.

The samples all displayed radial cracking, as shown in **Figure 53**, however they did not fail in planes. It appears that fiber reinforcement extended the fatigue life. **Figure 55**, found on page 77, shows the difference in pressure cycles between the SF and PP samples. The SF samples failed at 2-3 S-cycles while the PP samples failed at 5-6 S-cycles. The primary difference between the two slurry designs is the addition of 0.75% bvob polypropylene fibers. The addition of fibers lead to a change in density from 16.4 ppg to 16.0 ppg, but more importantly it extended the fatigue life of the cement sheath samples.

Figure 53: Radial cracking in PP cement sheaths

Table 10: Modified cyclic fatigue results for PP slurry

Slurry ID	Sample ID	Cycles to Failure	Failure Type/Observations
PP	9-1	6S	• No changes at 1S • 1 severe radial crack, 2 minor radial cracks at 2S, 3S, and 4S • 3 severe radial cracks, 1 minor radial crack at 5S • 3 severe radial cracks, 1 minor radial crack, severe debonding at 6S
	9-2	5S	• 1 minor radial crack at 1S • 1 severe radial crack, 2 minor radial cracks, 1 minor disk crack at 2S • 2 severe radial cracks, 1 minor radial crack, 1 minor disk crack at 3S • 2 severe radial cracks, 1 minor radial crack, 1 minor disk crack, minor debonding at 4S • 2 severe radial cracks, 1 minor radial crack, 1 minor disk crack, severe debonding at 5S
	9-3	6S	• 1 minor radial crack at 1S • 1 severe radial crack at 2S • 1 severe radial crack, 1 minor disk crack at 3S • 1 severe radial crack, 1 minor radial crack, 1 minor disk crack at 4S • 1 severe radial crack, 2 minor radial cracks, 1 minor disk crack, minor debonding at 5S • 1 severe radial crack, 2 minor radial cracks, 1 minor disk crack, severe debonding at 6S
	9-4	6S	• no changes at 1S, 2S, and 3S • 2 minor radial cracks at 4S • 3 minor radial cracks at 5S • 3 minor radial cracks, severe debonding at 6S

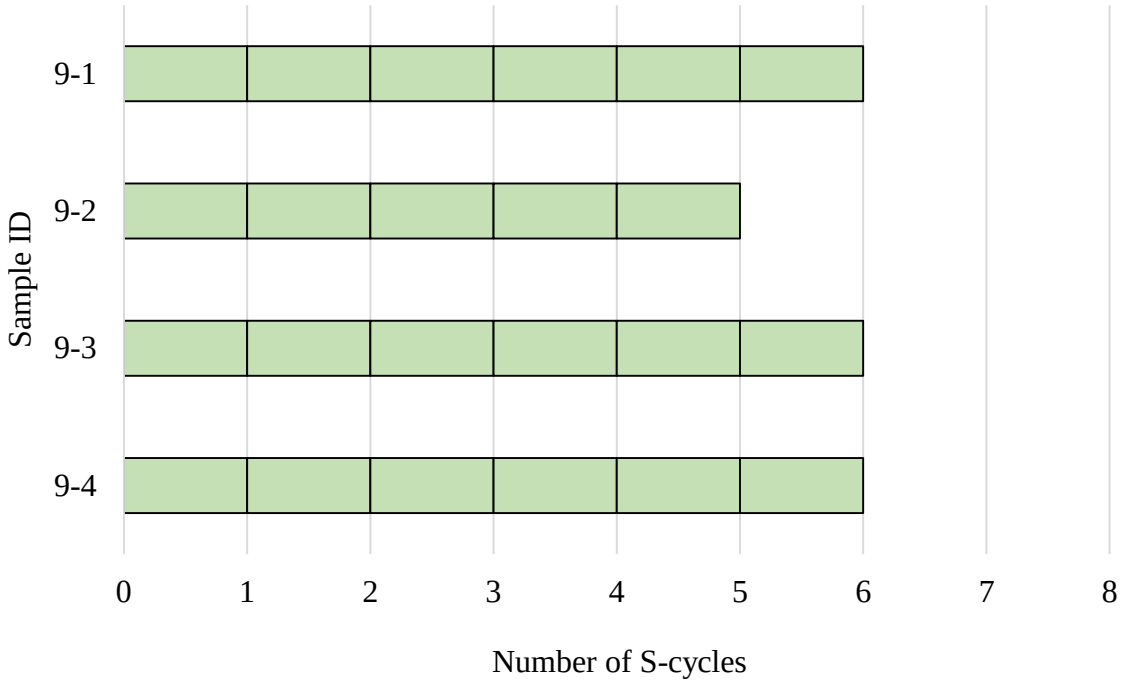

Figure 54: Bar chart for PP slurry

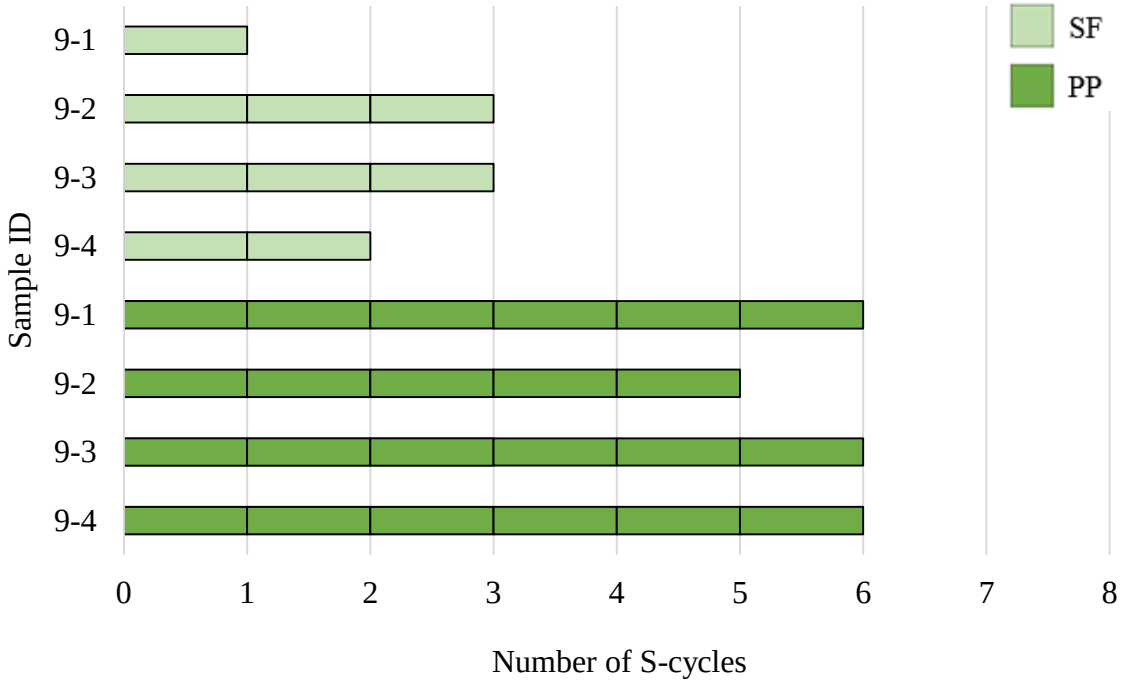

Figure 55: Bar chart for SF slurry vs. PP slurry

Four samples were tested for the BEN slurry design, all at 9,000 psi pressure differential. One sample, PP 9-4, was not considered for fatigue life analysis. After removal of its mold, the sample was observed to have a severe radial crack, as shown in **Figure 56**. The other three samples failed after 2-3 S-cycles. Two of the three samples did not exhibit radial cracks at any point during the test. The third sample developed a very minor radial crack after 2 S-cycles when it severely debonded. Results from the tests are shown in **Table 11** and **Figure 57**, found on the following page. The vertical lines on the bar chart represent the end of pressure cycles and initiation of a temperature cycle. It was also a checkpoint to look for cement sheath failure.

Figure 56: Bad sample, BEN 9-4

Table 11: Modified cyclic fatigue results for BEN slurry

Slurry ID	Sample ID	Cycles to Failure	Failure Type/Observations
BEN	9-1	3S	• No changes at 1S • Minor debonding at 2S • Severe debonding at 3S
	9-2	2S	• Minor debonding at 1S • 1 minor radial crack, severe debonding at 2S
	9-3	3S	• No changes at 1S • Minor debonding at 2S • Severe debonding at 3S
	9-4	n/a	• 1 severe radial crack at 0S following mold removal • 1 severe radial crack, severe debonding at 1S

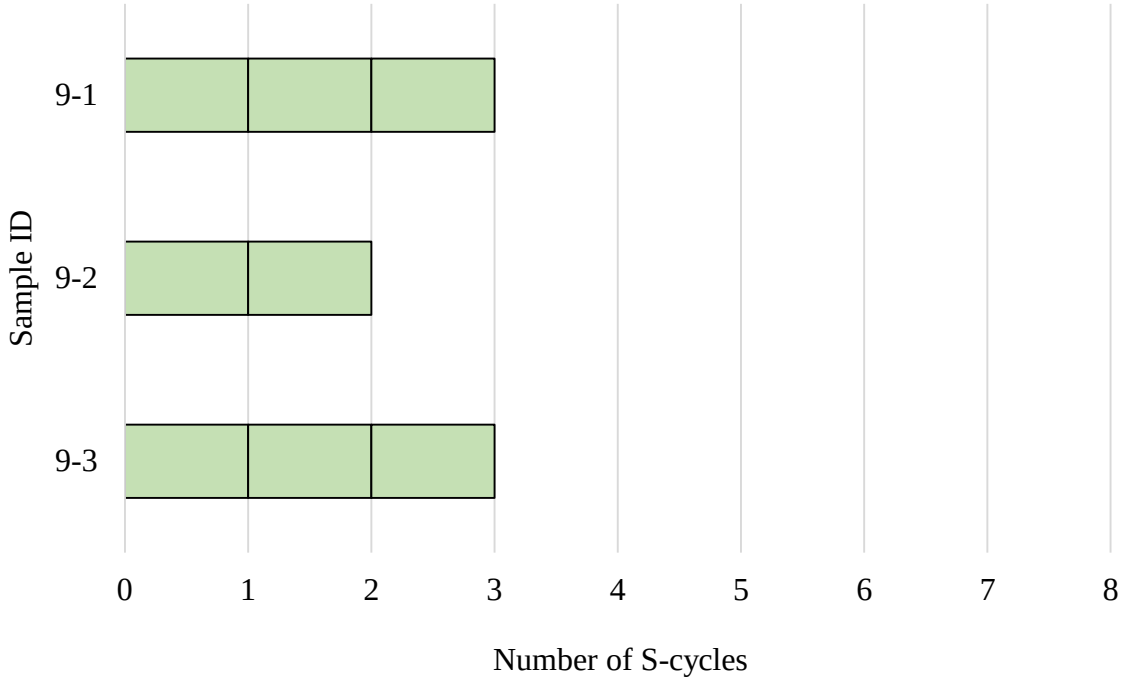

Figure 57: Bar chart for BEN slurry

Four samples were tested for the BENPP slurry design, all at 9,000 psi pressure differential. Three samples failed after 3 S-cycles and the fourth failed after 4 S-cycles. Results from the tests are shown in **Table 12** and **Figure 58**, found on the following page. The vertical lines on the bar chart represent the end of pressure cycles and initiation of a temperature cycle. It was also a checkpoint to look for cement sheath failure.

The samples did not display radial or disk cracks. Instead they showed minor debonding before failing after the next S-cycle in severe debonding. Fiber reinforcement did not significantly extend the fatigue life. **Figure 59**, found on the next page, shows the difference in pressure cycles between the BEN and BENPP samples. The BEN samples failed at 2-3 S-cycles while the BENPP samples failed at 3-4 S-cycles. The primary difference between the two slurry designs is the addition of 0.75% bvob polypropylene fibers.

Table 12: Modified cyclic fatigue results for BENPP slurry

Slurry ID	Sample ID	Cycles to Failure	Failure Type/Observations
BENPP	9-1	3S	• No changes at 1S • Minor debonding at 2S • Severe debonding at 3S
	9-2	3S	• No changes at 1S • Minor debonding at 2S • Severe debonding at 3S
	9-3	3S	• No changes at 1S and 2S • Severe debonding at 3S
	9-4	4S	• No changes at 1S and 2S • Minor debonding at 3S • Severe debonding at 4S

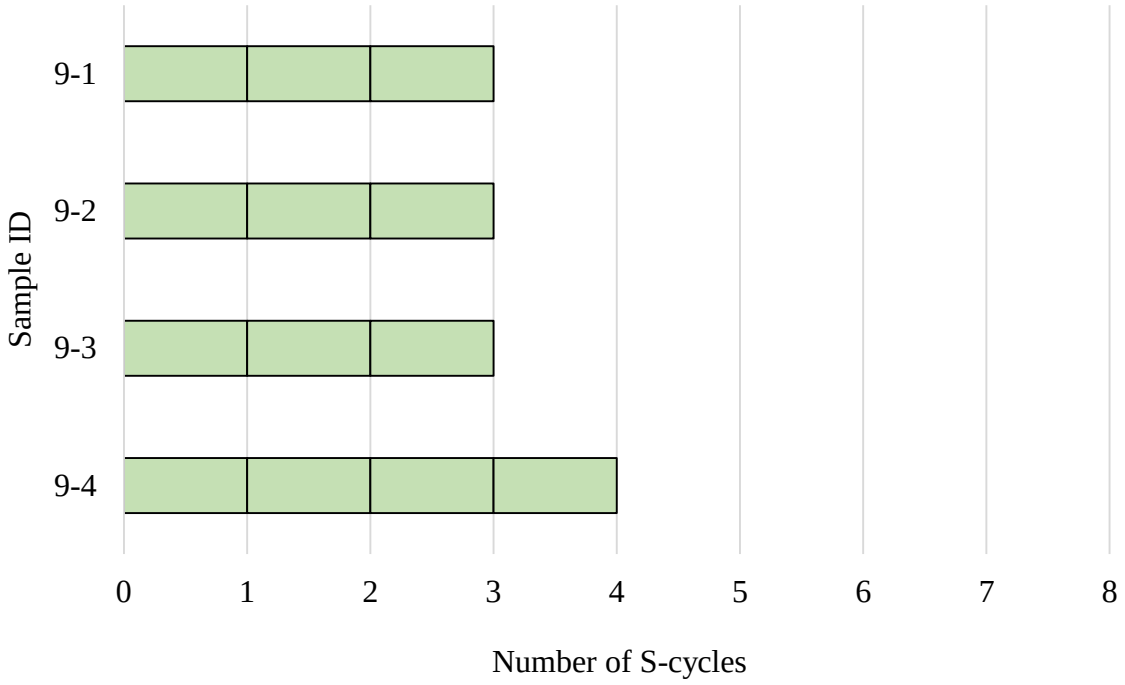

Figure 58: Bar chart for BENPP slurry

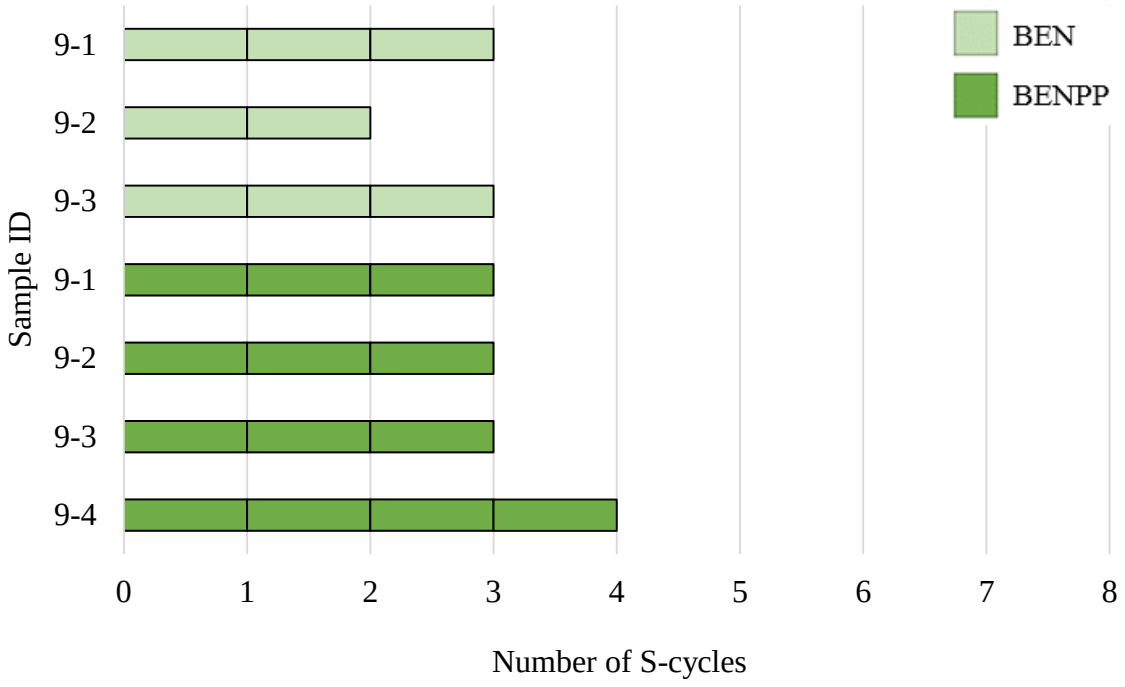

Figure 59: Bar chart for BEN slurry vs. BENPP slurry

Four BEN samples were contaminated with oil-based mud (OBM). A cuttings bed, commonly found in the lateral of unconventional wells, was created in the molds, as shown in **Figure 60**. In order to do this, OBM was mixed according to the design shown in **Table 13**. Diesel was used as the oil phase, bentonite as a weighting agent, and soap as an emulsifier. The oil-to-water ratio was 80:20 by volume. The placement process was straightforward. Popsicle sticks were set vertically in the mold and OBM was applied to the mold wall between the sticks. Space was left between the small pressure vessel and the cuttings bed to allow cement slurry to flow in-between them. As the cuttings bed grew larger, slurry was added to the other side of the mold. Once its level reached the top, the sticks were removed and the sample was placed in the surface curing tank at 120^{o}F for 26 hours.

Figure 60: Mixing and placing OBM into BEN cement molds

Table 13: Mass of mixture components for OBM

Mass of Components (g)				Batch Volume (mL)
Diesel	Water	Bentonite	Soap	
150.00	50.00	300.00	10.00	355

After 26 hours had passed, the samples were carefully removed from the curing tank and demolded. The cuttings bed for all four samples was poorly bonded with the hardened cement. Effort was required to ensure the two pieces did not separate prior to testing. **Figure 61** shows how a cuttings bed was attached to the cement sheath sample prior to testing. Once exposed to high temperature and hydraulic oil, the cuttings bed dissolved and separated from the cement sheath.

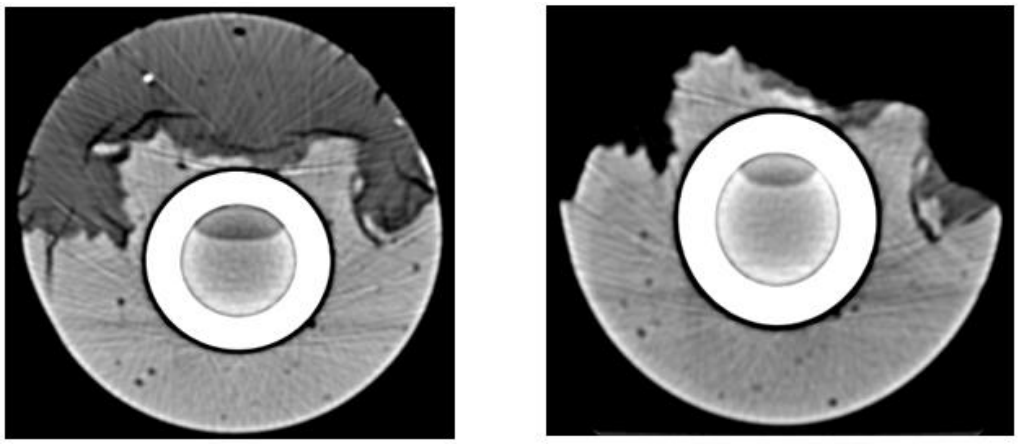

Figure 61: OBM sample pre-test (left) and post-test (right)

The samples were exposed to cyclic fatigue at a 9,000 psi pressure differential. Two samples, badly damaged upon removal of the molds, debonded after 1 S-cycle. The other two samples were in better shape and failed after 3 S-cycles. Results from the tests are shown in **Table 14** and **Figure 62**, found on the following pages. The vertical lines on the bar chart represent the end of pressure cycles and initiation of a temperature cycle. It was also a checkpoint to look for cement sheath failure.

The samples did not display obvious radial or disk cracks. Instead they showed minor debonding before failing after the next S-cycle in severe debonding. **Figure 63**, found on the next page, shows the similarity in pressure cycles between the BEN and OBM samples. Both sets failed at 2-3 S-cycles if the OBM sample was not damaged following the curing process.

Table 14: Modified cyclic fatigue results for BEN slurry contaminated with OBM

Slurry ID	Sample ID	Cycles to Failure	Failure Type/Observations
OBM	9-1	3S	• Good form at 0S • No changes at 1S and 2S • Severe debonding at 3S
	9-2	1S	• Badly damaged at 0S • Severe failure (1 plane, 2 points) at 0S • Severe debonding at 1S
	9-3	3S	• Good form at 0S • No changes at 1S and 2S • Severe debonding at 3S
	9-4	1S	• Badly damaged at 0S • Severe failure (1 plane, 2 points) at 0S • Severe debonding at 1S

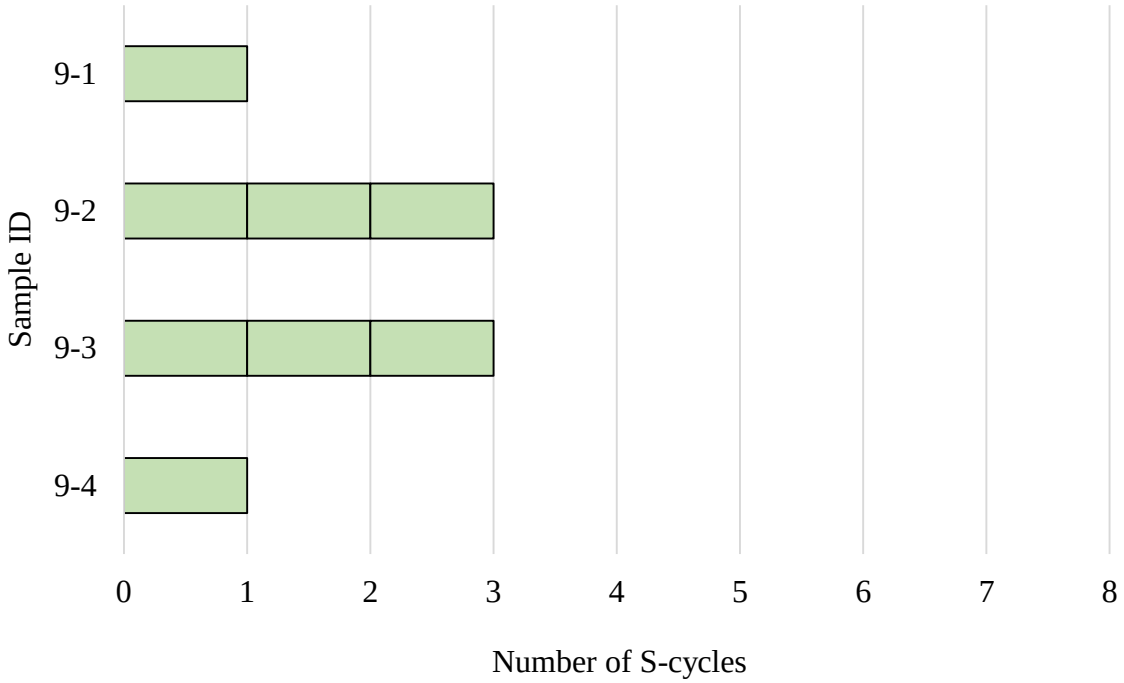

Figure 62: Bar chart for BEN slurry contaminated with OBM

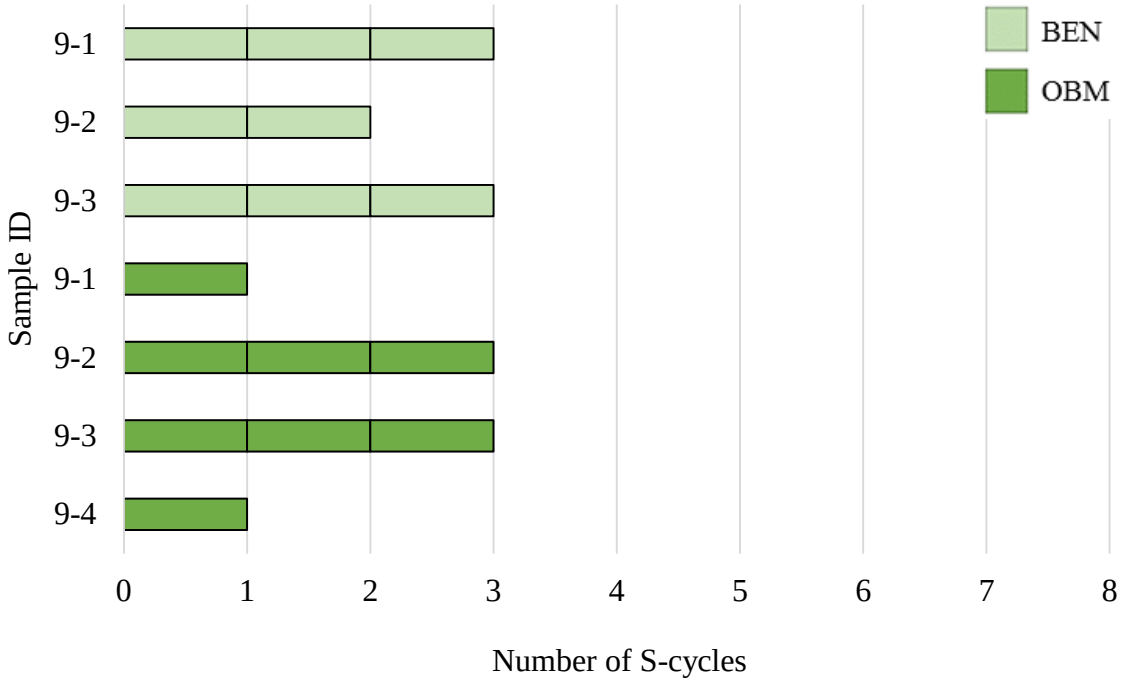

Figure 63: Bar chart for BEN slurry vs. OBM-contaminated slurry

CT Images

The objective of the CT images was to observe crack initiation and propagation during cyclic pressure and temperature tests. Samples were scanned following the curing process before the cyclic test started, then in-between rounds of cyclic fatigue, and finally once the sample had failed. An image processing program, ImageJ, was used to organize the image sequences.

Identification of mature cracks was successful because images showed major cracks within the cement sheath sample. Both radial and disk cracks could be viewed in the CT scans. However, there were limitations since debonding failure and crack propagation was not clearly observed. Mature cracks, as shown in **Figure 64**, were identified without difficulty, but significant time and effort was placed into finding small cracks that would propagate with continued fatigue testing This objective was not fulfilled.

Figure 64: Types of failure - radial crack (left), disk crack (center), debonding (right)

Figure 65 shows the same cross-section from one sample, identified by its unique pore spaces. Before cyclic testing, there were no cracks. After the test, a severe radial crack was visually observed which is shown here. **Figure 66** shows four images out of the image sequence for one cement sheath. The images display how a radial crack extends throughout the length of the sample.

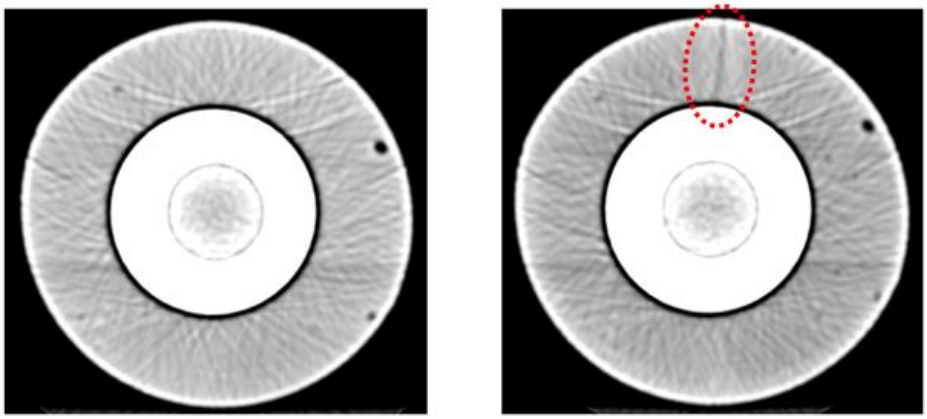

Figure 65: Cement sheath before (left) and after (right) radial crack development

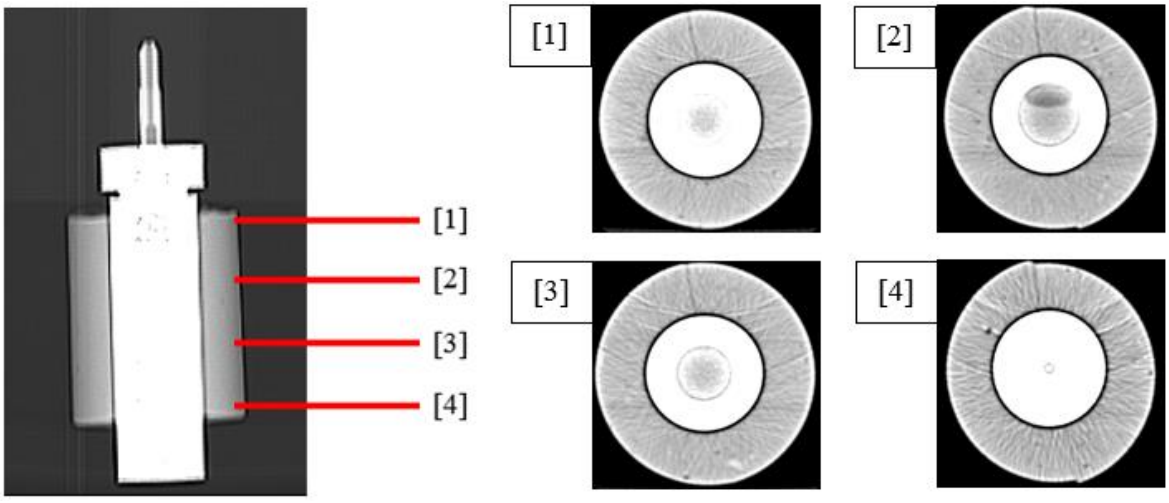

Figure 66: Single radial crack through four cross sections of a cement sheath

Disk cracks were rare compared to radial cracks and debonding. Disking was observed in NS and SF cement sheaths tested at wellbore conditions. It was also seen at modified conditions, but exclusively in PP samples. The cracks in PP samples typically propagated through the cement sheath to connect two or three radial cracks. The best CT image showing a disk crack can be observed in **Figure 67.**

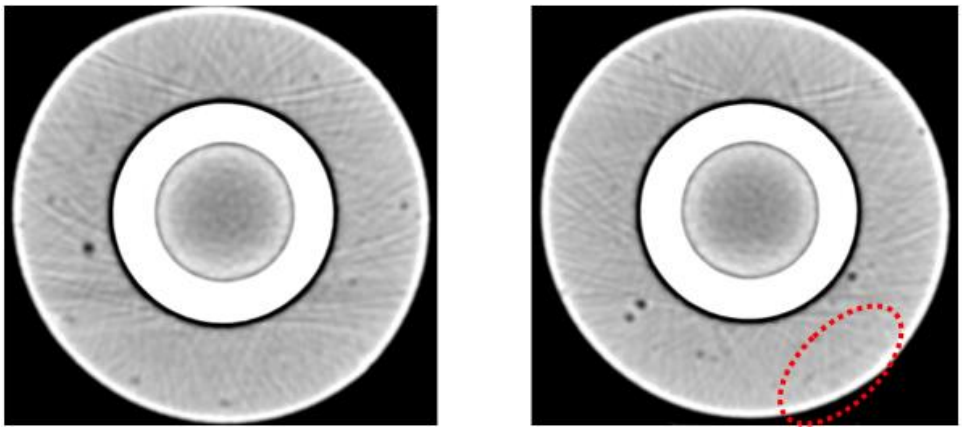

Figure 67: Cement sheath without (left) and with (right) disk crack

Cyclic tests were stopped once the cement sheath severely debonded from the small pressure vessel. At modified conditions, NS, SF, and PP samples typically exhibited radial or disk cracks before failing. BEN and BENPP samples did not, and the CT scans for these samples failed to provide insight into their failure mechanism. Debonding failure, as shown in **Figure 68** on the next page, is not observable in the CT images. The two images are of the same sample at different locations. The cement sheath in the second image (right) is not surrounding the small pressure vessel which implies debonding has occurred. The first image (left) does not show signs of severe debonding failure.

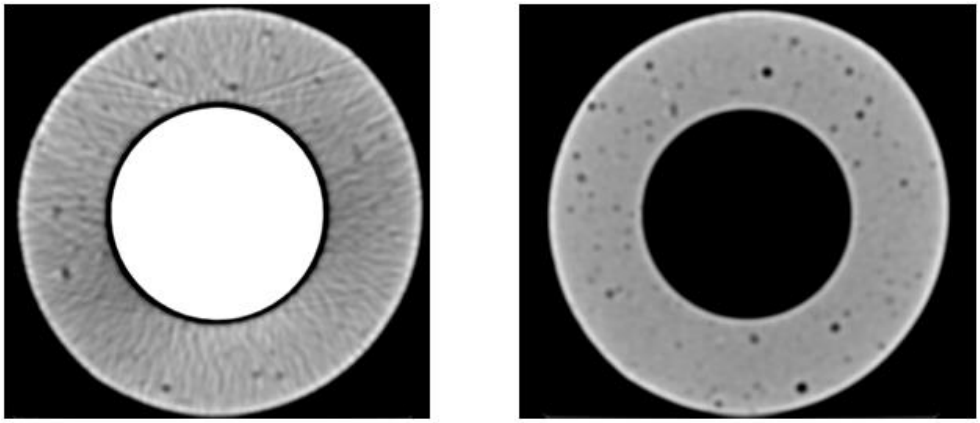

Figure 68: Images from one debonded sample

In addition to cracks, the CT scans showed large pore spaces in the cement sheath. It was observed that NS, SF, and BEN samples contained significantly smaller and fewer pore spaces than samples reinforced with polypropylene fibers such as PP and BENPP, as shown in **Figure 69**. The addition of fibers greatly reduced workability so this observation is not unexpected. The fibers themselves were too small to be observed.

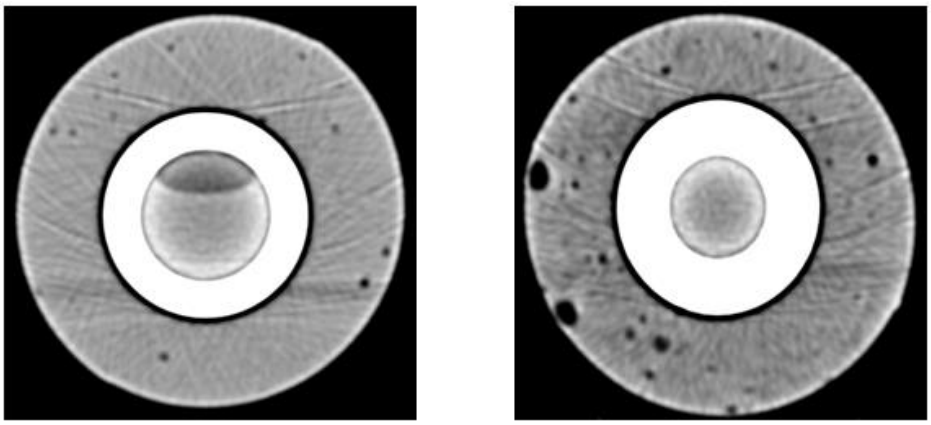

Figure 69: Pore space of BEN (left) and BENPP (right) samples

CHAPTER V

CONCLUSIONS

Discussion of Results

- An experiment was designed and built based off the Shadravan and Johns experimental set-up. They used a Model 7600 Ultra HPHT Viscometer to generate the pressure and temperature of wellbore conditions and log pressure data. Here, two Enerpac hand pumps, a roller oven, and DAQami software program was used. The new set-up ran several successful tests at wellbore conditions prior to equipment failure.

- NS samples displayed signs of strength retrogression. When the samples were removed from wellbore curing, a white foam was observed seeping out of radial cracks in the cement matrix. One explanation is that calcium hydroxide dissolved into solution at high temperature and pressure, whether in the confining hydraulic oil or just in the cement pore spaces. Then, rapid cooling upon removal from the large pressure vessel caused the calcium hydroxide ions to crystalize. Crystallization expelled the calcium hydroxide foam from the cracks. This behavior was not observed in samples containing 35% bwoc silica flour.

- Between 10 and 18 cube samples were prepared for each slurry design and tested in compression. The NS samples had an average compressive strength of 2,500 psi. The SF samples were weaker at 1,920 psi. The PP, BEN, and BENPP samples were even

weaker at 1,500, 370, and 460 psi, respectively. The results indicate that adding polypropylene fibers does not necessarily increase compressive strength. The BENPP samples were stronger than the BEN samples, however the PP samples were weaker than the SF samples. It is also interesting to note that 5% bwow $CaCl_2$ was added to neat slurry as an accelerator. The cubes from this batch broke at over 4,000 psi in 24 hours.

- Tests were conducted on two slurries, NS and SF, at wellbore conditions. The NS samples failed after 8 – 14 cycles at 2,000 psi differential. They failed at 3-9 cycles at 4,000 psi differential. A single SF sample was tested at wellbore conditions. It failed after 24 cycles at 2,000 psi differential.

- Equipment failure occurred unexpectedly after curing the SF 2-2 sample. The vessel cap became stuck in the large pressure vessel and could not be removed. The equipment was taken to a metal-works shop where they machined the cap out. They built a new cap and repaired the threads in the large pressure vessel. The equipment was returned as good as new and worked well.

- A parameter investigation was conducted to identify what conditions led to cement sheath failure. Failure was not observed from pressure cycles alone. Temperature cycles were essential to generating cracks and debonding in the cement sheaths. A modified experiment was developed without wellbore confining pressure. The

method introduced S-cycles which combine 5 pressure cycles with 1 temperature cycle simultaneously.

- Five different well cements were tested using the modified experiment. All samples were exposed to 9,000 psi pressure differential and 72 – 250^{o}F temperature changes.

    - The NS samples failed after 3 – 4 S-cycles and exhibited severe radial cracking and debonding.

    - The SF samples failed after 1 – 3 S-cycles which was surprising. The SF samples were expected to have a higher fatigue limit than the NS samples. However, the SF samples exhibited severe radial cracking and debonding which lead to major plane failure. This behavior, major plane failure, was not observed in any of the other slurry designs.

    - The PP samples failed after 5 – 6 S-cycles and exhibited severe radial cracking and debonding. Despite the cracks, the samples did not debond right away. The polypropylene fibers greatly improved the fatigue life when compared to the SF samples. The SF and PP slurry designs were almost identical, just the PP slurry had 0.75% bvob fiber addition.

    - The BEN samples failed after 2 – 3 S-cycles. The samples were observed to be highly ductile and did not generate cracks during the fatigue test. However,

they failed by debonding. This would suggest the samples deformed during high temperature and pressure cycles. When the casing contracted, the sample remained deformed and therefore debonded from the casing.

- The BENPP samples failed after 3 – 4 S-cycles. The samples were highly ductile and did not generate cracks during the fatigue test. They failed by debonding. Again, this suggests the samples deformed during the high temperature and pressure cycles, but debonded when the casing contracted. It is unclear whether the polypropylene fibers improved the fatigue life of the BENPP samples compared to the BEN samples. They did slightly on average, but realistically the performance was about the same.

- BEN slurry was contaminated with a cuttings bed to imitate a horizontal wellbore. Oil-based mud was produced using diesel as the continuous phase (80:20 oil-to-water volume ratio), bentonite as the weighting agent, and soap as an emulsifier. The samples were subjected to the modified cyclic fatigue test. Results show the cement sheaths exhibited performance similar to BEN samples without OBM contamination. However, the equal performance occurred only when the OBM samples were not badly damaged following curing and demolding. If the samples were damaged, they failed after the first S-cycle.

- The CT scanner could clearly show mature radial and disk cracks, but not debonding. A significant gap between the small pressure vessel and a debonded cement sheath was never observed. Additionally, crack initiation and propagation was not identified. Substantial time and effort was taken to find cracks that propagated axially along the cement sheath or radially through the cement sheath, however a small crack was not shown to grow larger with more pressure cycles. The process is assumed to occur very quickly, within one S-cycle, so only a more mature crack could be observed.

Recommendations for Future Work

- The most obvious recommendation is to finish testing the slurries batched in this research at wellbore conditions. The modified testing procedure had severe shortcomings. The samples were not cured at wellbore conditions, nor was testing carried out at wellbore confining pressure. The NS slurry does not outperform the SF slurry at wellbore conditions, as it did with the modified conditions. This outcome was observed prior to the equipment failure, as well as with Shadravan's results. It remains unknown whether polypropylene fibers would increase the fatigue life at wellbore testing conditions.

- The two vessel system was designed for Shadravan's experiments at HPHT conditions. These conditions included pressures between 10,000 to 20,000 psi and over 300^{o}F. It is possible that radial expansion/contraction of the small pressure vessels is too small at 10,000 psi internal pressure. The vessels do not deform enough to break their respective cement sheaths. Evidence for this concern originates from the parameter investigation and how the cement only failed when temperature cycles were introduced. An experiment could be conducted to reduce the OD, or increase the ID, of some of the small pressure vessels. This work could be done at the same metal-works shop that repaired the large pressure vessel. A reduced wall thickness would lead to more expansion and contraction from pressure opposed to temperature.

- The possibilities for changing the slurry design are limitless. An experiment could be conducted on slurries at a wider range of densities. The addition of polypropylene fibers greatly increased the fatigue life of the 16.4 ppg SF slurry, however it did not affect the fatigue life of the 14.0 ppg BEN slurry. An investigation could be conducted to find whether it was the change in density, the addition of bentonite, or something else that led to these results. The density cut-off point where fiber addition is beneficial could be studied. However, this is just one possibility. There are hundreds of different additives available in the cementing and concrete industry. Latex, foamed cement, fluid-loss additives, and other types of fibers could be incorporated in the slurry design and tested.

- The experimental set-up provides a way to cure and test cement sheaths at various pressure and temperature combinations. The temperature could be held constant while changing the confining pressure from one batch to another and vice versa. More practically, the wellbore conditions for different reservoirs around the world could be mimicked while testing the same slurry design. Then, modifications could be made to the slurry design for each reservoir to improve its fatigue life.

- The curing conditions could be modified to have a pressure differential during the curing process. Instead of setting the confining pressure equal to the casing pressure, it could be increased or decreased to observe changes in performance. This would correlate to the rig applying annular backpressure during the curing process or running a casing integrity test too soon after placement.

REFERENCES

Berndt, M., Philippacopoulos, A. (2002, December 1). Incorporation of Fibres in Geothermal Well Cements. Geothermics. 31. 643-656. 10.1016/S0375-6505(02)00028-7.

Bois, A.-P., Garnier, A., Galdiolo, G., & Laudet, J.-B. (2012, June 1). Use of a Mechanistic Model to Forecast Cement-Sheath Integrity. Society of Petroleum Engineers. doi:10.2118/139668-PA

Boukhelifa, L., Moroni, N., James, S. G., Le Roy-Delage, S., Thiercelin, M. J., & Lemaire, G. (2004, January 1). Evaluation of Cement Systems for Oil and Gas Well Zonal Isolation in a Full-Scale Annular Geometry. Society of Petroleum Engineers. doi:10.2118/87195-MS

Bourgoyne, A. T., Scott, S. L., & Regg, J. B. (1999, January 1). Sustained Casing Pressure in Offshore Producing Wells. Offshore Technology Conference. doi:10.4043/11029-MS

Carter, G., & Smith, D. K. (1958, January 1). Properties of Cementing Compositions at Elevated Temperatures and Pressure. Society of Petroleum Engineers.

Cementing Services. (2015). Retrieved March 14, 2018, from http://www.scmdaleel.com/category/cementing-services/91

Goodwin, K. J., & Crook, R. J. (1992, December 1). Cement Sheath Stress Failure. Society of Petroleum Engineers. doi:10.2118/20453-PA

Ingraffea, A. R., Wells, M. T., Santoro, R. L., & Shonkoff, S. B. (2014, July 29). Assessment and Risk Analysis of Casing and Cement Impairment in Oil and Gas Wells in Pennsylvania, 2000–2012. Retrieved March 22, 2018, from http://www.pnas.org/content/111/30/10955

Jackson, P. B., & Murphey, C. E. (1993, January 1). Effect of Casing Pressure on Gas Flow Through a Sheath of Set Cement. Society of Petroleum Engineers. doi:10.2118/25698-MS

Johns, A.W. (2014). Cyclic Loading of Fiber-Containing Cement Sheaths in HPHT Conditions. Master of Science, Texas A&M University, College Station, Texas.

Kosinowski, C., & Teodoriu, C. (2012, January 1). Study of Class G Cement Fatigue Using Experimental Investigations. Society of Petroleum Engineers. doi:10.2118/153008-MS

Nelson, E. B., & Guillot, D. (Eds.). (2006). Well Cementing (2nd ed.). Sugar Land, TX: Schlumberger.

Newman, K., & Wojtanowicx, A. (2001, September 22). Improving Gas Well Cementing Through Cement Pulsation (Tech. No. 6011). Retrieved March 7, 2018, from CTES, L.C. website: http://www.athenaeng.com/Content/publications/1999_2001_GRI_Cement_Pulsation_Project_Report.pdf

Rapier, R. (2017, July 3). Oil And Natural Gas Demand Set Records While Coal Slumps. Forbes Business / Energy. Retrieved March 15, 2018, from https://www.forbes.com/sites/rrapier/2017/07/03/oil-and-natural-gas-demand-set-records-while-coal-slumps/#1018a4c8590b

Shadravan, A. (2013). A Method for Cement Integrity Evaluation in Unconventional Wells. Master of Science, Texas A & M University, College Station, Texas.

Shadravan, A., Schubert, J., Amani, M., & Teodoriu, C. (2014, March 17). HPHT Cement Sheath Integrity Evaluation Method for Unconventional Wells. Society of Petroleum Engineers. doi:10.2118/168321-MS

Shadravan, A., Schubert, J., Amani, M., & Teodoriu, C. (2015, March 1). Using Fatigue-Failure Envelope for Cement-Sheath-Integrity Evaluation. Society of Petroleum Engineers. doi:10.2118/168321-PA

Tinsley, J. M., Miller, E. C., Sabins, F. L., & Sutton, D. L. (1980, August 1). Study of Factors Causing Annular Gas Flow Following Primary Cementing. Society of Petroleum Engineers. doi:10.2118/8257-PA

Total Energy Consumption. (2017). Retrieved March 13, 2018, from https://yearbook.enerdata.net/total-energy/world-consumption-statistics.html

Ugwu, I.O. (2008). Cement Fatigue and HPHT Well Integrity with Application to Life of Well Prediction. Master of Science, Texas A&M University, College Station, Texas.

United States, Energy Information Administration, Independent Statistics and Analysis. (2018, March 8). How Much Shale (tight) Oil Is Produced in the United States? Retrieved March 18, 2018, from https://www.eia.gov/tools/faqs/faq.php?id=847&t=6

Watson, T. L., & Bacchu, S. (2009, March 1). Evaluation of the Potential for Gas and CO2 Leakage Along Wellbores. Society of Petroleum Engineers. doi:10.2118/106817-PA

APPENDIX A

STANDARD OPERATING PROCEDURES

Appendix A details the equipment, materials, and steps used in this research. All procedures were followed as closely as possible to standardize the tests, maintain controlled variables, and isolate independent variables. Notes and recommendations are based off the author's experience running the tests. This appendix is meant to assist future researchers who aspire to continue cementing research using similar equipment as the author.

The necessary equipment and materials are listed for each procedure along with personal protective equipment and potential hazards. Notes, recommendations, and pictures offer further insight into the author's methods. All procedures were written based off API recommended practices, ASTM standards, instruction manuals, and past research theses.

Table A.1: Mold preparation

Equipment:	cube mold paint brush PVC pipe mold small pressure vessel wire brush ½" plywood molding board with 1" OD holes ½" plywood retaining board
PPE:	plastic or rubber gloves – handle the acetone safety glasses – repel acetone splash, repel dust particles
Materials:	acetone solvent form release agent packaging tape sandpaper silicone
Procedures:	1. Bolt the two plywood boards together and tighten the wing nuts. Ensure the molding board is on top. 2. Clean the small pressure vessel using acetone, wire brush, and sandpaper Then fully dry it. 3. Apply a small amount of silicone to the bottom ½" of the vessel and insert it into one hole of the molding board. 4. Twist the vessel in place, then use a paper towel to remove any silicone attached to the vessel that is visible above the plywood board. 5. Use the packaging tape to connect two halves of the PVC pipe mold. Centralize the mold into position over the 1" OD hole of the molding board. 6. Liberally apply silicone to the exterior surface of the mold where it contacts the molding board. **Note:** low density cement slurry will leak through the base of the mold if not properly sealed. **7.** Allow the silicone to cure at room temperature for 24 hours before adding cement slurry. **Note:** the silicone is water resistant after 30 minutes, however it is recommended to wait the full 24 hours to achieve the most effective seal. 8. Assemble the cube mold using the provided bolts and wing nuts. Apply one spray of form release agent per cube and evenly coat the surface using the paint brush

References:	A Method for Cement Integrity Evaluation in Unconventional Wells. (Shadravan, 2013) Cyclic Loading of Fiber-Containing Cement Sheaths in HPHT Conditions. (Johns, 2014)

Figure A.1: Cement sheath sample preparation

Figure A.2: Cement cube sample preparation

Table A.2: Mixing

Equipment:	electric blender (1-Liter capacity, blade-type, capable of 4,000 and 12,000 rpm) – OFITE 120-60 Model 115V electronic balance – Mettler Toledo PB 3002-L funnel small bucket spatula
PPE:	plastic or rubber gloves – handle the slurry and admixtures respirator mask – repel dust particles (particularly silica flour or silica fume) safety glasses – repel slurry splash, repel dust particles
Materials:	cement chemical admixtures mineral admixtures tap water
Procedures:	1. Use the balance to weigh cement and dry admixtures according to the slurry design. Add to the fully dry small bucket. Blend the components thoroughly and uniformly with spatula. 2. Use the balance to weight mix water and wet admixtures according to the slurry design. Add to the surface-saturated dry blender container. Stir the components with the spatula. **Note:** surface-saturated dry (SSD) is defined as the condition of a material in which the surfaces are dry but the inter-particle voids are saturated with water. **Recommend:** use a water-moist paint brush to wet the entire surface, then a paper towel to remove any pooling or visible collection. This achieves SSD. 3. Place the blender container which holds the mix water and wet admixtures on the blender base. Turn the blender on to 4,000 ± 250 rpm using the variable speed option. **Note:** the blender and display must turn on together. The blender speed on the blender base must be set to high, then flip the display switch on and adjust the blade speed using the variable dial. **Note:** the display shows the speed of the blade. On the model 120-60 for cement testing, the displayed value is multiplied by 10 to determine the actual rpm of the blade. For example, 400 * 10 = 4,000 rpm and 1,200 *

	10 = 12,000 rpm. The display should show 400 or 1,200 while mixing. 4. Use the funnel to add the cement and dry additives to the blender container in 15 seconds or less. Then place the cover on the mixing container and continue mixing at 12,000 ± 250 rpm for 35 seconds. 5. Turn off the blender and remove the blender container from the base. 6. Consider the cement slurry in the blender container. Hand mixing with the spatula may be needed.
References:	API RB 10B-2, 2nd Edition, 2013 OFITE Model 20 Instruction Manual

Figure A.3: Cement mixing set-up

Figure A.4: Control box

Figure A.5: Blender base

Table A.3: Placement

Equipment:	cube mold paint brush puddling rod (0.25” OD) PVC pipe mold spatula small pressure vessel strike-off bar ½” plywood molding board with 1” OD holes ½” plywood retaining board
PPE:	plastic or rubber gloves – handle the slurry and admixtures safety glasses – repel slurry splash, repel dust particles
Materials:	cement slurry mold release agent tap water
Procedures:	Procedure for cement sheath mold: 1. Pour cement slurry into the mold until the level is half of the desired sample height. **Note:** take care not to spill slurry onto the top of the small pressure vessel. If it happens, use a paper towel to clean the surface of slurry. 2. Puddle the sample with a puddling rod 20 times, but do not forcibly strike the molding board. Then lightly tap the sides of the PVC mold 10 times. **Note:** the objective is to remove a majority of air bubbles. 3. Stir the remaining slurry with the spatula to ensure the slurry is uniform. Then fill the mold until slightly above the desired sample height. 4. Puddle the sample and tap the sides of the PVC mold as before. Ensure the top of the sample is as close to level as possible. More vibration may be needed. Procedure for cube mold: 1. Use the paint brush to coat mold release agent to the interior faces of the mold. Use a paper towel to remove any pooling or excessive collection. 2. Pour cement slurry into the mold to approximately ½ the height of the 2 inch tall retaining well. 3. Puddle the sample with a puddling rod 20 times, but do not forcibly strike the base of the mold. Then lightly tap the sides 10 times.

	Note: the objective is to remove a majority of air bubbles. 4. Stir the remaining slurry with the spatula to ensure the slurry is uniform. Then fill the mold until slightly above the 2 inch mark. 5. Puddle the sample and tap the sides of the mold as before. Then, strike-off the surface to make the top of the sample level and smooth. 6. Run water over the mold lid and place it onto the mold base.
References:	API RB 10B-2, 2nd Edition, 2013 ASTM C192-00

Figure A.6: Cement sheath placement

Figure A.7: Cube mold placement

Table A.4: Curing

Equipment:	casing pressure line: P-2282 hand pump, isolation valve 1 and 2, pressure gauge confining collar confining pressure line: P-39 hand pump, isolation valve 1 and 2, pressure gauge combination wrenches cooking thermometer – Maverick HD 32 cube mold curing tank flathead screwdriver hammer and punch large pressure vessel metal lidless can oil pan (8.5 x 8.5 x 2.25”) pipe wrench portable vice probe thermometer (2) PVC pipe mold razor blade small pressure vessel Styrofoam cubes vessel cap vessel head weight ½” plywood molding board with 1” OD holes ½” plywood retaining board
PPE:	fire-resistant lab coat – protect body from contact burns or hot oil splash heat-reflective face guard – protect face from contact burns or hot oil splash long jeans – protect hip to ankle from contact burns or hot oil splash safety glasses – repel slurry splash, repel dust particles steel-toe shoes – handle the heavy large pressure vessel welding gloves – protect hands and forearms from contact burns or hot oil splash **Recommend:** prior to touching hot surfaces that are visibly wet, use a paper towel to remove moisture from the surface. The welding gloves are much less effective when moisture is introduced.

Materials:	cement cube samples (2 x 2 x 2”) cement sheath sample hydraulic oil – Mobile DTE 24 mineral base oil lime – $Ca(OH)_2$
Procedures:	Procedure for cement sheath mold: 1. Within 10 minutes since cement placement into the sheath mold, place the sample attached to the molding and retaining boards into the curing tank set at the desired temperature. **Note:** if necessary, place weights on the plywood boards to ensure they do not float. **Note:** 3 grams / liter of lime is added once to the curing tank to prevent calcium carbonate or calcium hydroxide from leaching out of the cement samples during curing. 2. Insert two probe thermometers into a small cube of Syrofoam so they float and monitor temperature. **Note:** the water level in the curing tank consistently decreases due to evaporation. **Recommend:** add water once or twice daily to the desired level. This level is about 5 inches of water, or 1 inch from the top of the tank. **Note:** do not allow the water level to cover the nipple of the small pressure vessel. Lime-saturated water could damage it internally. 3. After 6 hours, or the first surface curing period, remove the mold and plywood boards from the curing tank. 4. Use a razor blade to cut away the hard silicone holding the PVC mold in place. Also, cut the packaging tape holding the two halves of the PVC mold together. 5. Insert a flathead screwdriver into the groove between the two halves of the PVC mold. Force the two halves to separate and unbind them from the hardened cement. 6. Remove the sample from the molding board. **Note:** if necessary, loosen the wing nuts and remove the retaining board from the molding board. Use a hammer and punch to lightly tap the bottom of the pressure vessel until it breaks free of the molding board. 7. Place the sample back into the curing tank for the remainder of the surface curing period. 8. Once surface curing is complete, prepare the sample for wellbore curing. 9. Attach the sample to the vessel head. Slip the threaded vessel cap and confining collar over the vessel head into place.

Note: it can be difficult to ensure a tight secure connection between the small pressure vessel and vessel head.

Recommend: the problem was solved by using a cheaper wrench. The cheap wrench was thinner than the standard Craftsmen wrench and could tighten the small vessel more effectively.

10. Screw the vessel head into the large pressure vessel. This process may require a portable vice and pipe wrench to achieve a good seal.

Note: do not overtighten the vessel cap onto the large pressure vessel. After the curing process is complete, it becomes very difficult to remove the cap.

11. Place the arrangement into the oil pan within the oven.

Note: the oven is set to the desired curing temperature, however the temperature-setting dial is inaccurate. A cooking thermometer probe is inserted into a metal lidless can containing hydraulic oil to better monitor temperature.

Recommend: it is best to run the oven constantly and place the large pressure vessel into the oven 2-3 hours before the wellbore curing process is started. Then, momentarily remove the large pressure vessel to attach the vessel head holding the cement sheath sample.

12. Attach the casing and confining pressure flow lines to the vessel head.

Note: this is likely the most unpleasant procedure in Appendix A. It is difficult to attach the coned and threaded high pressure connections to the high pressure adapters while reaching into the oven. Also, the casing pressure line is much easier to connect than the confining pressure line.

Recommend: to handle the confining pressure connection, remove the tubing below the downstream isolation valve at the NPT connection. Remove the tubing section from the oven and attach it to the adapter. Then, attach the adapter and tubing to the large pressure vessel. Finally, replace the arrangement back into the oven and remake the NPT connection.

13. Apply pressure in both lines in equal steps of 400 psi until the desired curing pressure is reached. The two pressure lines should always show approximately the same pressure.

14. Close the upstream isolation valves at the same time. Then open the pressure release valve on each pump to relieve its pressure contribution.

Note: closing the isolation valve will cause an increase in line pressure. Must close the two valves at the same time.

15. Check the pressure gauges. The pressure readings increase with time due to the expansion of the hydraulic fluid at high temperatures.
16. Slowly and carefully open the isolation for one line. Allow the pressure reading to drop and quickly close the isolation valve once the correct pressure is achieved. Repeat the process for the other line.
17. If the pressure reading is less than desired, quickly open both isolation valves and try Steps 13-16 again.

Note: sometimes pressure cannot be maintained at a constant level by closing the isolation valves. This means there is a downstream leak, likely inside the oven at one of the connections.

Recommend: release the pressure on both flow lines. Then, try tightening the connections inside the oven. If that doesn't work, disconnect and reconnect the equipment inside the oven.

Note: if there is pressure communication between the flow lines, then the small pressure vessel is leaking inside the curing chamber. This condition is easy to diagnose by watching the pressure gauges. If the applied pressures always converge to each other, then there is communication.

18. Allow thermal equilibrium to be reached inside the oven. During this process, thermal expansion of the hydraulic fluid will cause an increase in pressure in both flow lines.

Recommend: every 15 minutes, check the pressure readings and relieve increases in pressure following Step 16. Do this until 30 minutes passes without a noticeable increase in pressure (<100 psi). It usually takes about 2 to 2 ½ hours.

19. Wellbore pressure and temperature are achieved. The sample is ready for the remaining wellbore curing time.

Procedure for cube mold:

1. Within 10 minutes since cement placement into the cube mold, place the samples inside the mold into the curing tank maintained at the desired surface curing temperature.
2. Insert two probe thermometers into a small cube of Syrofoam so they float and monitor temperature.

Note: the water level in the curing tank consistently decreases due to evaporation.

	Recommend: add water once or twice daily to the desired level. This level is about 5 inches of water, or 1 inch from the top of the tank. 3. Raise the mold off the bottom of the curing tank so the mold does not contact any heating surface. A permeable spacer such as cardboard or the molding and retaining boards is acceptable. The spacer allows water to completely circulate around the mold. 4. Allow the samples to cure undisturbed for the desired surface curing period. 5. At 45 ± 5 minutes before testing, remove the mold from the water bath. Alter the heat setting on the curing tank so the curing temperature changes to 80 ± 5^{o}F. 6. Disassemble the cube mold using a hand pliers to remove the necessary wing nuts and bolts. 7. Use the flathead screwdriver to wedge between the two retaining wall pieces of the mold and force them apart. 8. Remove the cured samples from the retaining wall piece and immediately place the samples back into the curing bath. **Note:** do this even if the curing temperature is outside the desired range. The samples must be saturated with water when tested. 9. At the time of compression testing, remove the cube samples from the curing tank. Test the samples as soon as possible.
References:	API RB 10B-2, 2nd Edition, 2013 A Method for Cement Integrity Evaluation in Unconventional Wells. (Shadravan, 2013)

Figure A.8: Surface curing tank

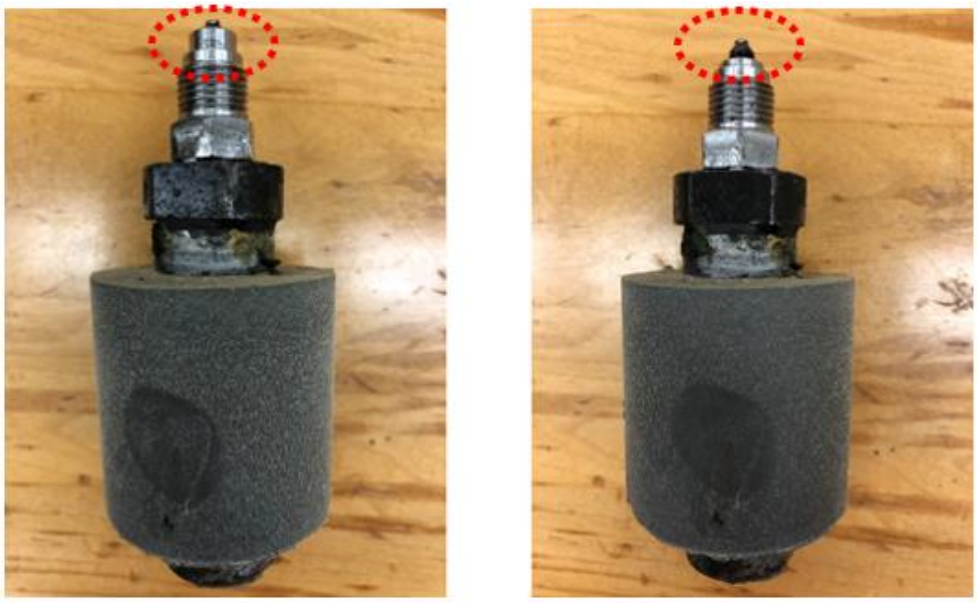

Figure A.9: Incorrect (left) vs. correct (right) gland and collar positioning

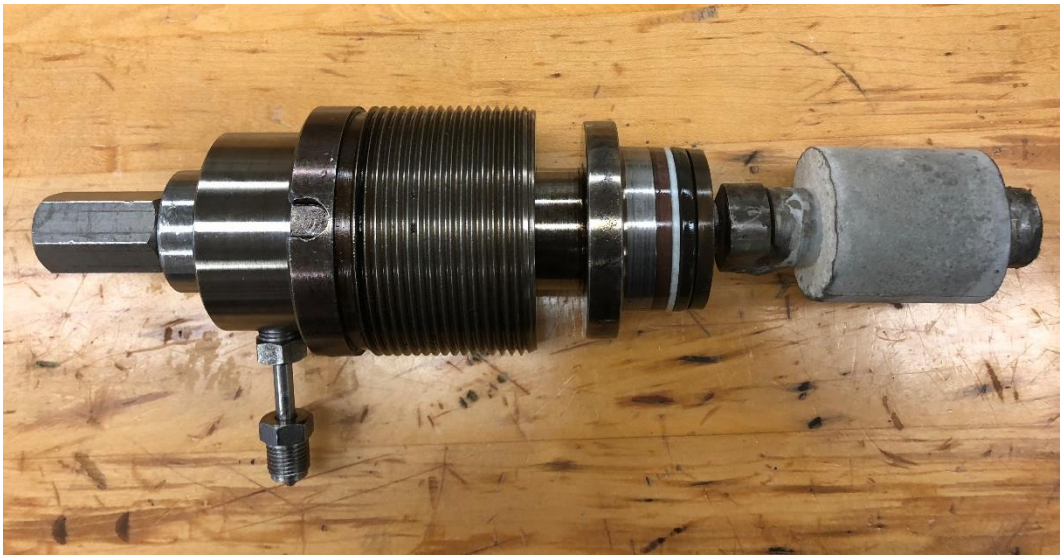

Figure A.10: Cement sample loaded to vessel head with vessel cap and confining collar

Figure A.11: Portable chain vice and pipe wrench

Figure A.12: Wellbore curing

Table A.5: Slurry density test

Equipment:	mud balance – OFITE 4 – Scale: #115-00 paint brush spatula
PPE:	plastic or rubber gloves – handle the slurry and admixtures safety glasses – repel slurry splash, repel dust particles
Materials:	cement slurry tap water
Procedures:	1. Place the mud balance container on a flat level surface. Ensure the components are completely dry except for the volume cup. It should be surface-saturated dry. **Note:** surface-saturated dry is defined as the condition of a material in which the surfaces are dry but the inter-particle voids are saturated with water. **Recommend:** use a water-moist paint brush to wet the entire surface, then a paper towel to remove any pooling or visible collection. This achieves SSD. 2. Fill the surface-saturated dry cup to the top with fresh cement slurry using the spatula. 3. Place the lid on the volume cup and twist it shut. Check that some cement slurry is expelled through the hole in the cap or the cap sides. It is desirable to ensure the cup is completely full. 4. Cover the hole in the lid and wash all cement from the outside of the volume cap and arm. Then thoroughly dry the entire balance. 5. Place the balance on the knife edge and move the rider along the outside of the arm until the cup and arm are balanced as indicated by the bubble. 6. Read the cement weight at the edge of the rider toward the volume cup. Record to the nearest 0.1 ppg. 7. Empty the cement from the volume cup back into the 1-Liter blender container. **Note:** slurry used for this test is reused to make cube or cement sheath molds. 8. Clean the mud balance, volume cup, and cap of any cement slurry.
References:	OFITE 4 – Scale #115-00 Instruction Manual, Version 1.5

Figure A.13: Mud balance for density testing

Figure A.14: Volume cup is balanced with rider arm

Table A.6: Compression strength test

Equipment:	compressive testing equipment – Instron 5982 testing frame and Bluehill computer software hex wrench swivel plate top platen
PPE:	safety glasses – impact protection, repel dust particles
Materials:	cement cube samples (2 x 2 x 2")
Procedures:	1. Remove the cube sample from the curing bath and transport to the testing area. **Note:** this area is located in building 0325 or CVLB, the Civil Engineering Lab Building, in Room 115 and overseen by lab coordinator Dave Dillon. 2. Attach the top platen to the testing block. Insert the pin, then use a hex wrench to tighten the top ring, and lastly hand tighten the bottom ring. 3. Place the swivel plate on the bottom cross frame and center the first sample on the swivel plate under the top platen. **Note:** place the sample on its side so the top surface faces forward. Never place the sample with the top surface facing upward or downward. 4. Launch the Bluehill computer software on the computer and select the testing procedure labeled "API Cubes" meant specifically for 2 x 2 x 2 inch cement cubes. 5. Navigate the Bluehill program to label the sample and select testing parameters. **Note:** one important parameter is loading rate. API standards recommend require applying 4,000 lbf per minute for expected strength less than or equal to 500 psi and 16,000 lbf per minute for expected strength greater than 500 psi. However, this loading rate was not achieved on the provided Instron testing frame. The proportional gain factor could not be calculated despite several attempts. **Recommend:** instead of loading the cement cube with a force rate of foot pounds per minute, use an extension rate of 0.035 inches per minute. 6. Once the testing parameters are selected, calibrate the load so it considers the weight of the top platen to equal zero lbf.

	7. Jog down to manually lower the top platen until almost touching the sample. Then use the dial to lower the top platen until 50 lbf is measured. 8. Zero out the extension and start the test. Once the cube is broken, stop the test. 9. Use the dial to raise the top platen until no lbf is measured. Then jog up to raise the top platen a couple more inches. 10. Remove the broken sample and replace it with the next sample, if there are more. Once finished, download the generated report onto a flash drive and clean the testing area.
References:	API RP 10B-2, 2nd Edition, 2013 ASTM C109/C109M-07

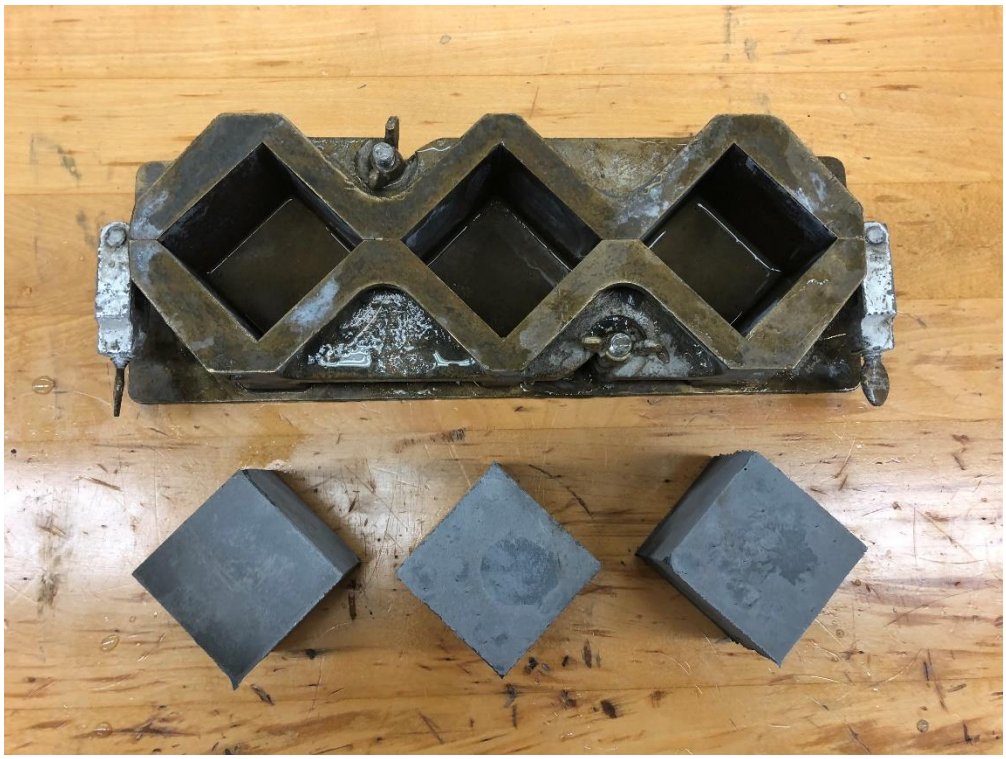

Figure A.15: Cube samples for compression testing

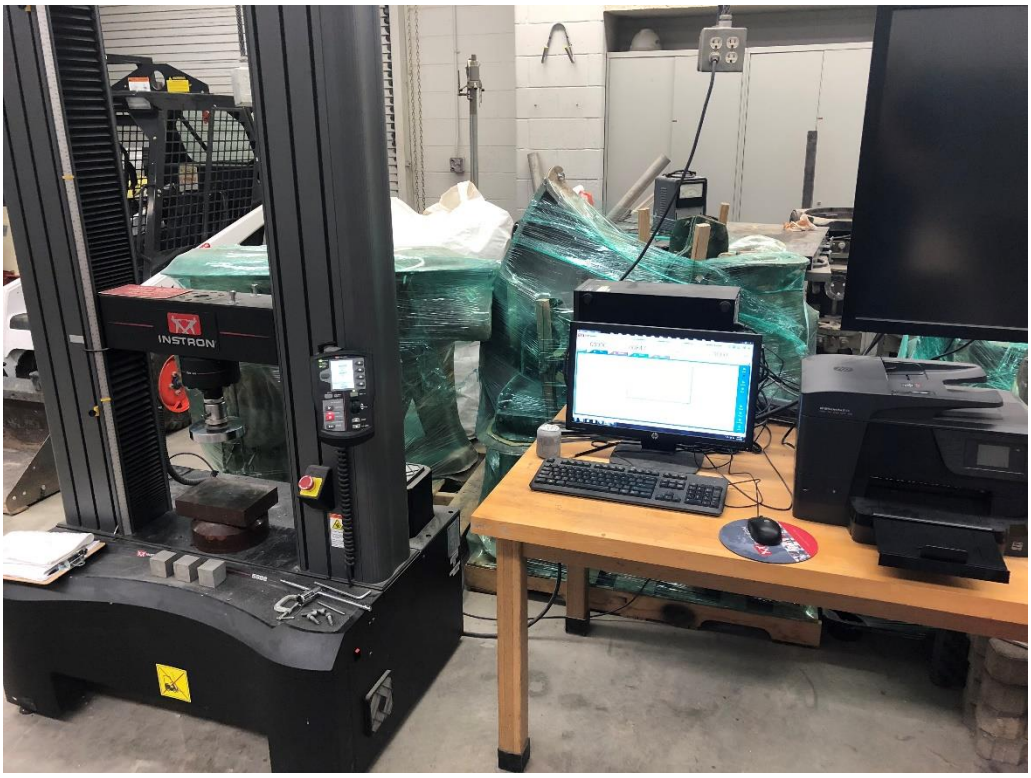

Figure A.16: Instron 5982 testing frame and computer

Figure A.17: Top platen, swivel plate, and control panel

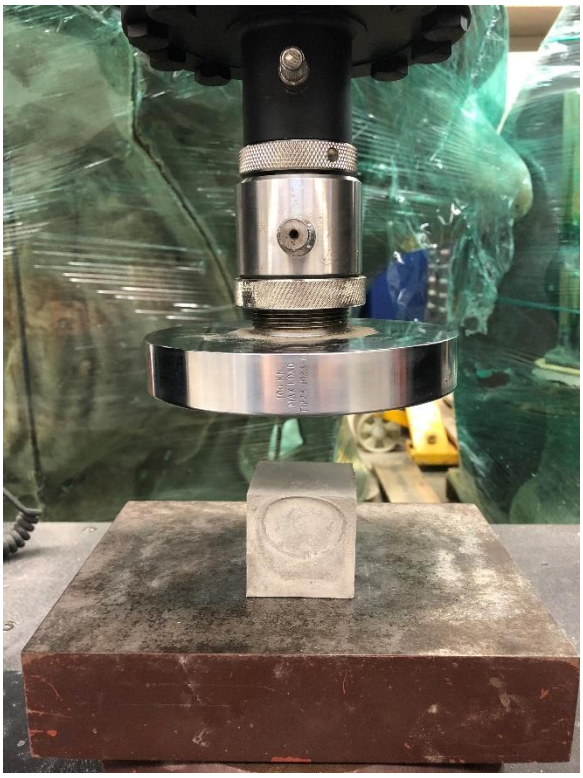

Figure A.18: Sample placement for compression test

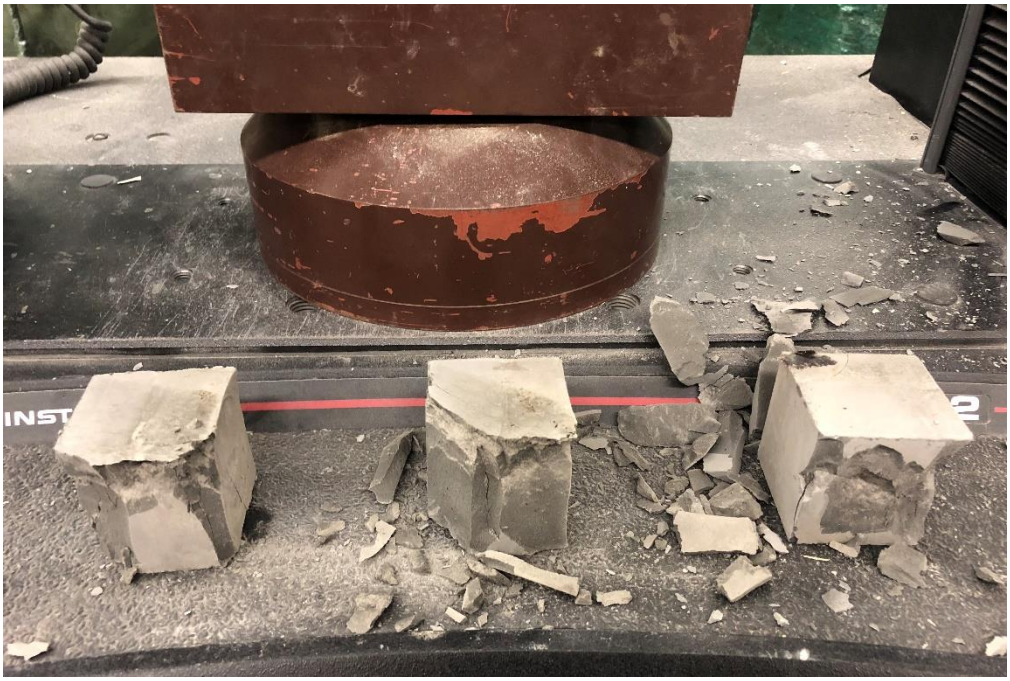

Figure A.19: Broken samples

Navigating the Bluehill program:

Step 1 – Select the test icon, then “API Cubes” from the displayed list.

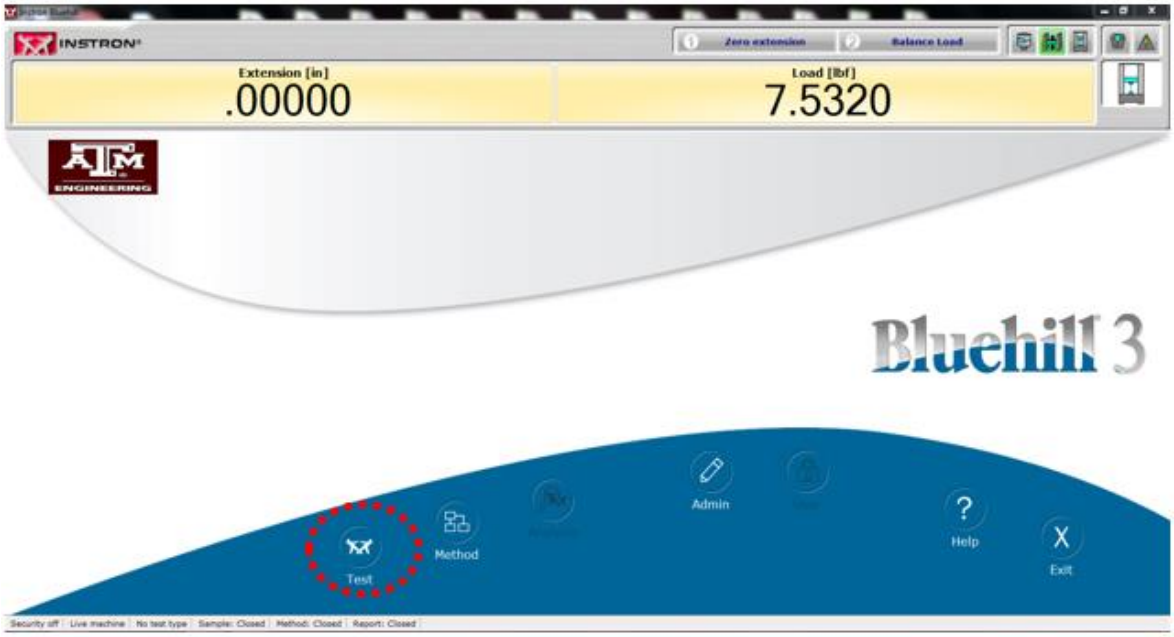

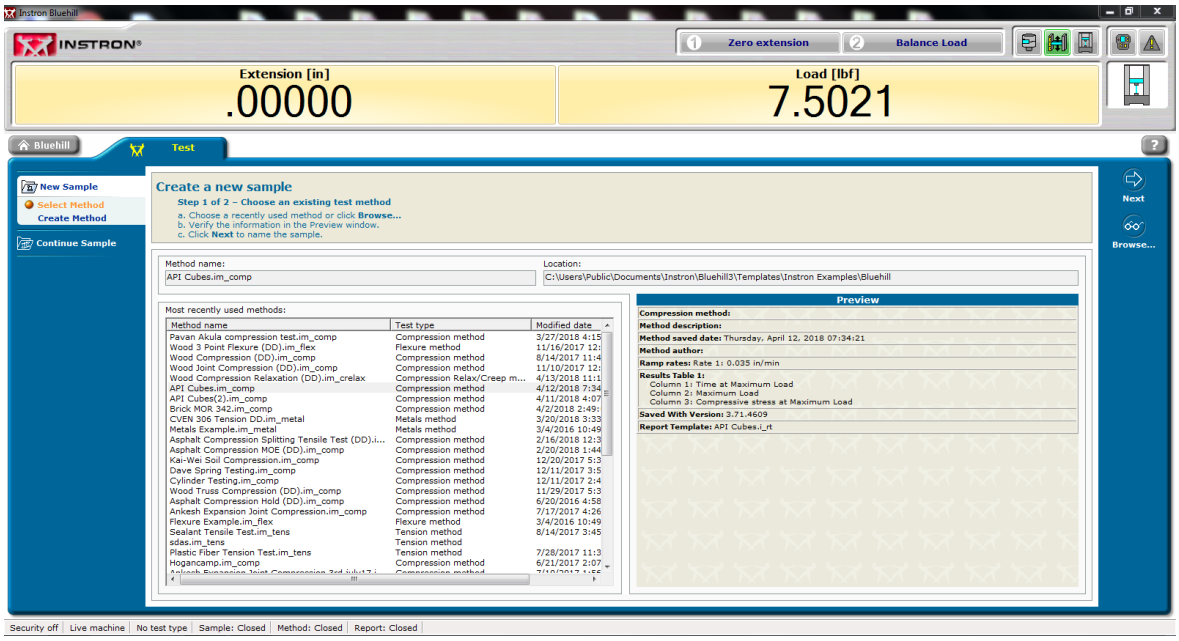

Step 2 – Provide a sample name. This will be the file name once the test is finished and the results downloaded.

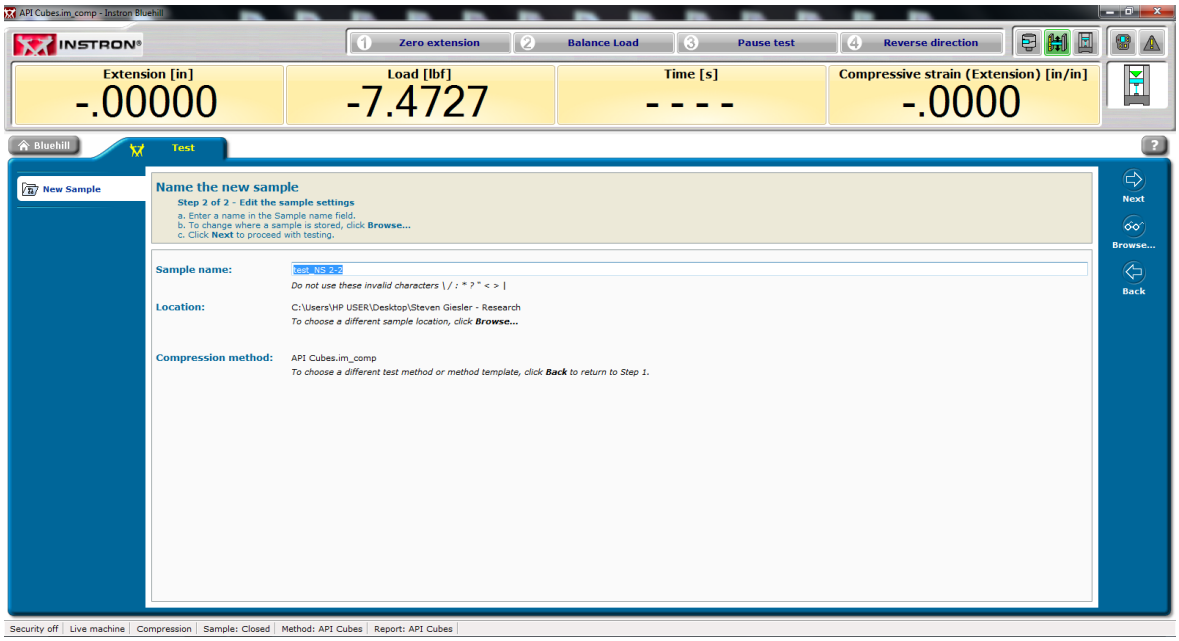

Step 3 – Go through the various options under the red Method tab. Change the sample name as desired for the final report pdf in the Sample tab. Click the Test Control tab on the left and observe the loading rate. **Note:** testing parameters which includes the loading rate cannot be changed between samples on the same file.

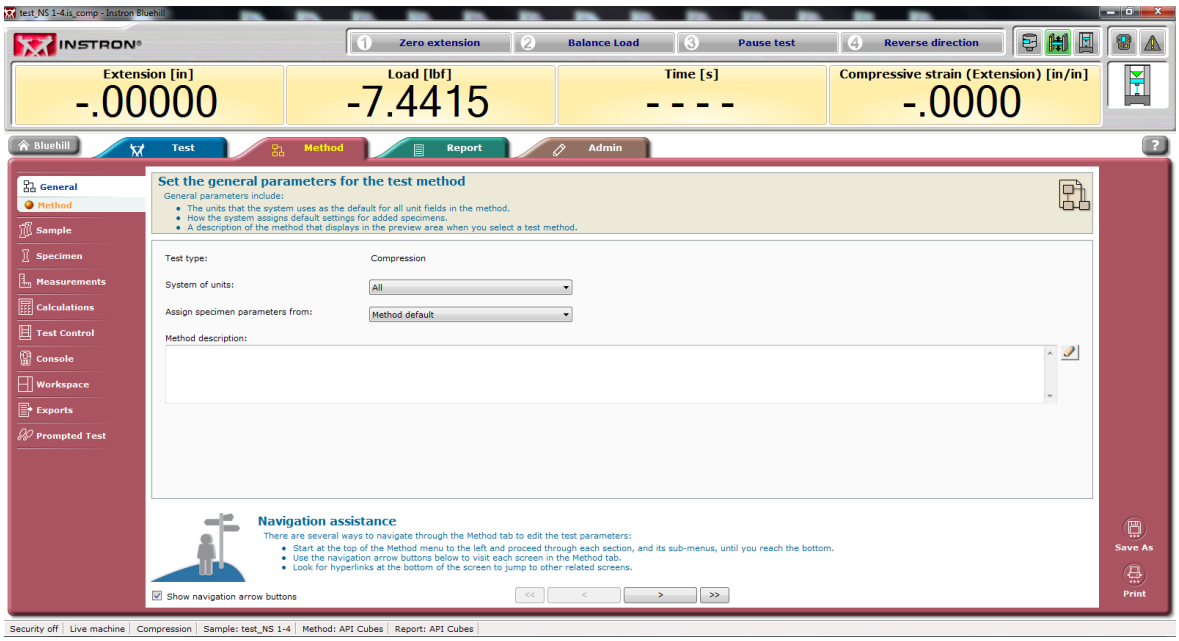

Step 4 – Calibrate the load applied by the weight of the top platen. Open the cell in the top right corner, then select the load tab in the new window and click calibrate.

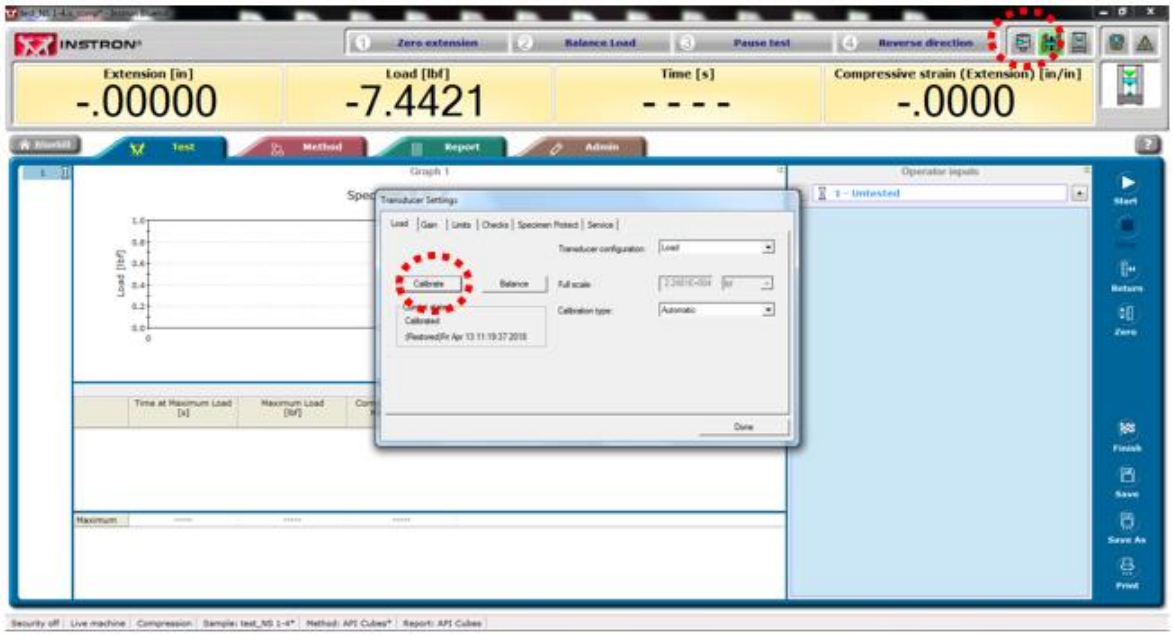

Step 5 – Once calibrated and ready for testing, open the blue Test tab. Manually pre-load the cement sample to 50 lbf, zero the extension, and click the Start icon to begin the compression test. Once the sample is broken, click the Stop icon and unload the sample.

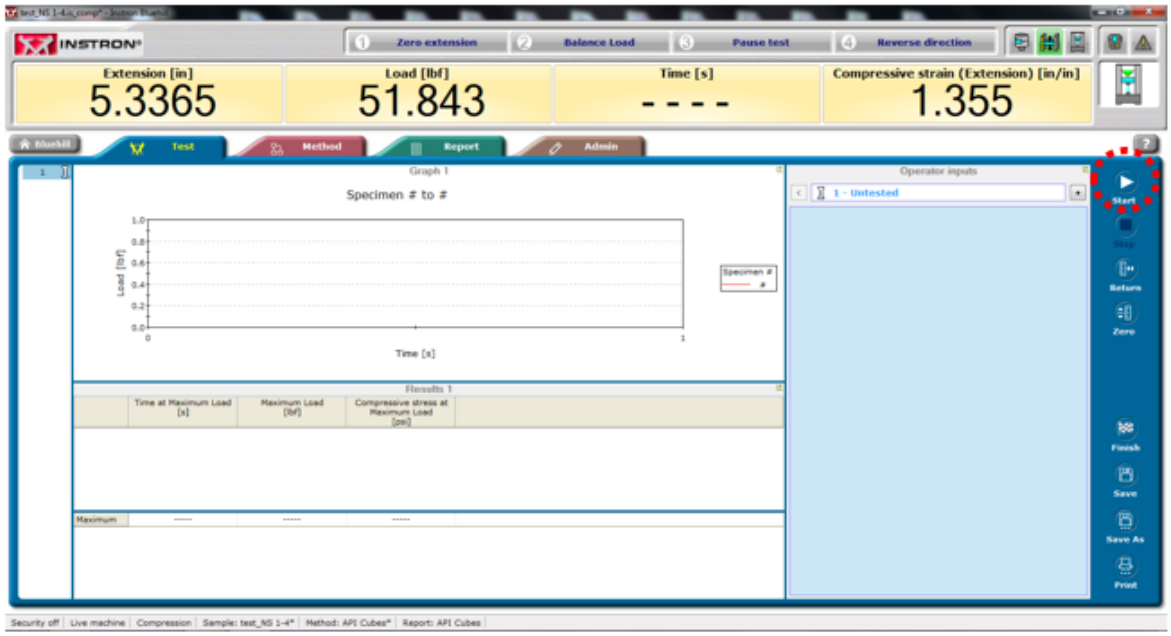

Step 6 – After breaking all the samples, click the Finish icon and save the files to the desired folder. Access the folder to export the files via e-mail or a flash drive. Ensure that the top platen has been raised from the cement cube and close the program.
Note: the loading block will not raise or lower unless the Bluehill program is open.

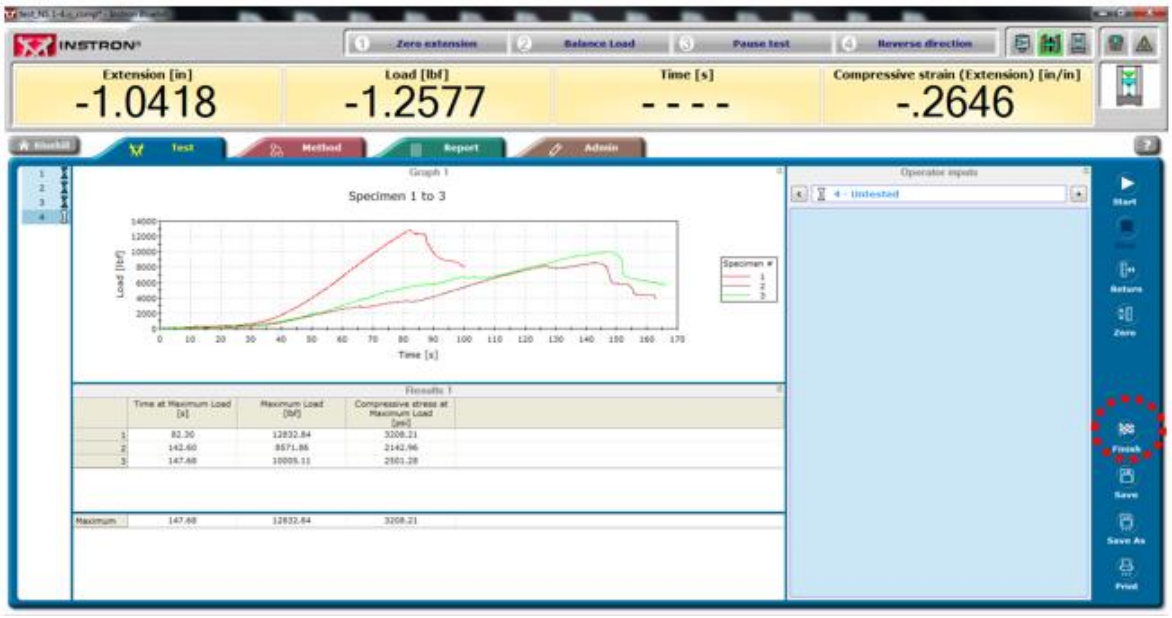

Table A.7: Cyclic fatigue test

Equipment:	casing pressure line: P-2282 hand pump, isolation valve 1 and 2, pressure gauge confining collar confining pressure line: P-39 hand pump, isolation valve 1 and 2, pressure gauge combination wrenches cooking thermometer – Maverick HD 32 data acquisition system: laptop computer, DAQami software, pressure transducers, power supply – Posweed 36w 15v, measurement compact – USB-1208FS large pressure vessel metal lidless can oil pan (8.5 x 8.5 x 2.25”) pipe wrench portable vice small pressure vessel vessel cap vessel head
PPE:	fire-resistant lab coat – protect body from contact burns or hot oil splash heat-reflective face guard – protect face from contact burns or hot oil splash long jeans – protect hip to ankle from contact burns or hot oil splash safety glasses – repel slurry splash, repel dust particles steel-toe shoes – handle the heavy large pressure vessel welding gloves – protect hands and forearms from contact burns or hot oil splash **Recommend:** prior to touching hot surfaces that are visibly wet, use a paper towel to remove moisture from the surface. The welding gloves are much less effective when moisture is introduced.
Materials:	cement sheath sample hydraulic oil – Mobil DTE 24 mineral base oil

Procedures:

1. The wellbore curing period is complete. Open the isolation valves and the pumps' pressure release valves. Ensure that line pressure is 0 psi.
2. Disconnect the large pressure vessel from the pressure lines and remove it from the oven.
3. Strap the large pressure vessel securely to the portable vice and use the pipe wrench to unscrew the vessel cap. Once fully unscrewed, remove the vessel head and sample from the large pressure vessel.

Note: it is not necessary to disconnect the sample from the vessel head.

4. Wipe the cement sheath sample with a paper towel to remove oil and other waste. Then check for cracks or debonding in the sample.

Note: neat slurry experiences strength retrogression and exhibits sever cracking and debonding following wellbore curing. Silica flour is added to combat this.

Recommend: debonding is diagnosed by applying a slight torque on the cement sheath sample. If the sample is well-bonded to the small pressure vessel, nothing happens and debonding has not occurred. If the sample is loose or breaks free, debonding has occurred.

5. If the sample has failed by cracking or debonding, the test is over. If the sample has not failed, continue with the test.
6. Attach the sample to the vessel head. Slip the threaded vessel cap and confining collar over the vessel head into place.

Note: it can be difficult to ensure a tight secure connection between the small pressure vessel and vessel head.

Recommend: the problem was solved by using a cheaper wrench. The cheap wrench was thinner than the standard Craftsmen wrench and could tighten the small vessel more effectively.

7. Screw the vessel head into the large pressure vessel. This process may require a portable vice and pipe wrench to achieve a good seal.

Note: do not overtighten the vessel cap onto the large pressure vessel. After the testing process is complete, it becomes very difficult to remove the cap.

8. Place the arrangement into the oil pan within the oven.

Note: the oven is set to the desired curing temperature, however the temperature-setting dial is inaccurate. A cooking thermometer probe is inserted into a metal lidless can containing hydraulic oil to better monitor temperature.

9. Attach the casing and confining pressure flow lines to the vessel head.

Note: this is likely the most unpleasant procedure in Appendix A. It is difficult to attach the coned and threaded high pressure connections to the high pressure adapters while reaching into the oven. Also, the casing pressure line much easier to connect than the confining pressure line.

Recommend: to handle the confining pressure connection, remove the tubing below the downstream isolation valve at the NPT connection. Remove the tubing section from the oven and attach it to the adapter. Then, attach the adapter and tubing to the large pressure vessel. Finally, replace the arrangement back into the oven and remake the NPT connection.

10. Apply pressure in both lines in equal steps of 400 psi until the desired confining pressure is reached. The two pressure lines should always show approximately the same pressure.

11. Check the pressure gauges to ensure pressure remains constant in both lines.

Note: if pressure quickly decreases, tighten the pressure release valve on the pump. If pressure still quickly decreases, there is likely a leak inside the oven at one of the connections.

Recommend: release the pressure on both flow lines. Then, try tightening the connections inside the oven. If that doesn't work, disconnect and reconnect the equipment inside the oven.

Note: if there is pressure communication between the flow lines, then the small pressure vessel is leaking inside the curing chamber. This condition is easy to diagnose by watching the pressure gauges. If the applied pressures always converge to each other, then there is communication.

12. Set up the data acquisition equipment and open the software program on the laptop computer. Click the play button to ensure the program is recording pressure data, then click stop.

Note: ensure that there are two channels open in the configuration, one for each pressure transducer. Also, select a modest sample rate. 10 samples per second works well.

13. Click the record button to start the test. Wait for two minutes with confining pressure applied in both lines.

	14. After two minutes, use the pump to quickly raise pressure in the casing pressure line to the desired pressure differential. 15. Wait two minutes, then slowly relieve pressure in the casing pressure line until it matches the confining pressure. 16. Repeat steps 14 – 15 for the desired number of cycles. **Note:** steps 14 – 15 is one cycle of 4 minutes. **Recommend:** the data acquisition software program allows the user to increase or decrease the scale on the x-axis (time). A scale of 2 minutes can be used to observe when to pressure up or down. Another option is to use a stopwatch which makes noise to alert the user. Then the user can multitask while running the experiment. 17. After a predetermined number of cycles, the test is halted to check whether the cement sheath sample failed. **Recommend:** allow two minutes of equal casing and confining pressure before stopping the test. It makes consolidating and analyzing the pressure data easier. 18. Click the stop button to end pressure sampling. Then export the data to the desired folder and rename it. 19. Open the isolation valves and the pumps' pressure release valves. Ensure that line pressure is 0 psi. 20. Disconnect the large pressure vessel from the pressure lines and remove it from the oven. 21. Strap the large pressure vessel securely to the portable vice and use the pipe wrench to unscrew the vessel cap. Once fully unscrewed, remove the vessel head and sample from the large pressure vessel. **Note:** it is not necessary to disconnect the sample from the vessel head. 22. Wipe the cement sheath sample with a paper towel to remove oil and other waste. Then check for cracks or debonding in the sample. **Recommend:** debonding is diagnosed by applying a slight torque on the cement sheath sample. If the sample is well-bonded to the small pressure vessel, nothing happens and debonding has not occurred. If the sample is loose or breaks free, debonding has occurred. 23. If the sample has failed by cracking or debonding, the test is over. If the sample has not failed, continue with the test by repeating steps 6 – 22.
References:	A Method for Cement Integrity Evaluation in Unconventional Wells. (Shadravan, 2013)

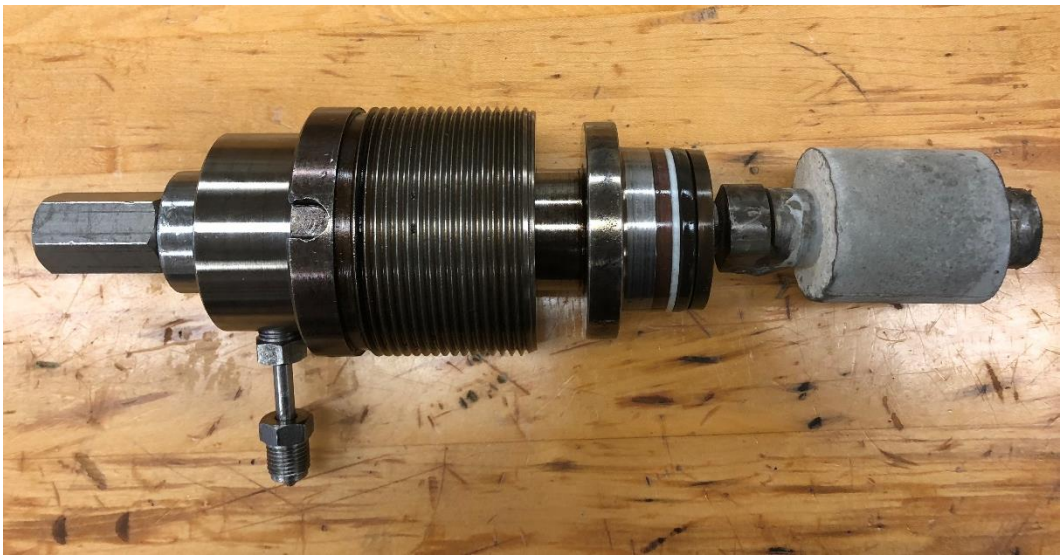

Figure A.20: Cement sample loaded to vessel head with vessel cap and confining collar

Figure A.21: Large vessel connected to flow lines

Figure A.22: As-built experimental set-up

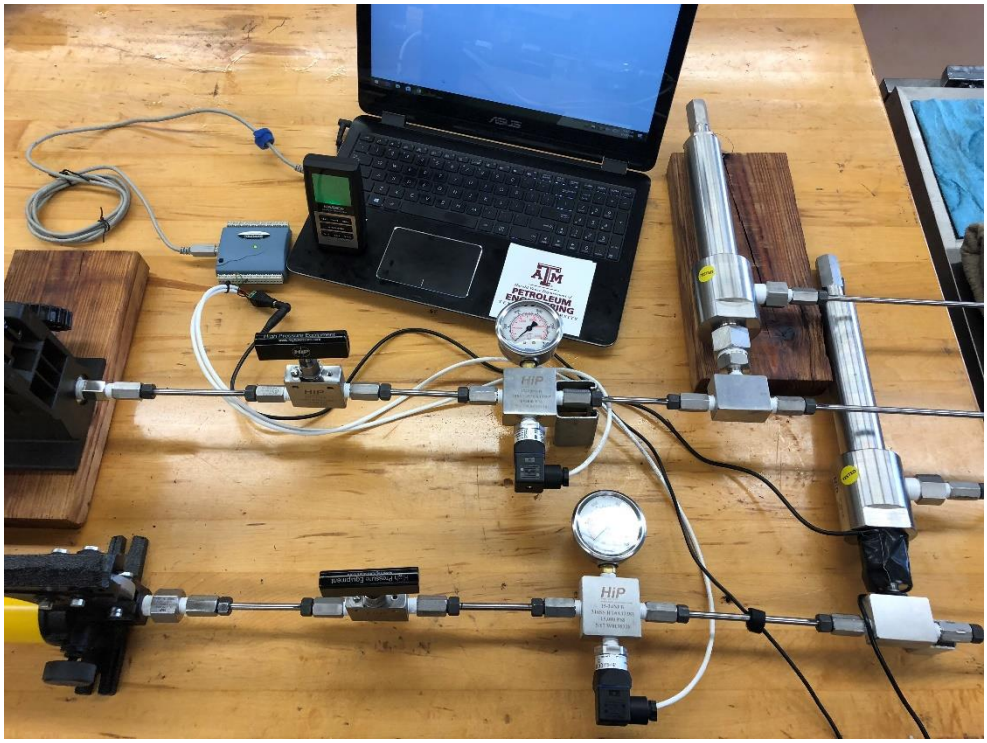

Figure A.23: Data acquisition equipment

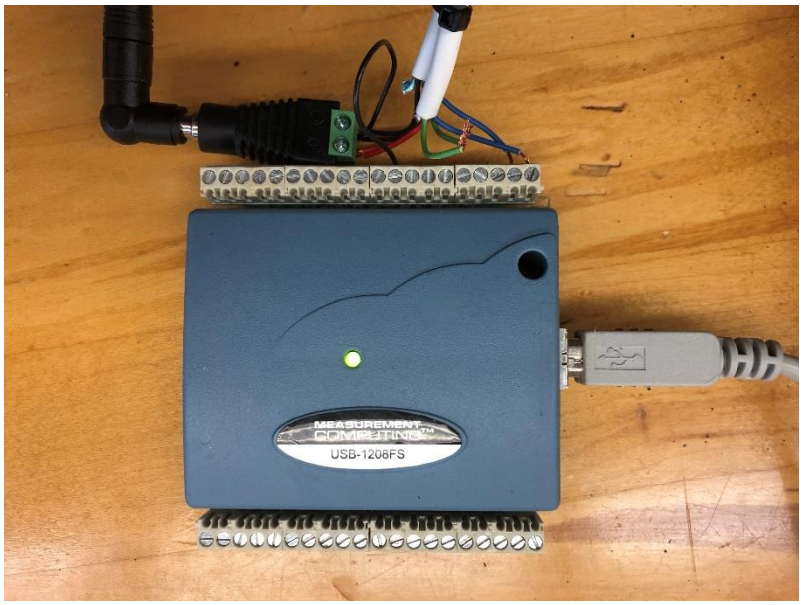

Figure A.24: USB measurement compact

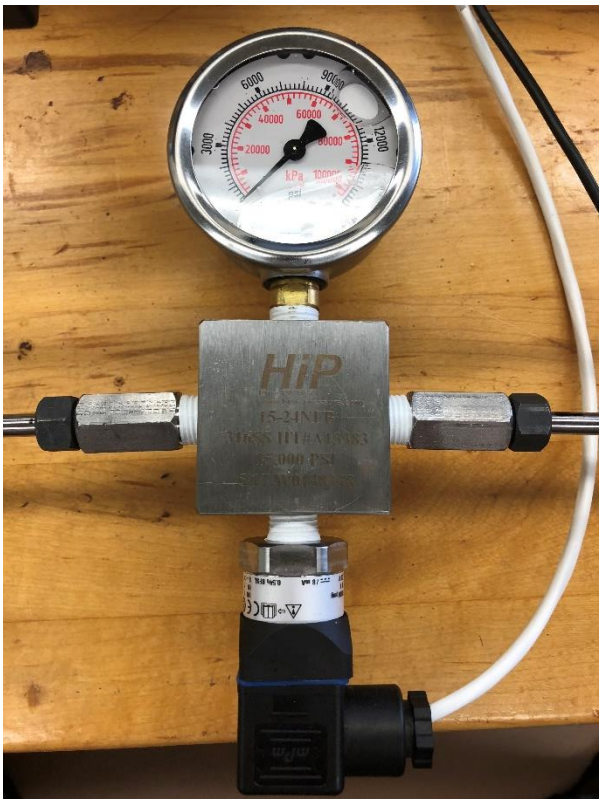

Figure A.25: Pressure gauge and transducer

Figure A.26: Radial cracking failure (left) and debonding failure (right)

Navigating the DAQami program:

Step 1 – Open the program and select New Configuration. Once a configuration is prepared, the user can save it and run same configuration for all tests.

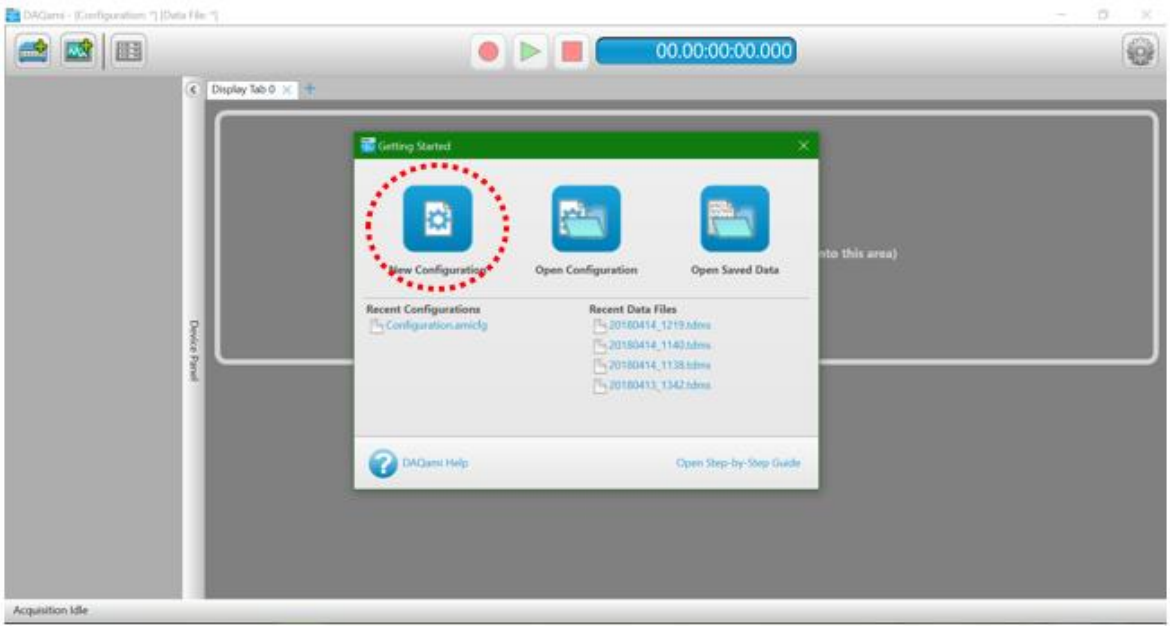

Step 2 – Click the Manual button to open a new configuration.

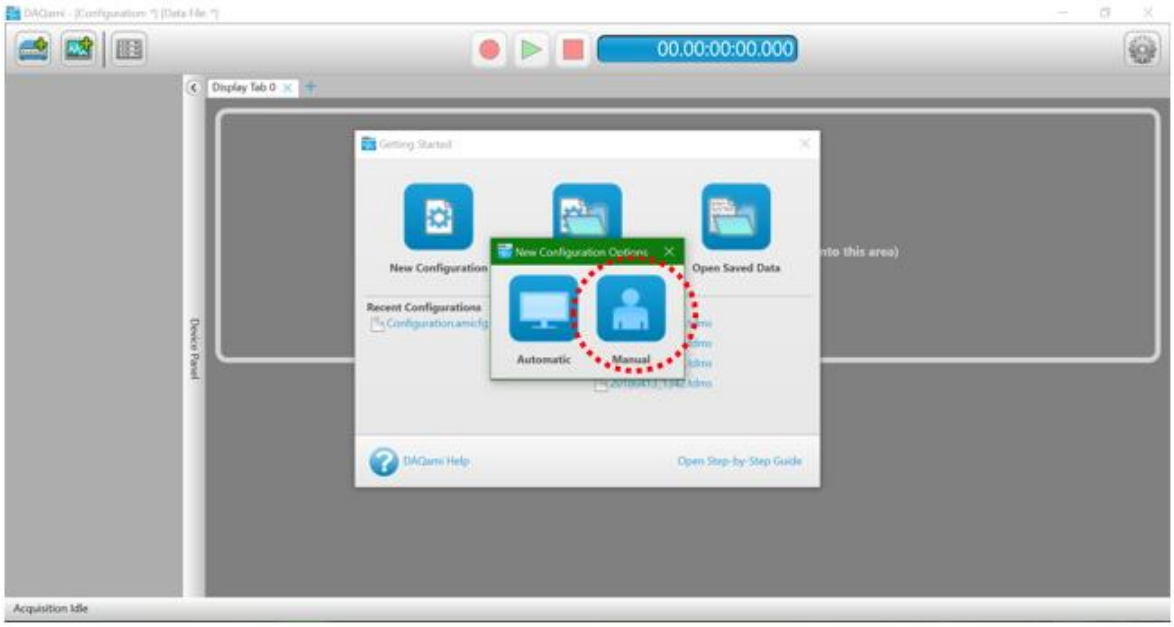

Step 3 – Plug the USB-1208FS into the laptop computer. This allows the DAQami software to find the device. Click on the Available Devices icon in the upper left corner. Select the USB-1208FS.

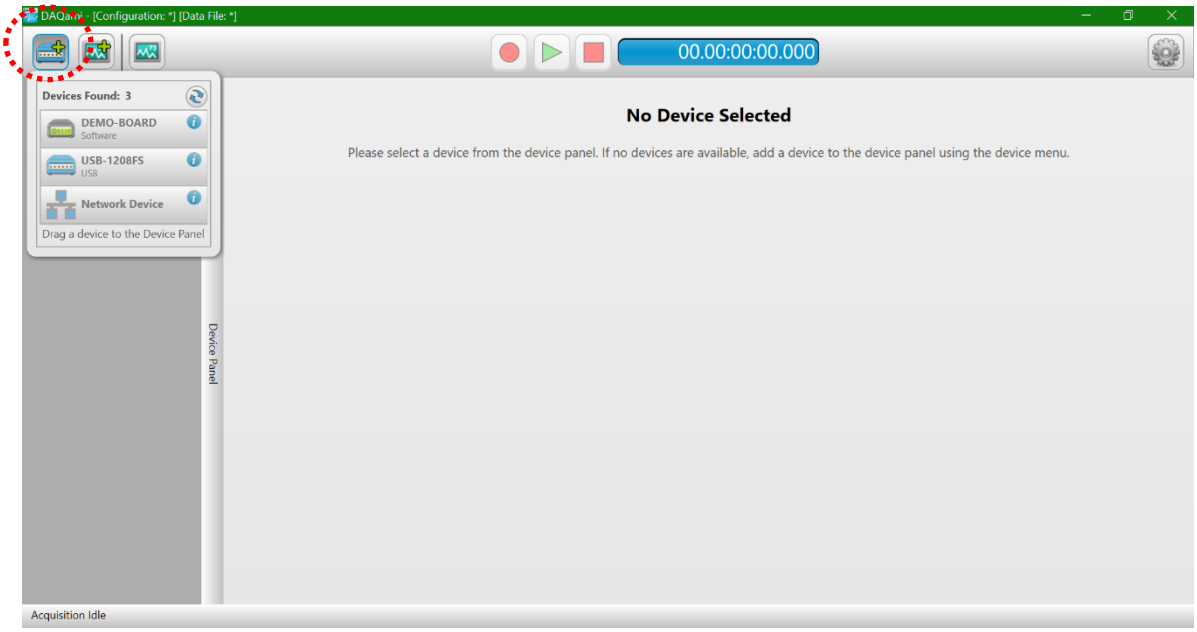

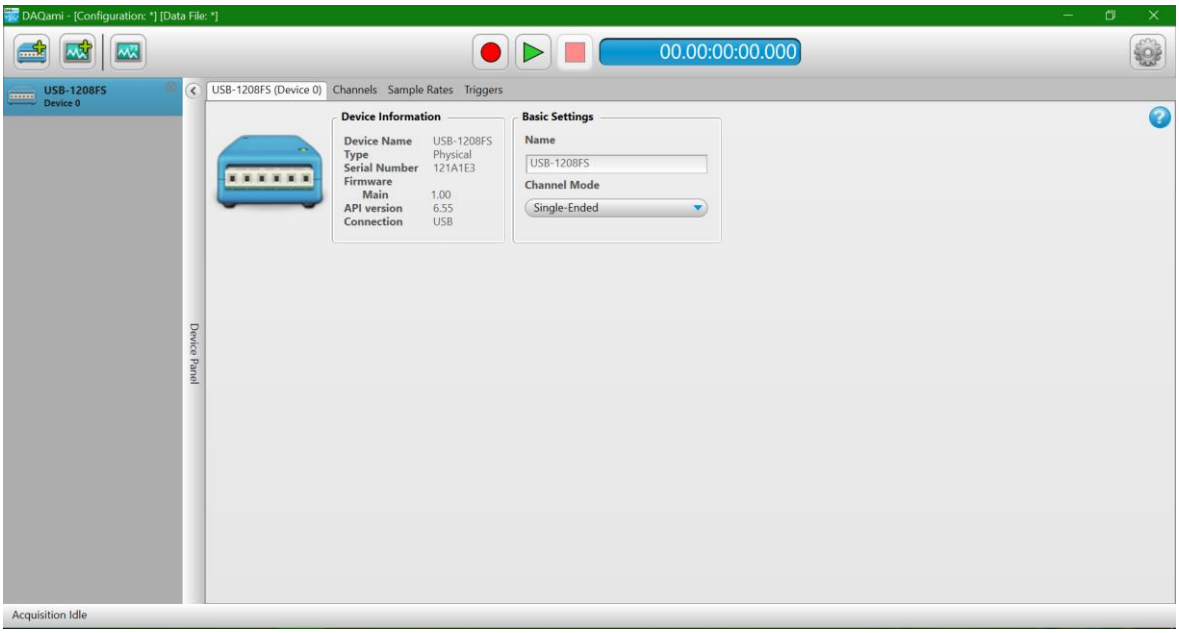

Step 4 – Open the Channels tab on the ribbon and select two channels to be active. Then, choose ± 10 V on the range dropdown box and V for units.

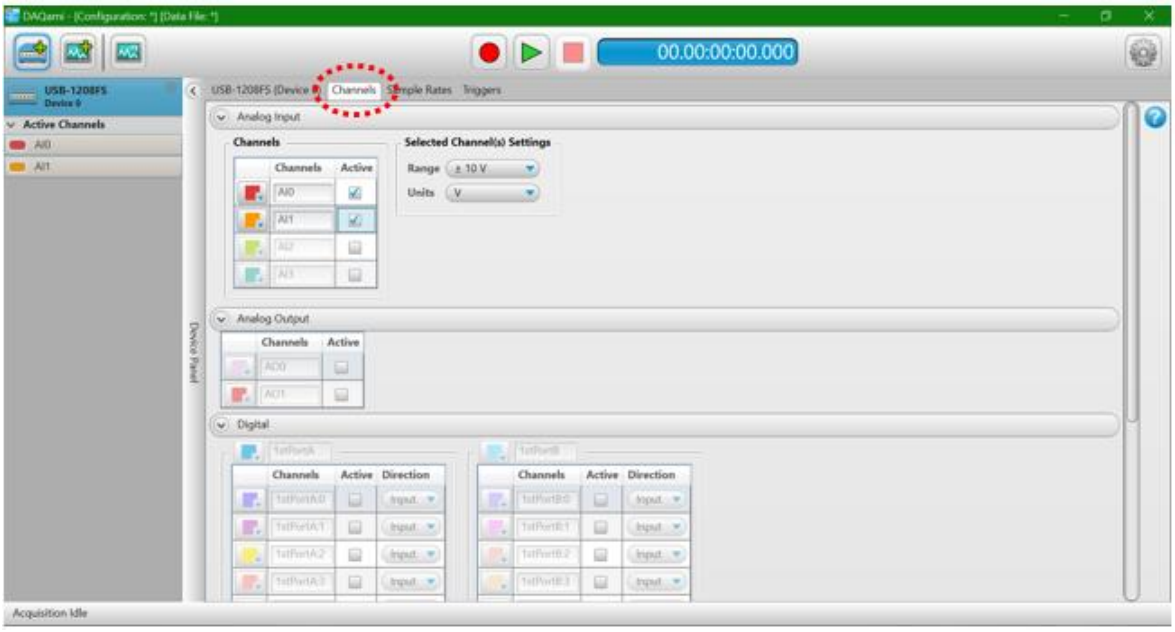

Step 5 – Open the Sample Rates tab on the ribbon and enter the desired sample rate.
Note: the data acquisition software can handle 1,000 samples per second, but 10 samples per second is satisfactory. An excessive sample rate records more than 1 million samples for a longer test. The program can only record and export 1 million samples, so all samples over 1 million are lost.

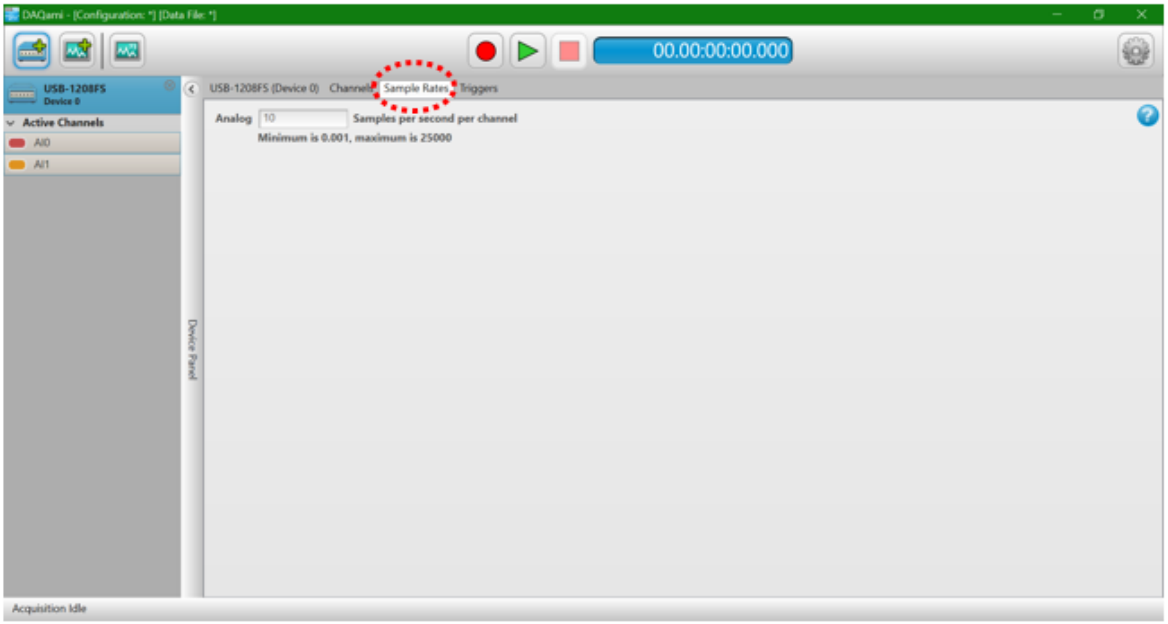

Step 6 – Prepare the configuration display by selecting Strip from the Displays icon. Drag the Strip display into the dark grey area. Then, individually select the active channels and drag them onto the newly-appeared graph.

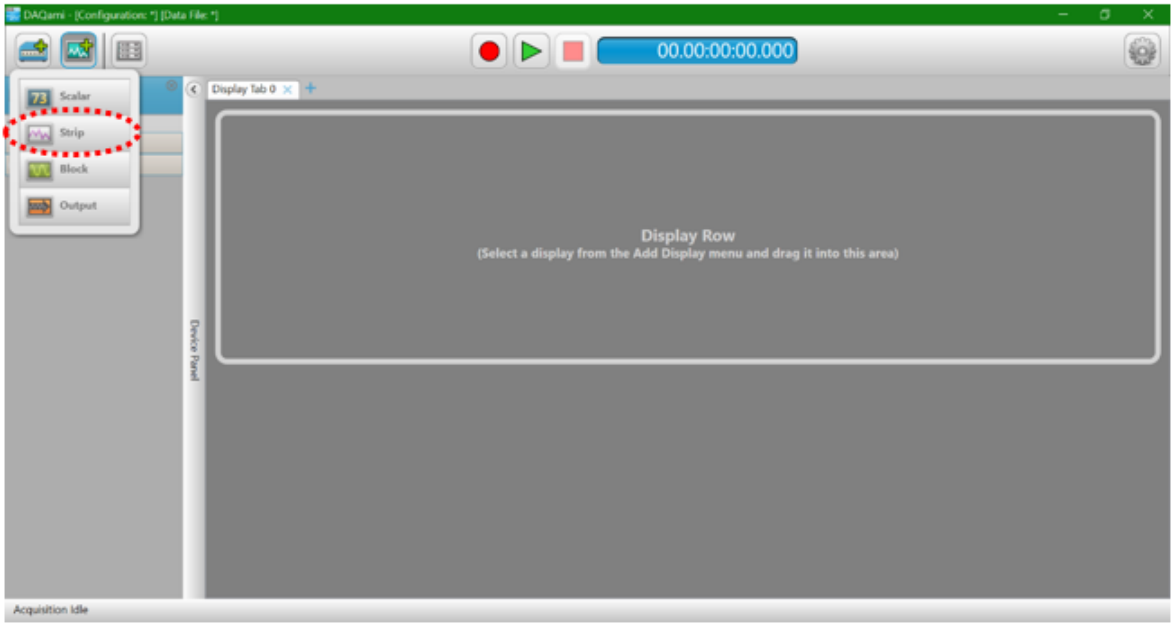

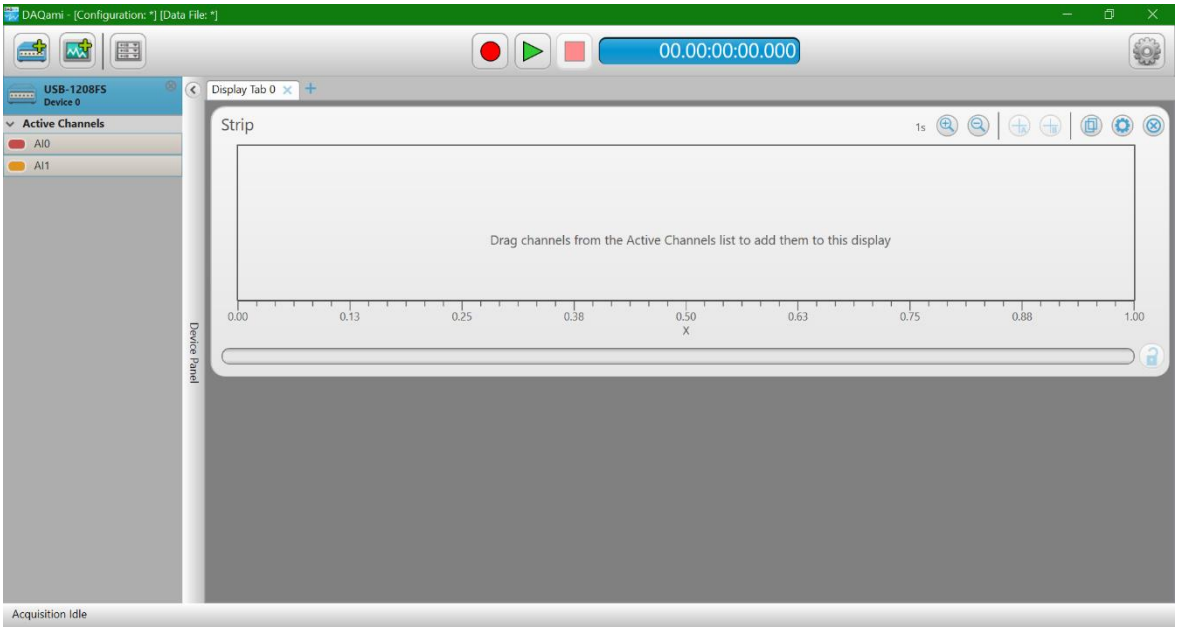

Step 7 – The DAQami software offers two options to record pressure data. The red stop sign records data and automatically logs to the disk. This means the user can easily export the data once the test is finished. The green arrow records data, but does not automatically log to the disk. The red square stops the data recording.
Note: if the recorded data does not automatically offer to export, click on the File and configuration options icon in the upper right corner. Then choose to export data.

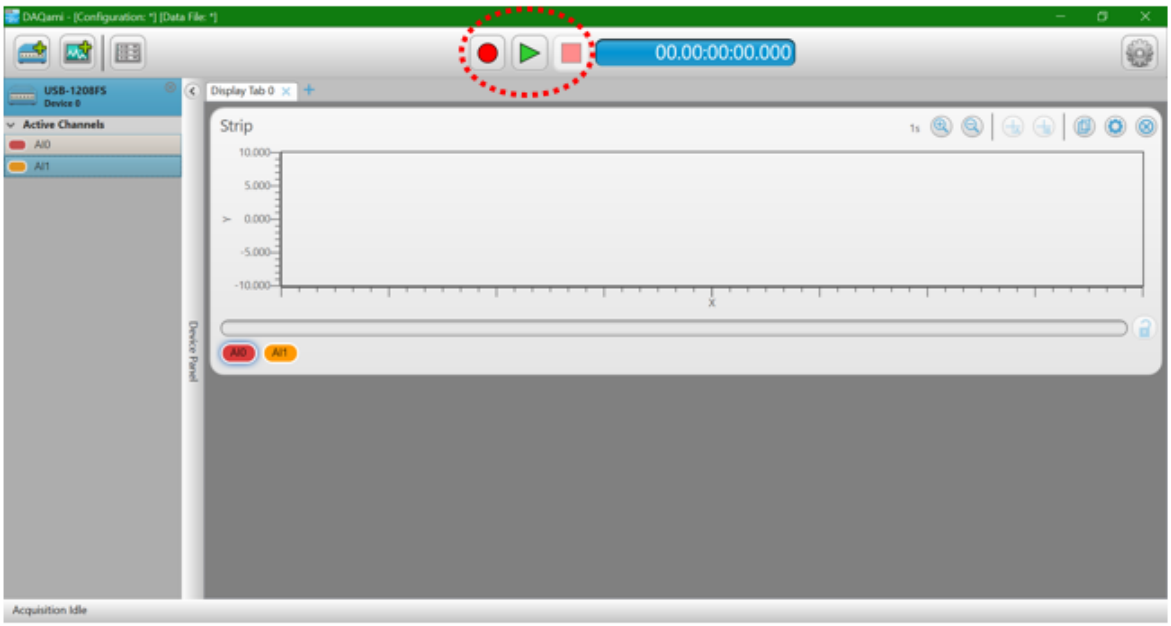

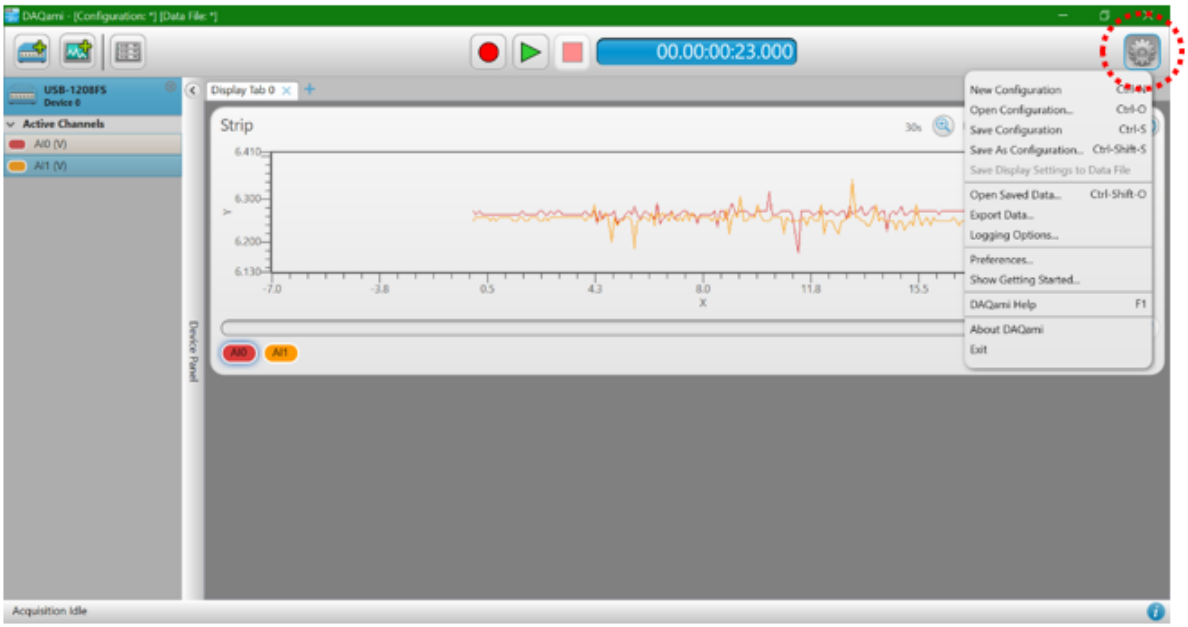

APPENDIX B

RESULTS – FIGURES AND TABLES

Appendix B contains exhaustive results from the compressive strength and cyclic fatigue tests. The density test acted as a specification, so results are not included in the appendix. Slurry that failed its density test was discarded and a new batch mixed to replace it.

This appendix is meant to catalog results from the numerous tests conducted by the author. Perhaps future researchers who use similar equipment will find the information useful.

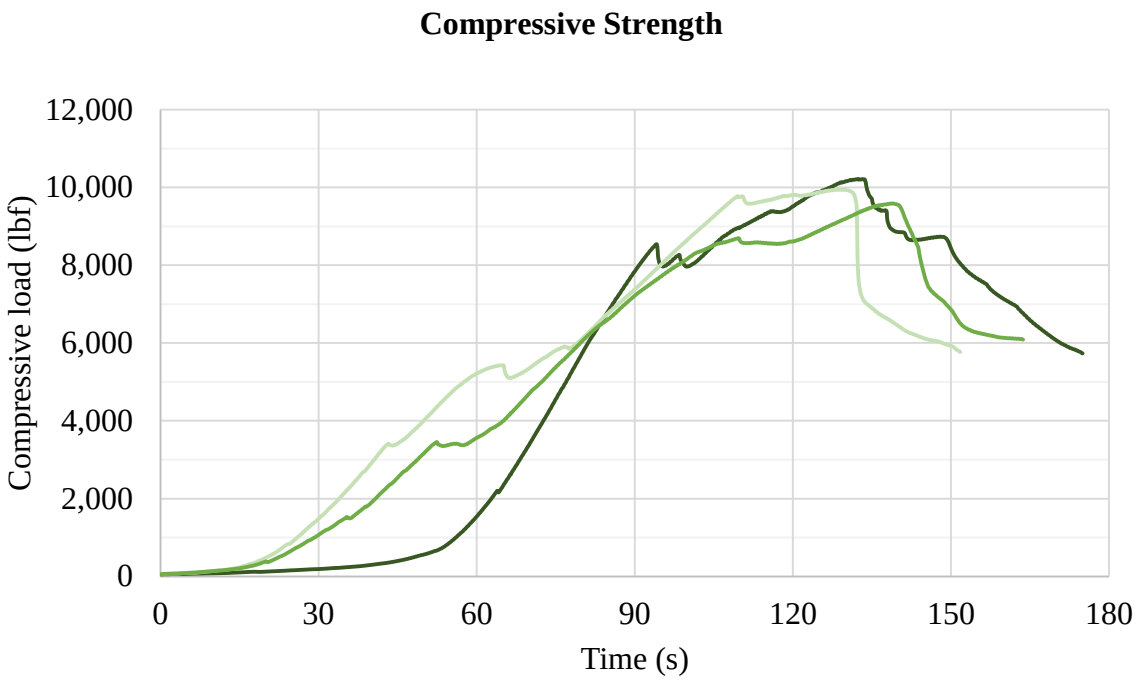

Figure B.1: Compressive strength test for NS 2-1 batch

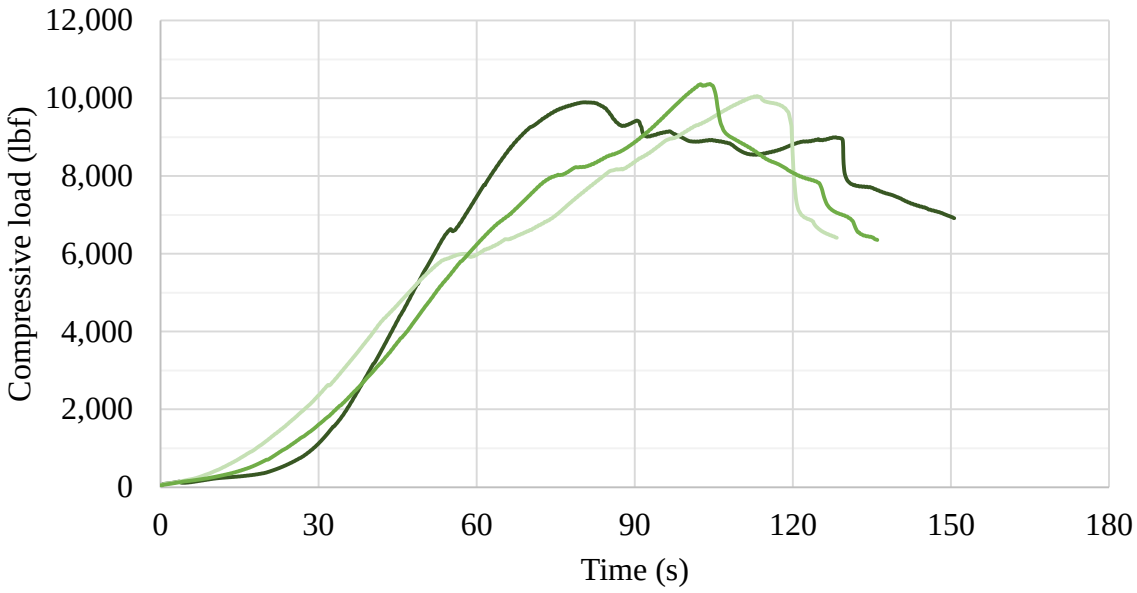

Figure B.2: Compressive strength test for NS 2-2 batch

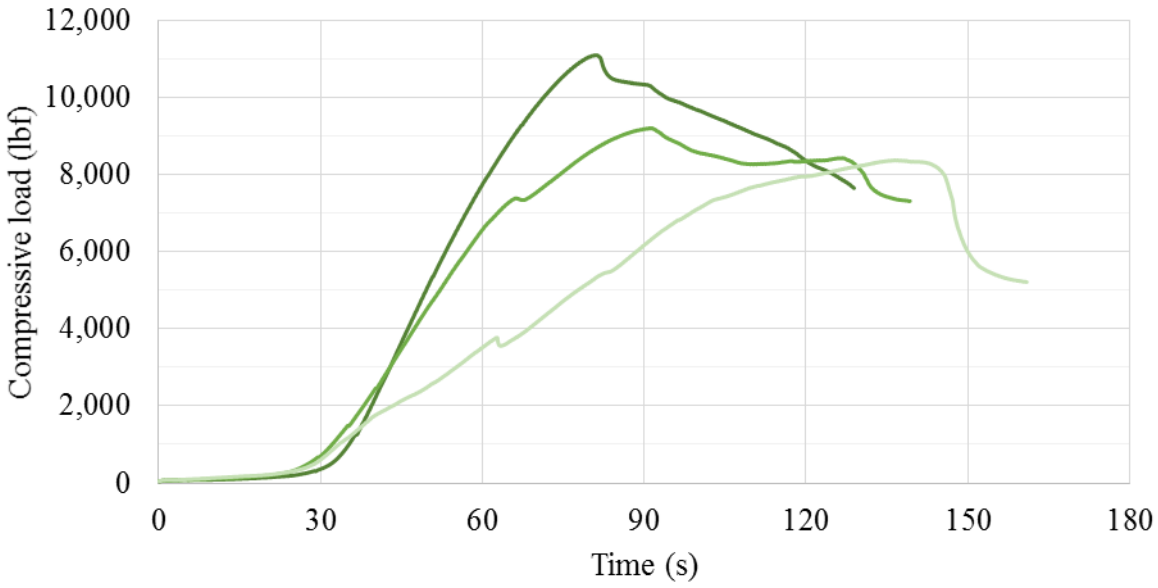

Figure B.3: Compressive strength test for NS 2-3 batch

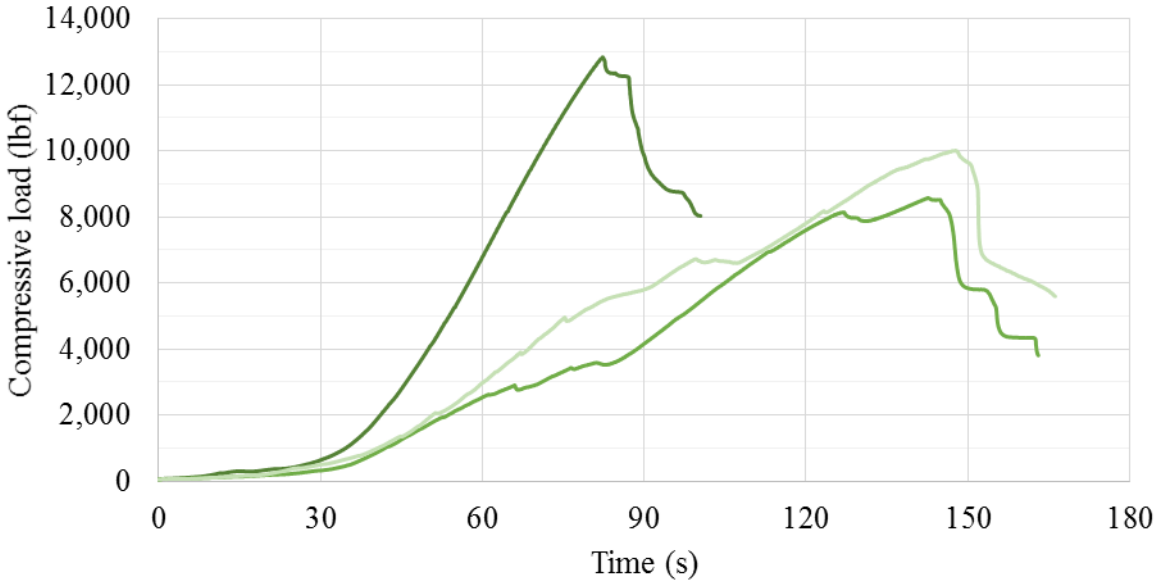

Figure B.4: Compressive strength test for NS 4-1 batch

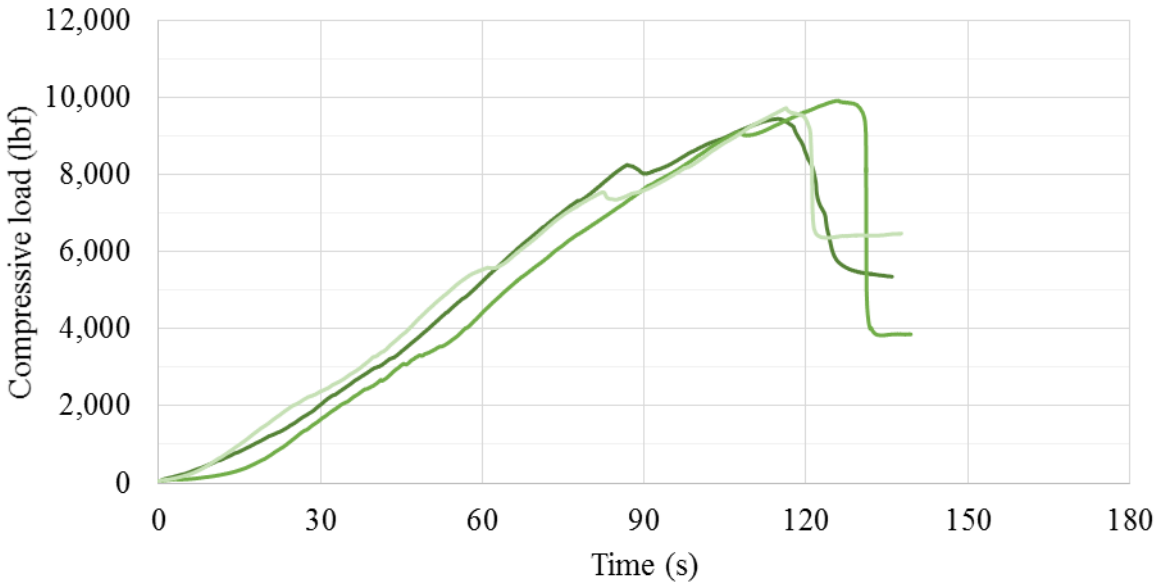

Figure B.5: Compressive strength test for NS 4-2 batch

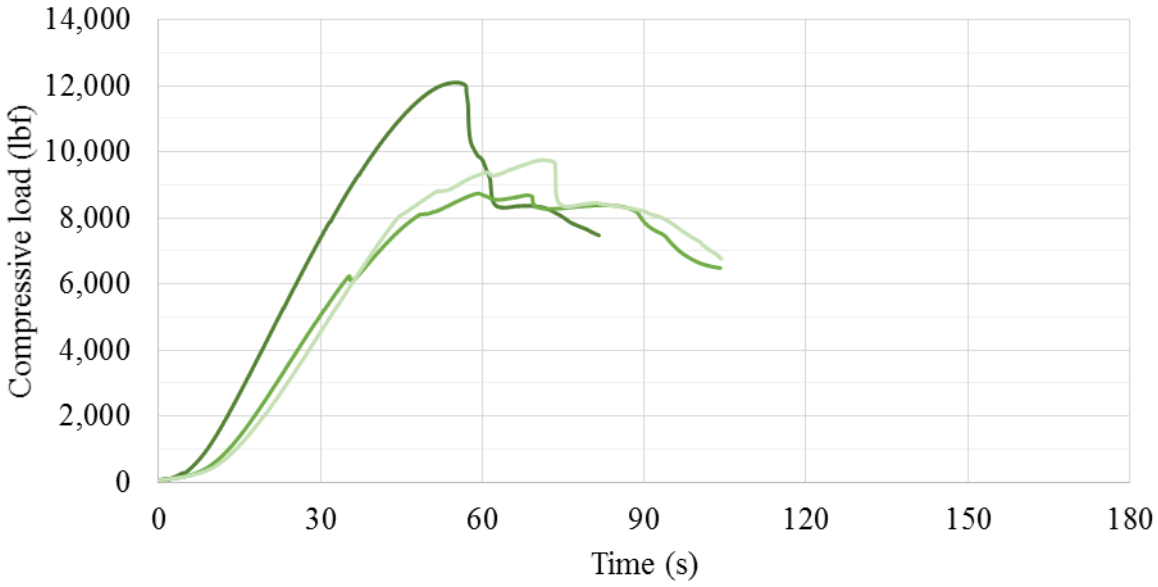

Figure B.6: Compressive strength test for NS 4-3 batch

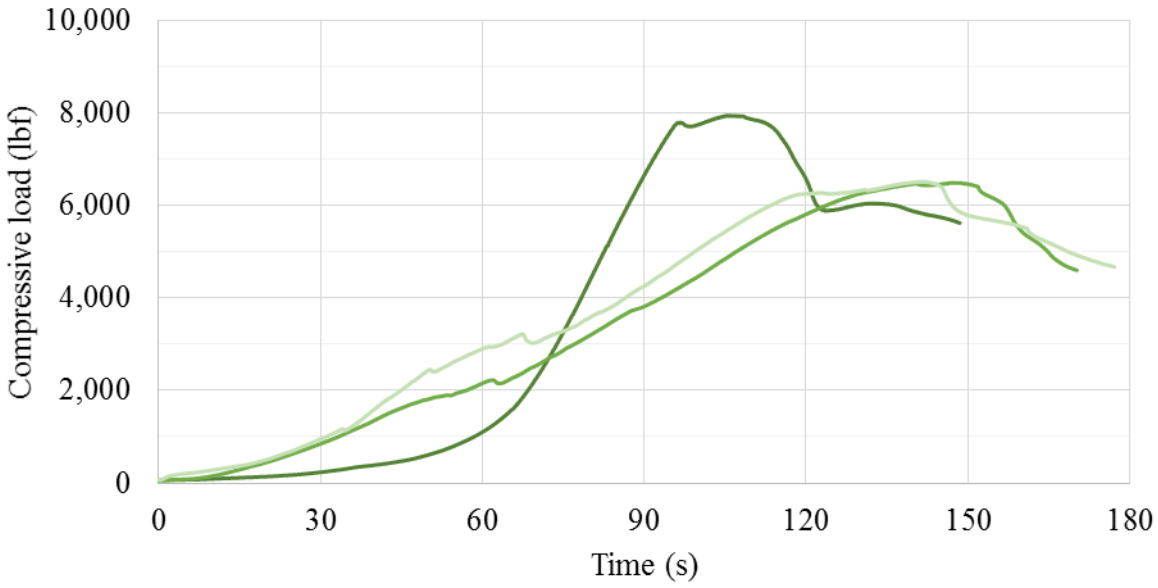

Figure B.7: Compressive strength test for SF 2-1 batch

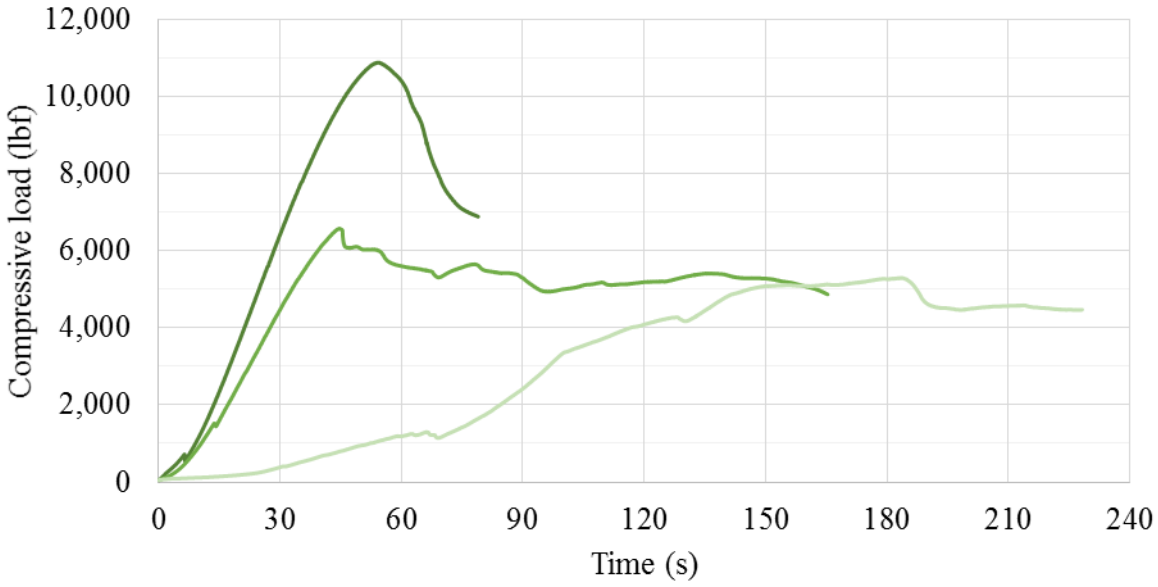

Figure B.8: Compressive strength test for SF 2-3 batch

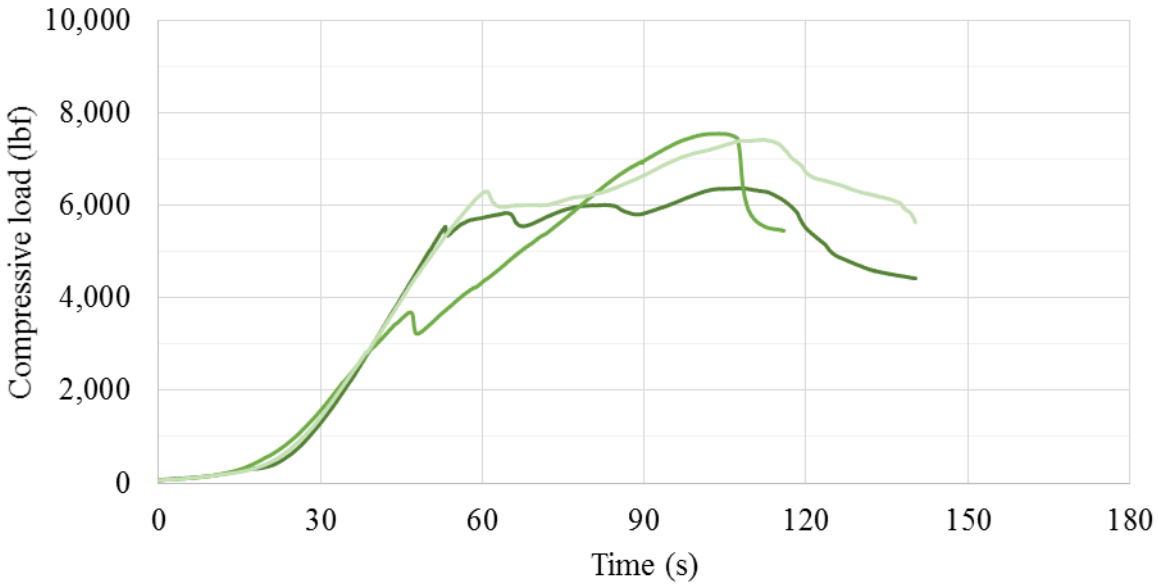

Figure B.9: Compressive strength test for SF 2-1 (no confining) batch

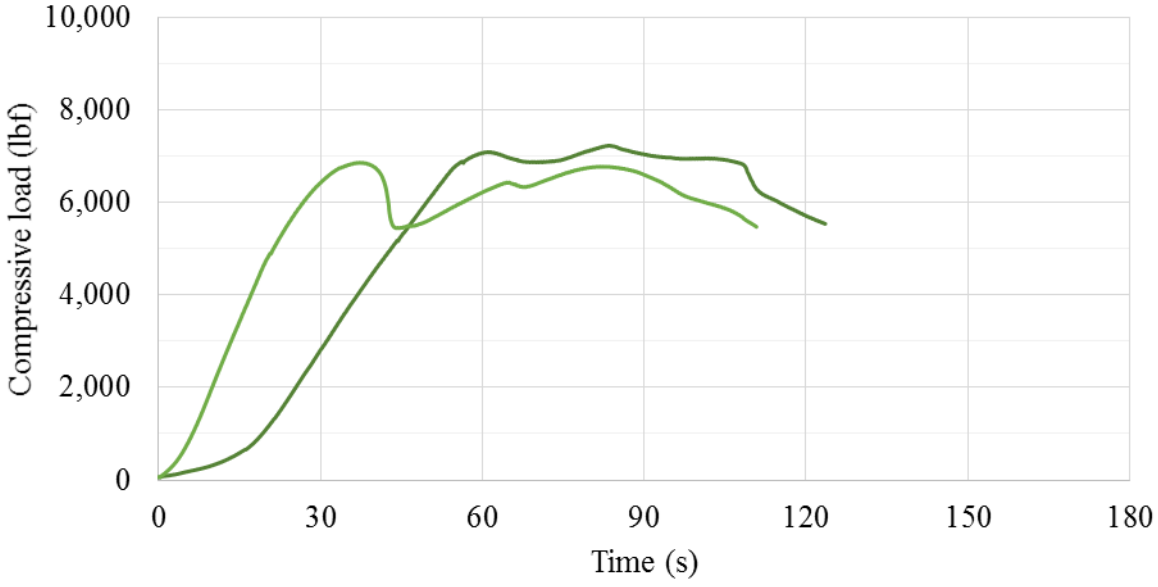

Figure B.10: Compressive strength test for SF 10-1 (no confining) batch

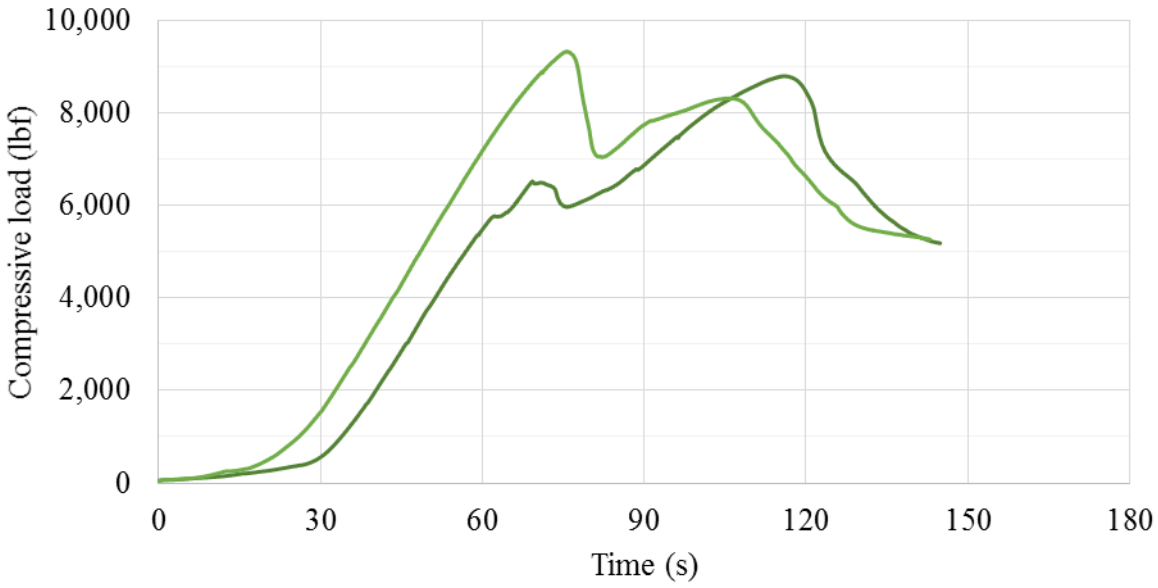

Figure B.11: Compressive strength test for SF 4-1 (Sch. 40 PVC confining) batch

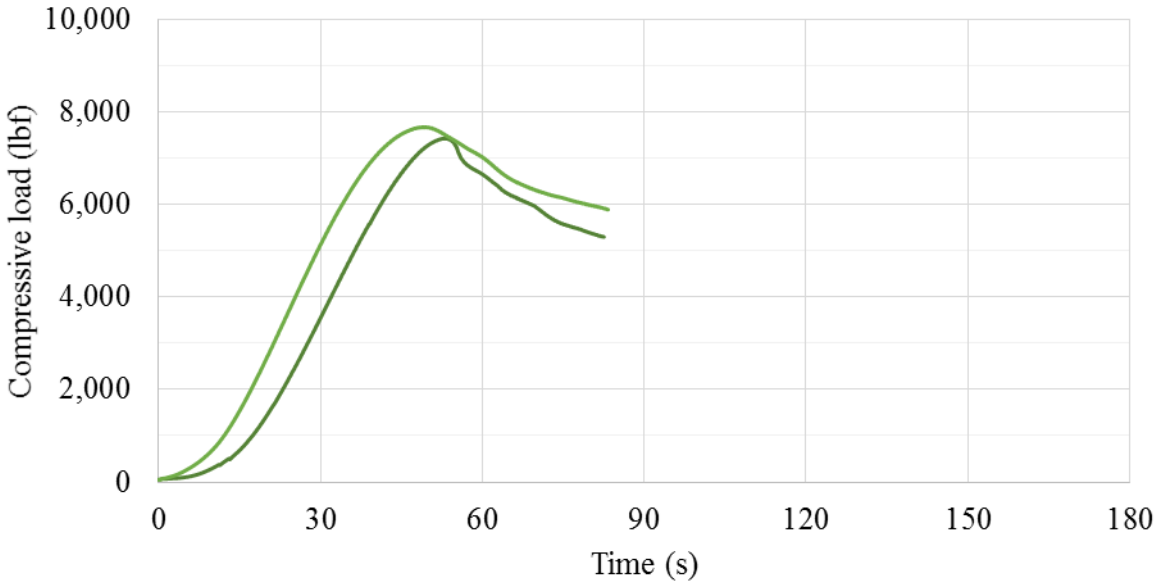

Figure B.12: Compressive strength test for SF 8-1 (Sch. 40 PVC confining) batch

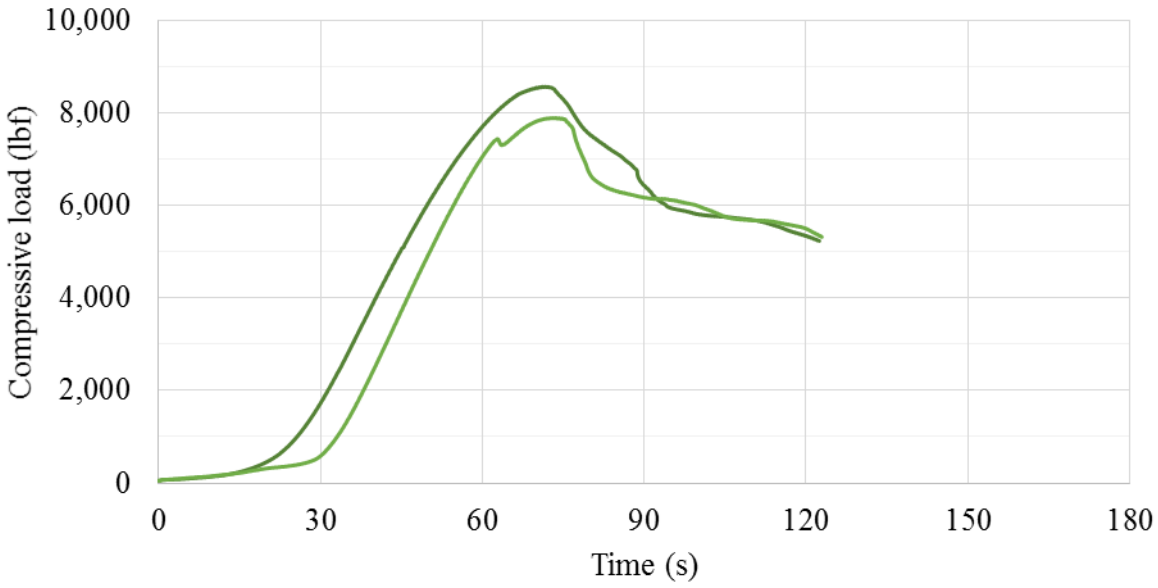

Figure B.13: Compressive strength test for SF 4-1, 8-1 (Sch. 80 PVC confining) batch

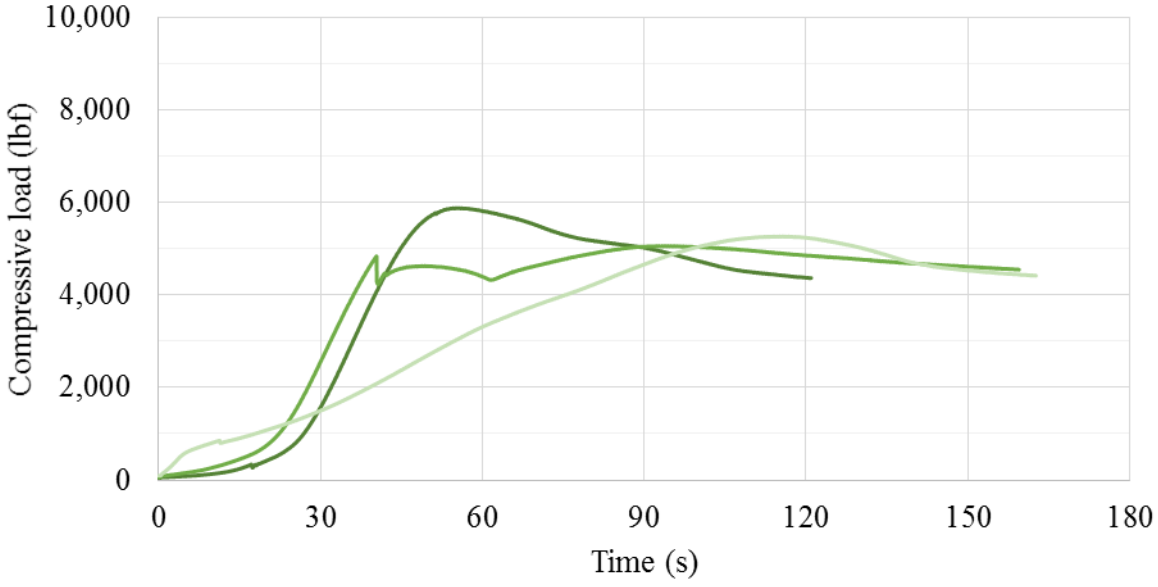

Figure B.14: Compressive strength test for PP 9-1 batch

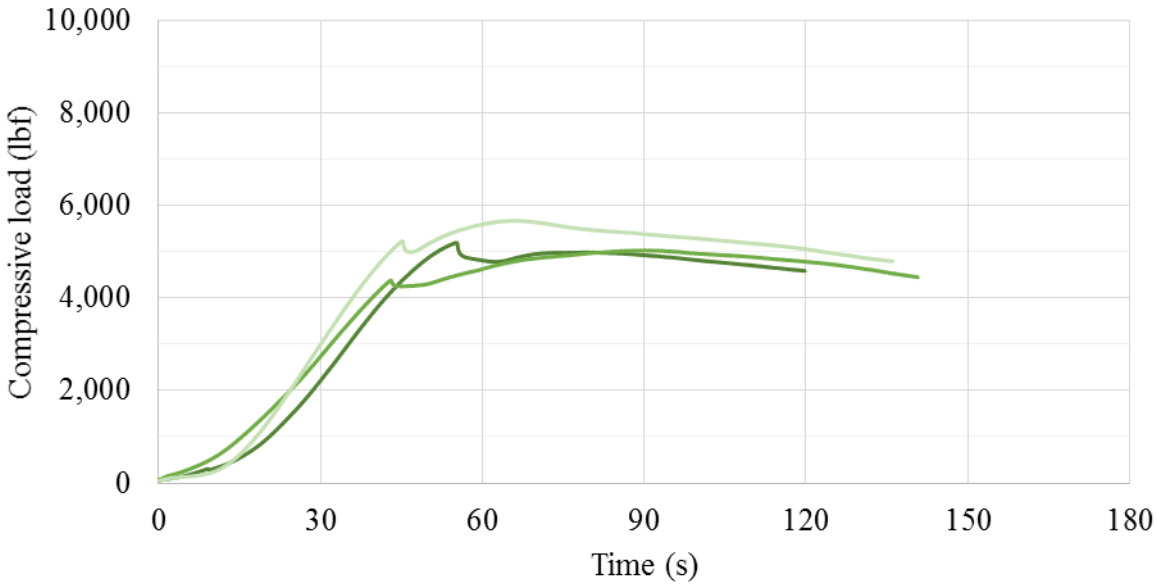

Figure B.15: Compressive strength test for PP 9-2 batch

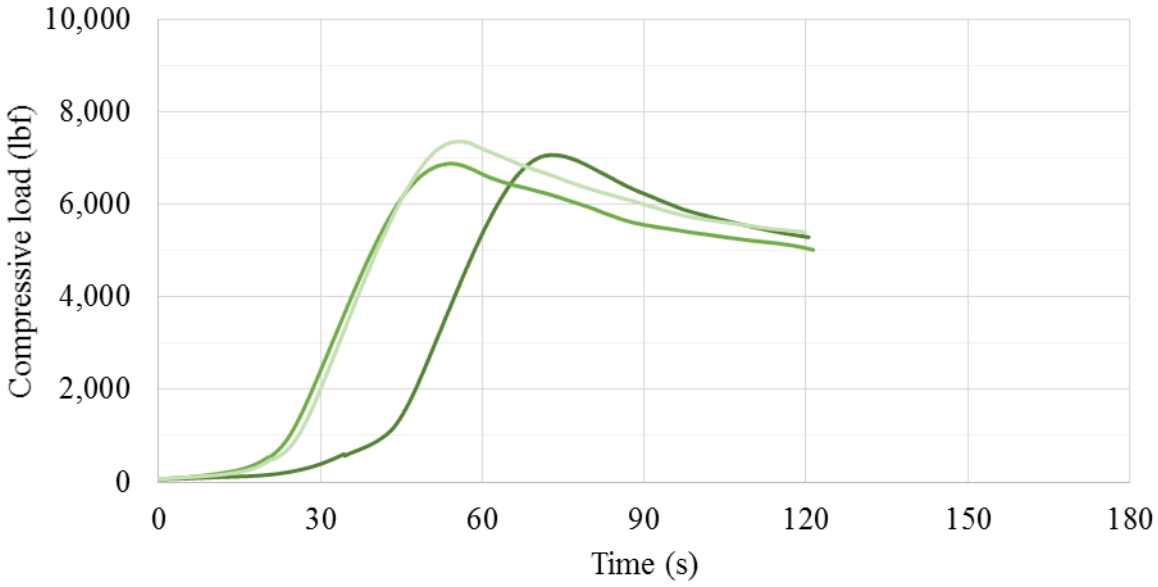

Figure B.16: Compressive strength test for PP 9-3 batch

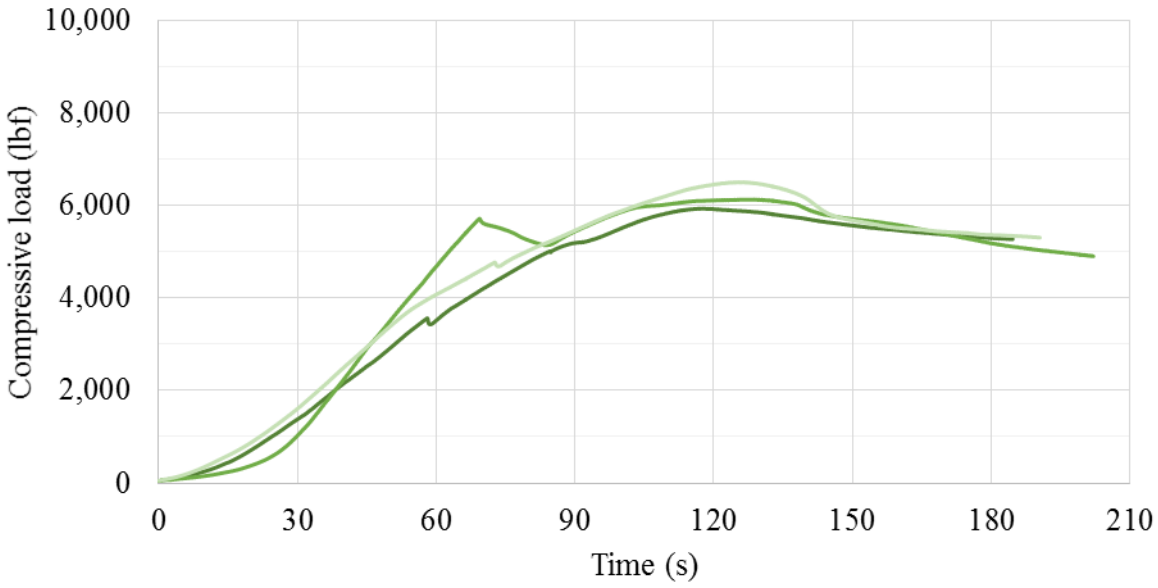

Figure B.17: Compressive strength test for PP 9-4 batch

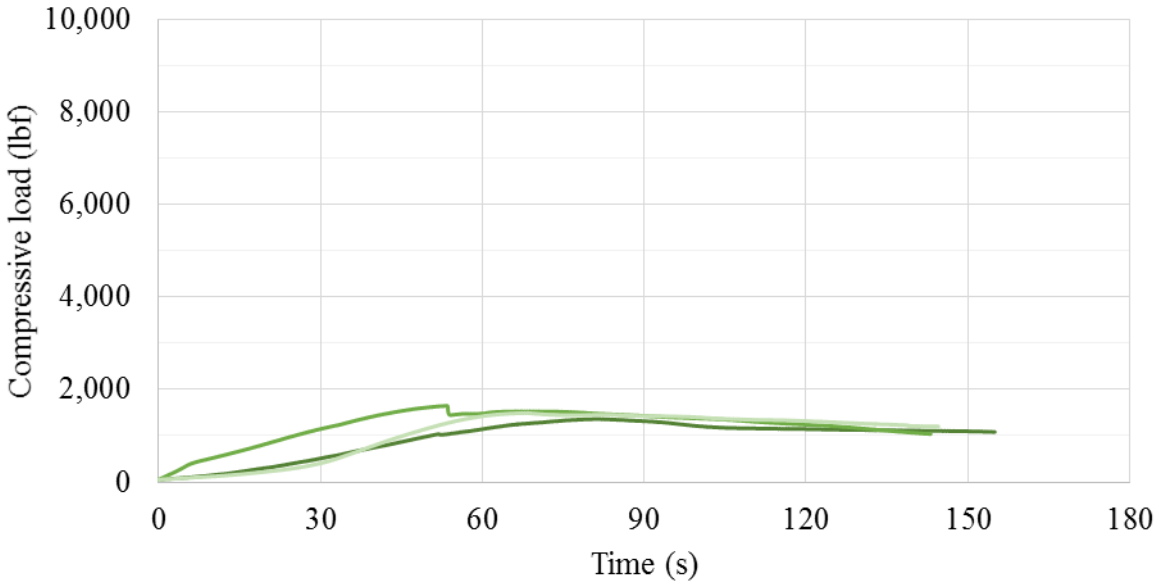

Figure B.18: Compressive strength test for BEN 9-1 batch

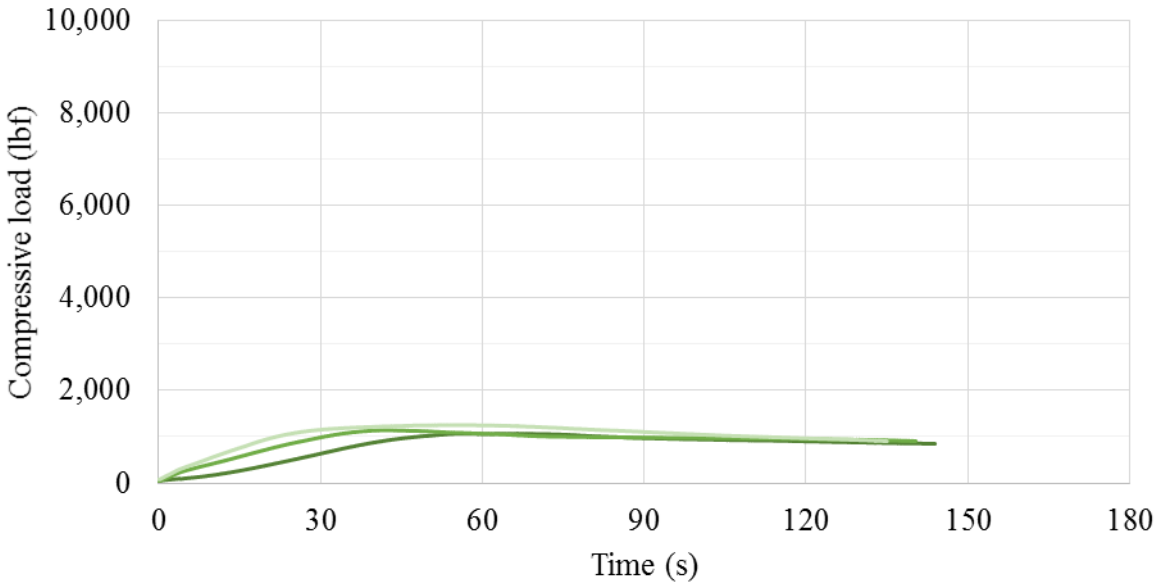

Figure B.19: Compressive strength test for BEN 9-2 batch

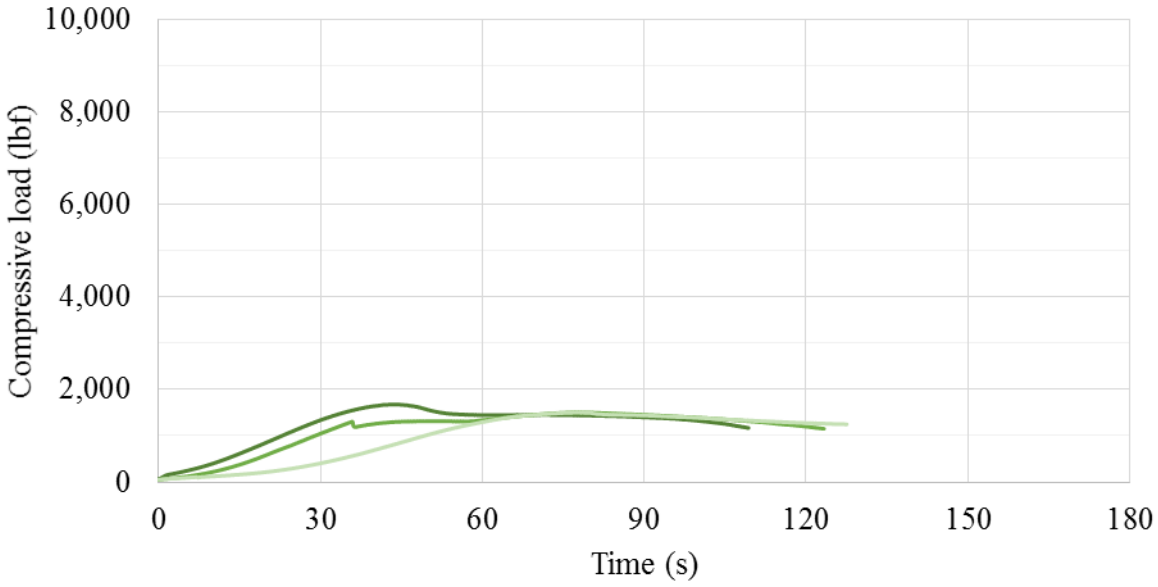

Figure B.20: Compressive strength test for BEN 9-3 batch

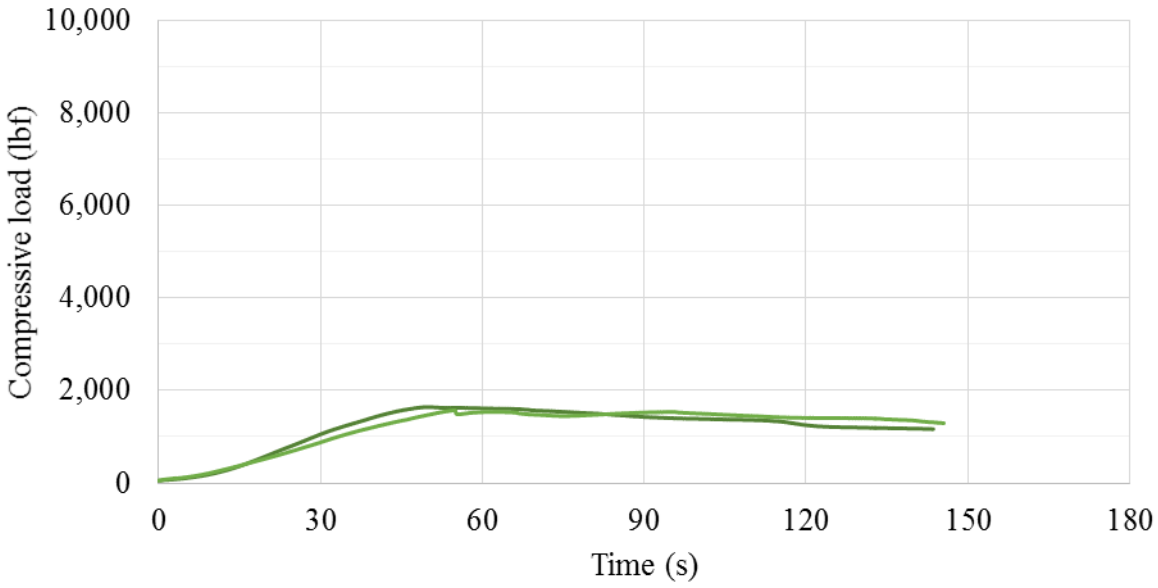

Figure B.21: Compressive strength test for BEN 9-4 batch

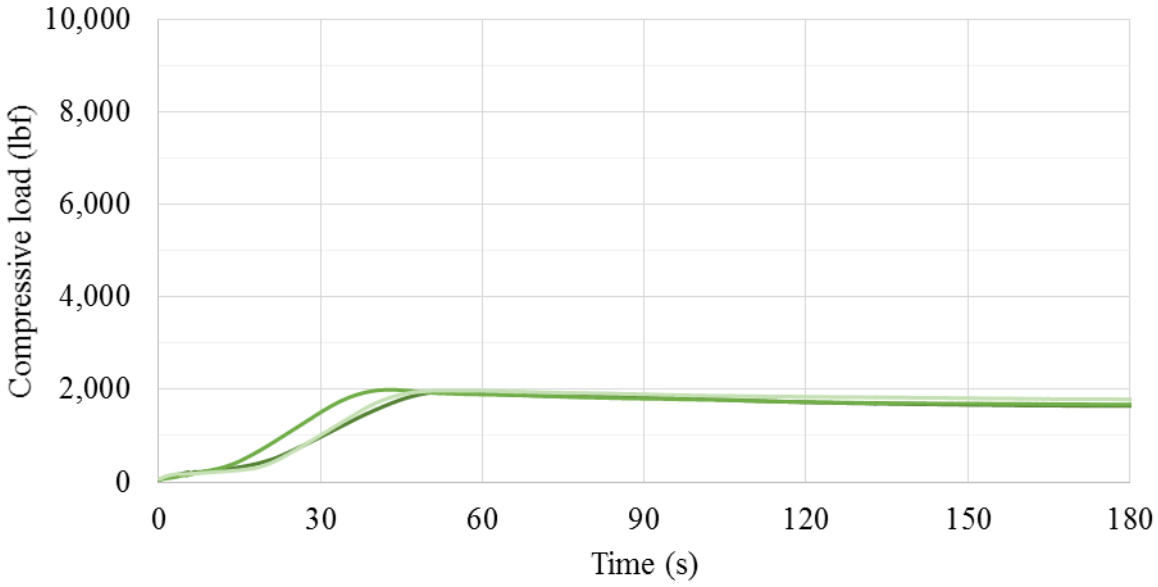

Figure B.22: Compressive strength test for BENPP 9-1 batch

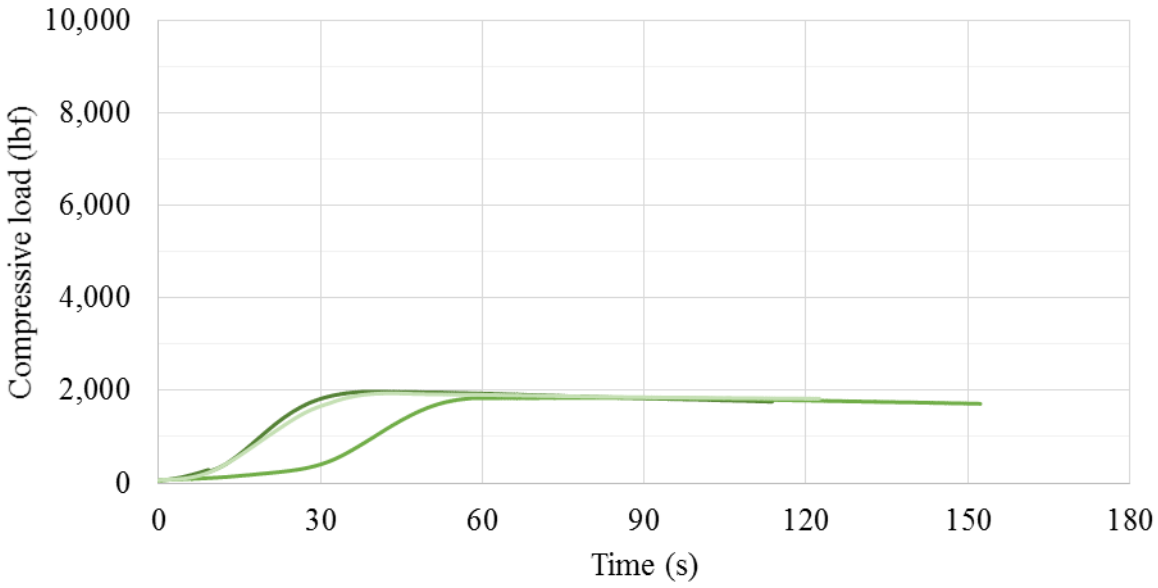

Figure B.23: Compressive strength test for BENPP 9-2 batch

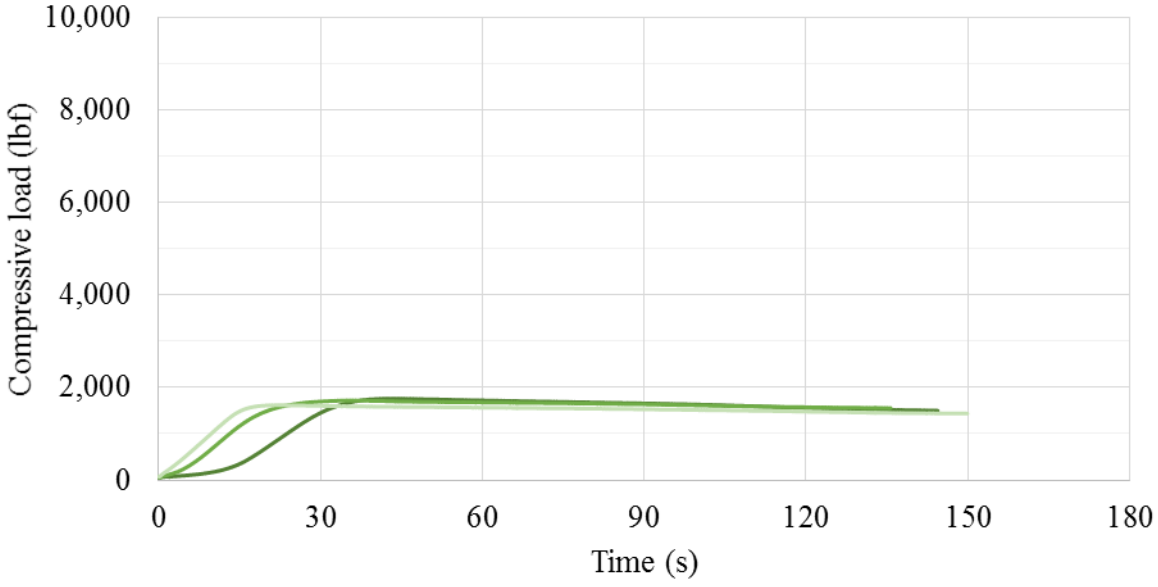

Figure B.24: Compressive strength test for BENPP 9-3 batch

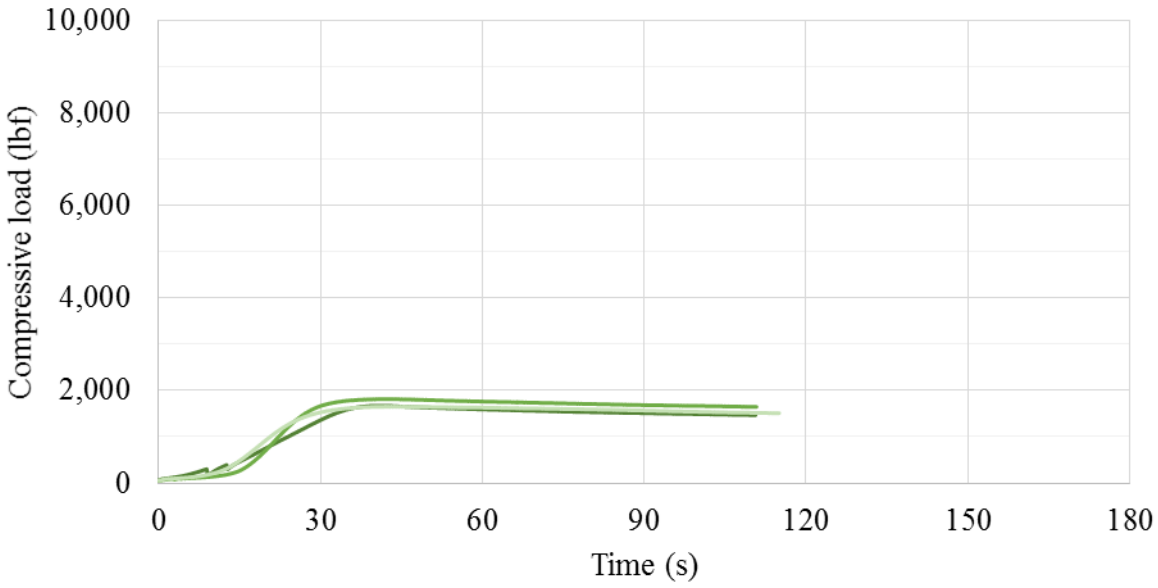

Figure B.25: Compressive strength test for BENPP 9-4 batch

Cyclic Fatigue Pressure Data

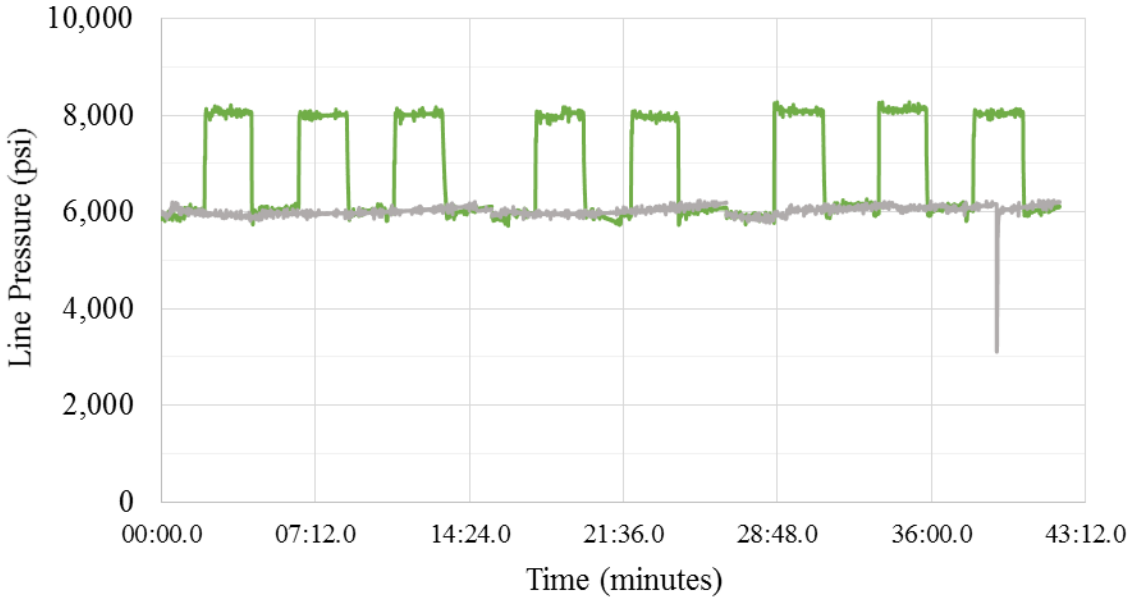

Figure B.26: Cyclic fatigue pressure data for NS 2-2

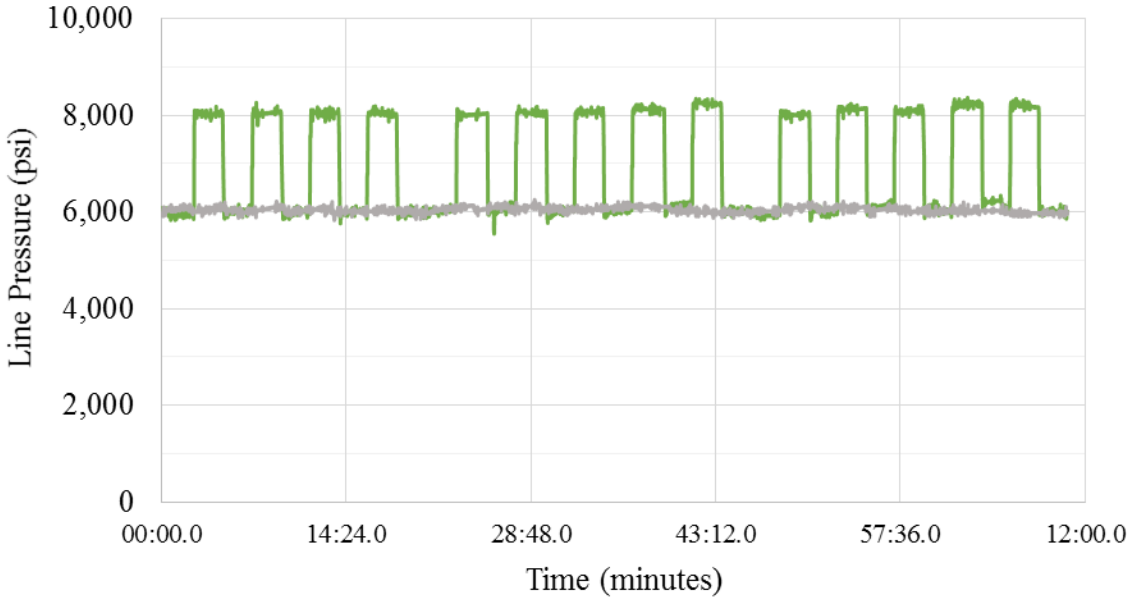

Figure B.27: Cyclic fatigue pressure data for NS 2-3

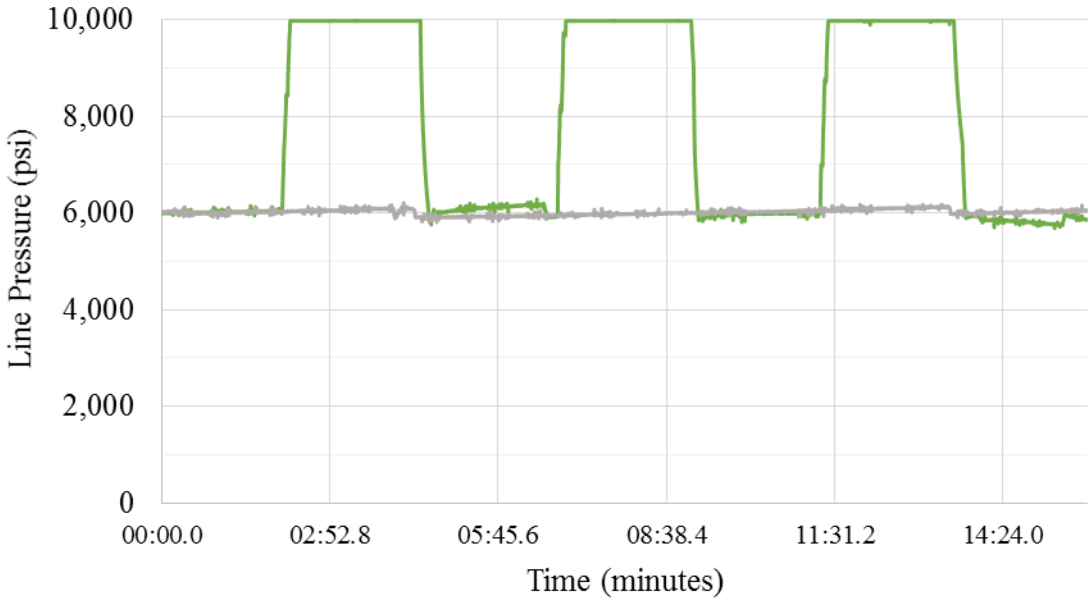

Figure B.28: Cyclic fatigue pressure data for NS 4-1

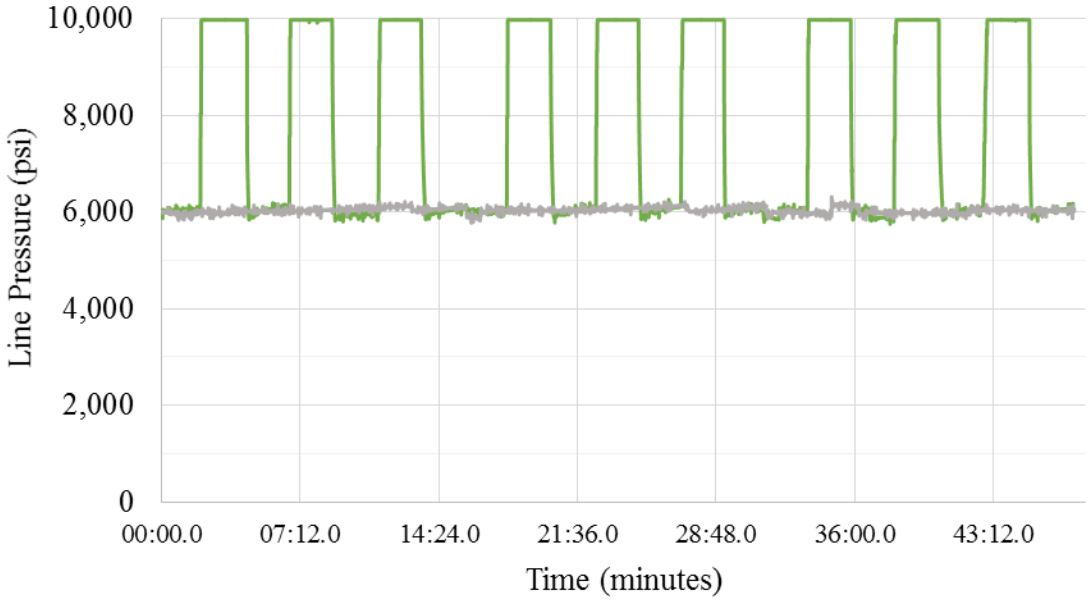

Figure B.29: Cyclic fatigue pressure data for NS 4-2

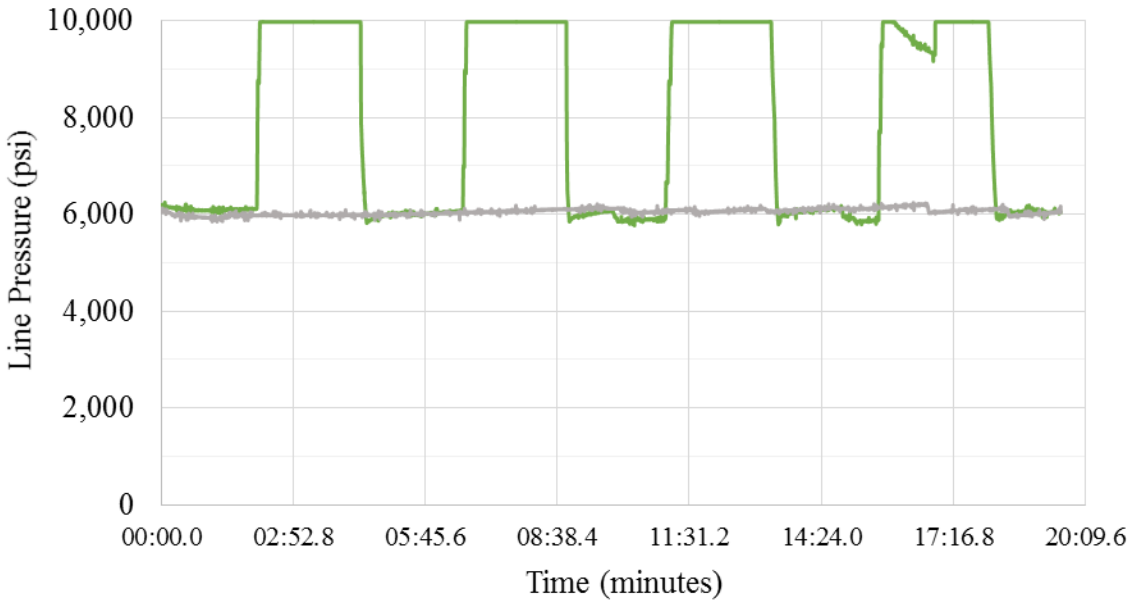

Figure B.30: Cyclic fatigue pressure data for NS 4-3

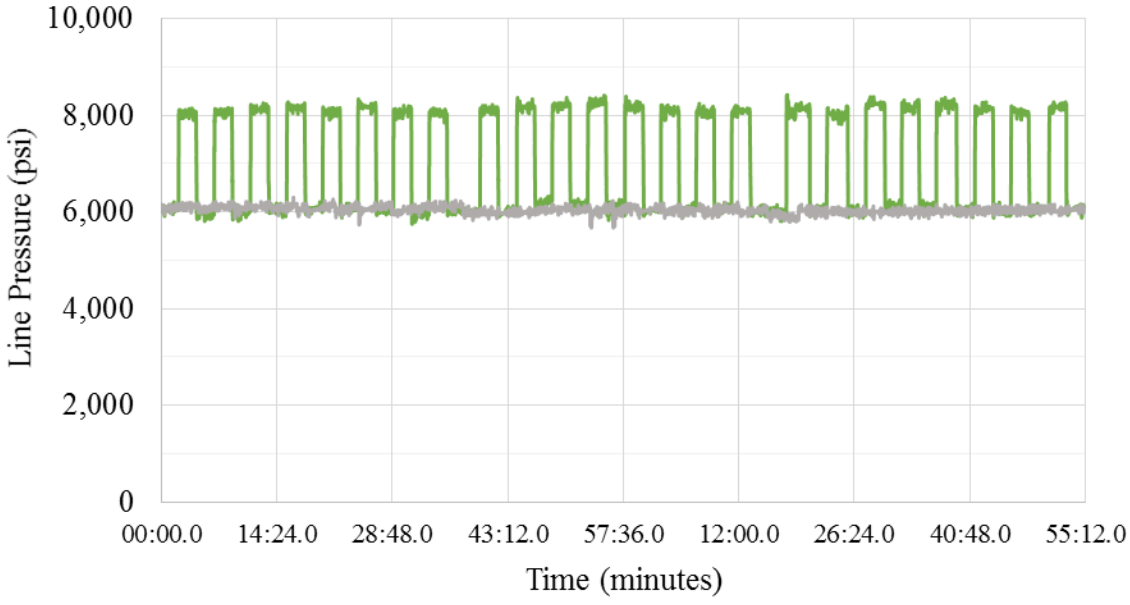

Figure B.31: Cyclic fatigue pressure data for SF 2-1

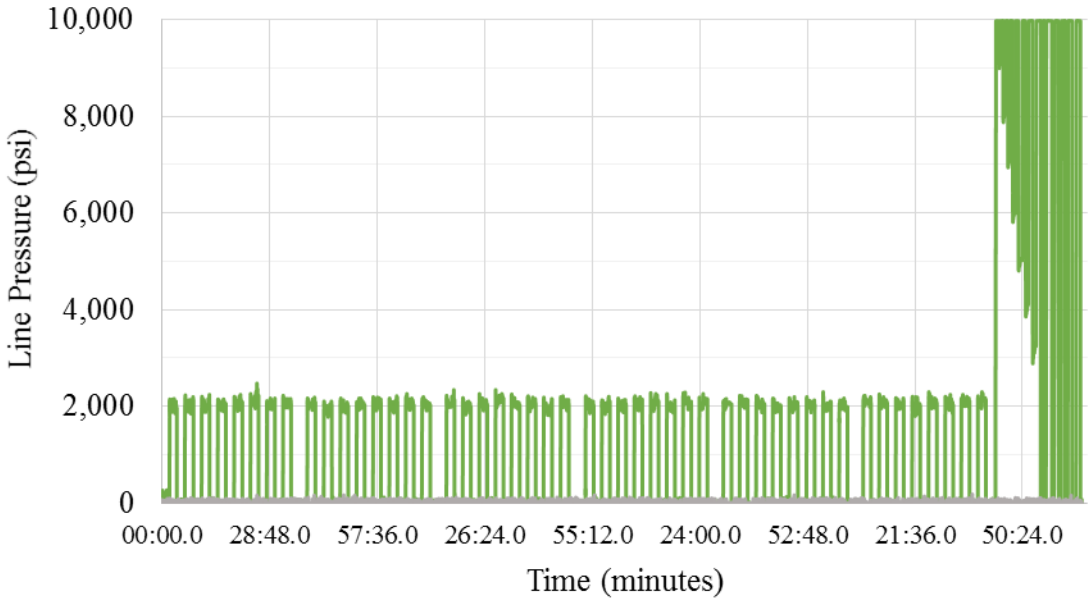

Figure B.32: Cyclic fatigue pressure data for SF 2-1 (no confining pressure)

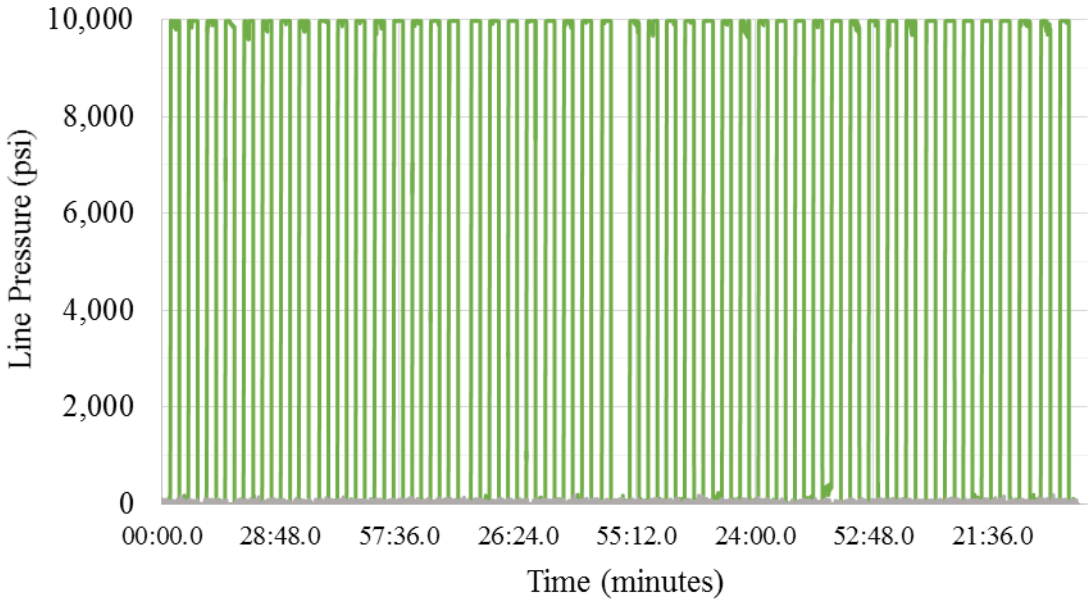

Figure B.33: Cyclic fatigue pressure data for SF 10-1 (no confining pressure)

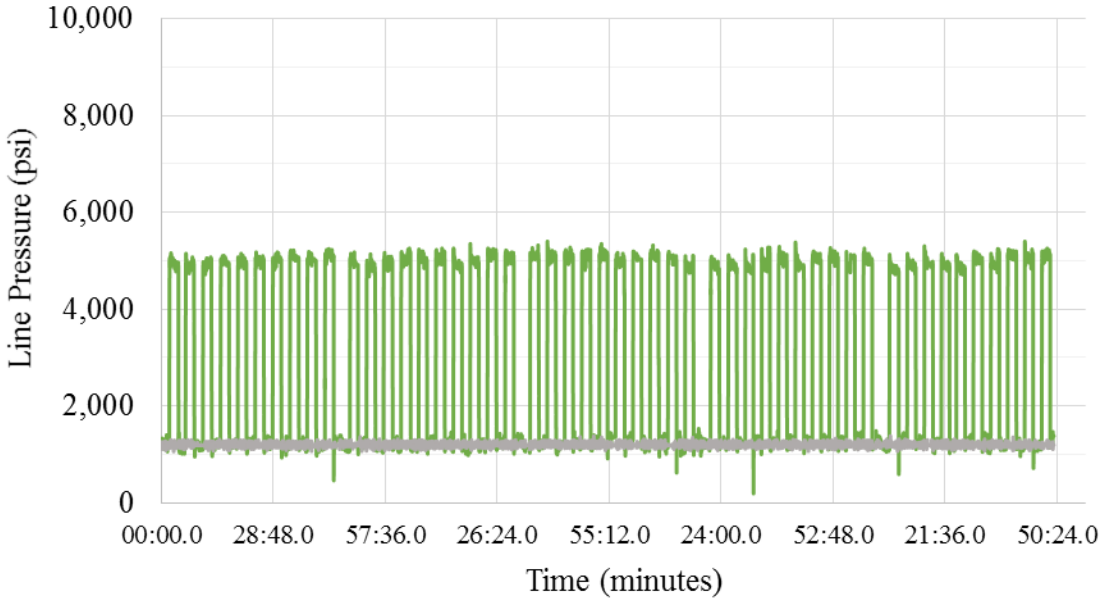

Figure B.34: Cyclic fatigue pressure data for SF 4-1 (Sch. 40 PVC confining)

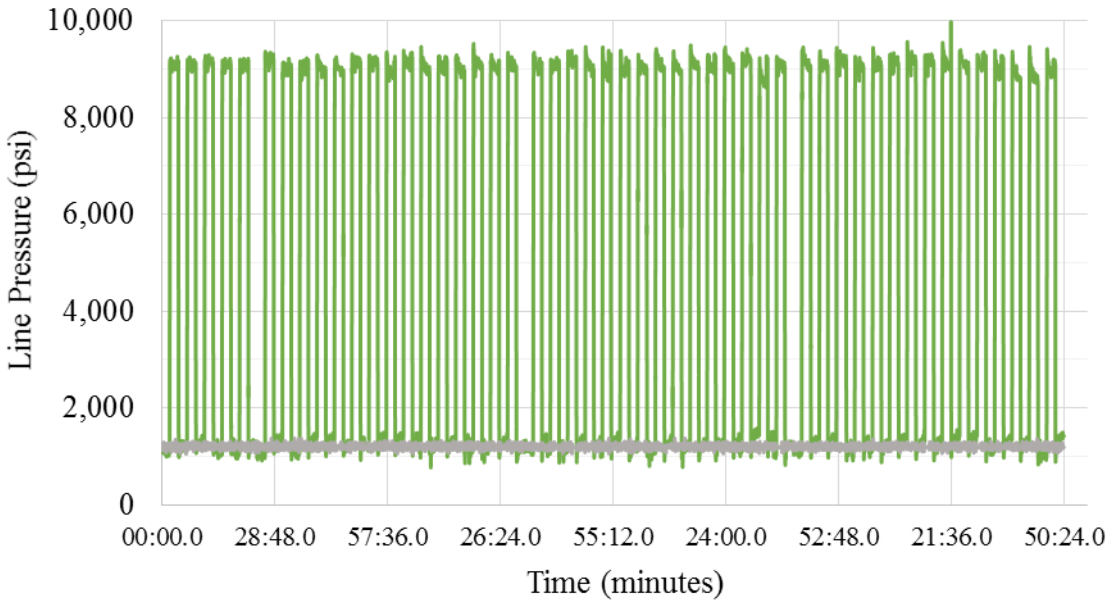

Figure B.35: Cyclic fatigue pressure data for SF 8-1 (Sch. 40 PVC confining)

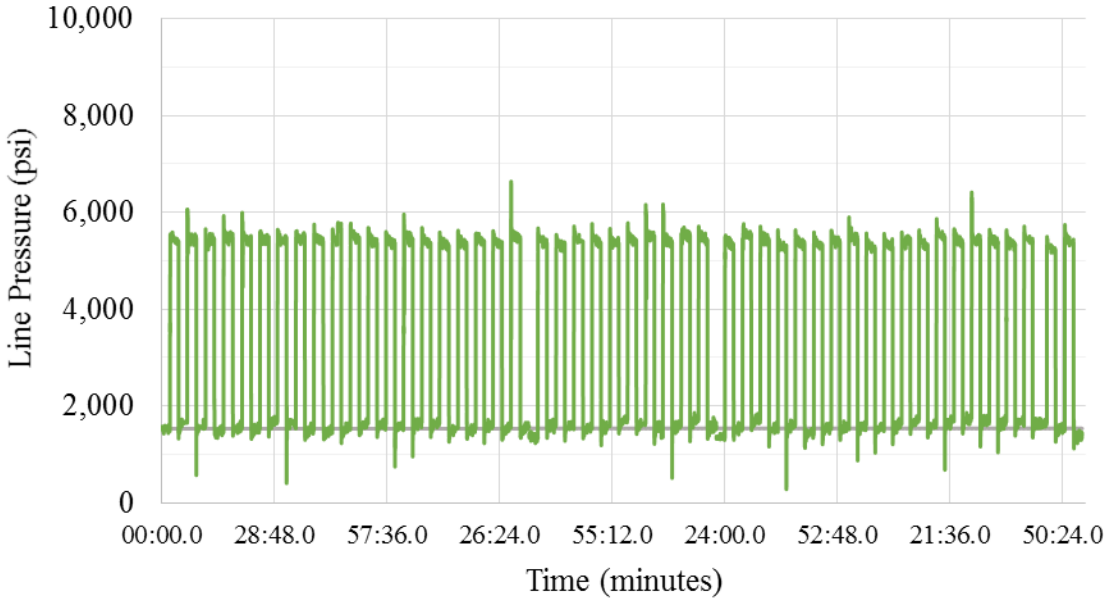

Figure B.36: Cyclic fatigue pressure data for SF 4-1 (Sch. 80 PVC confining)

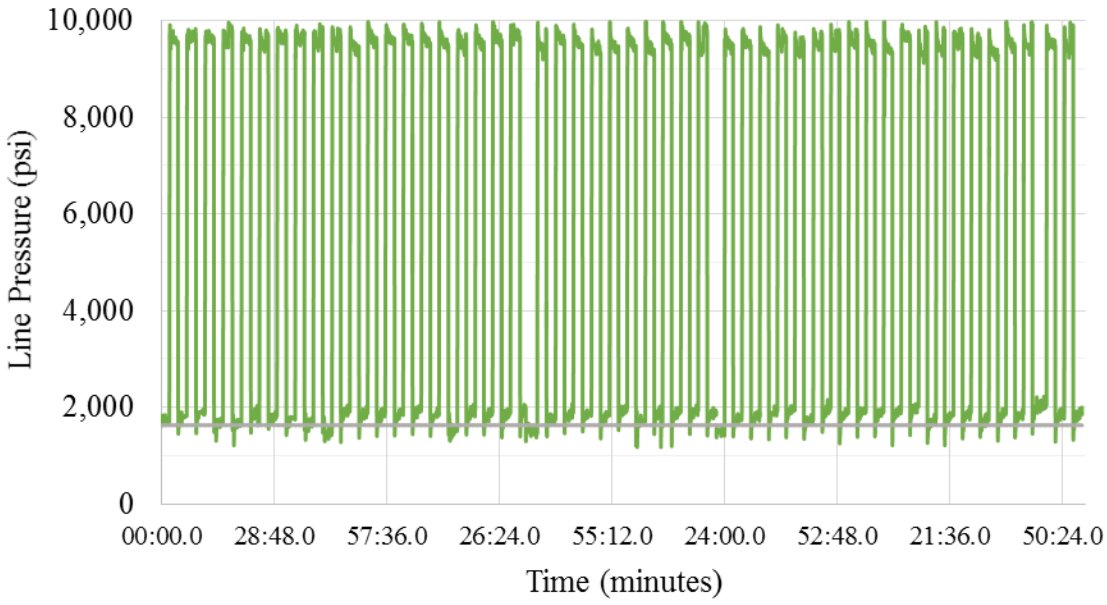

Figure B.37: Cyclic fatigue pressure data for SF 8-1 (Sch. 80 PVC confining)

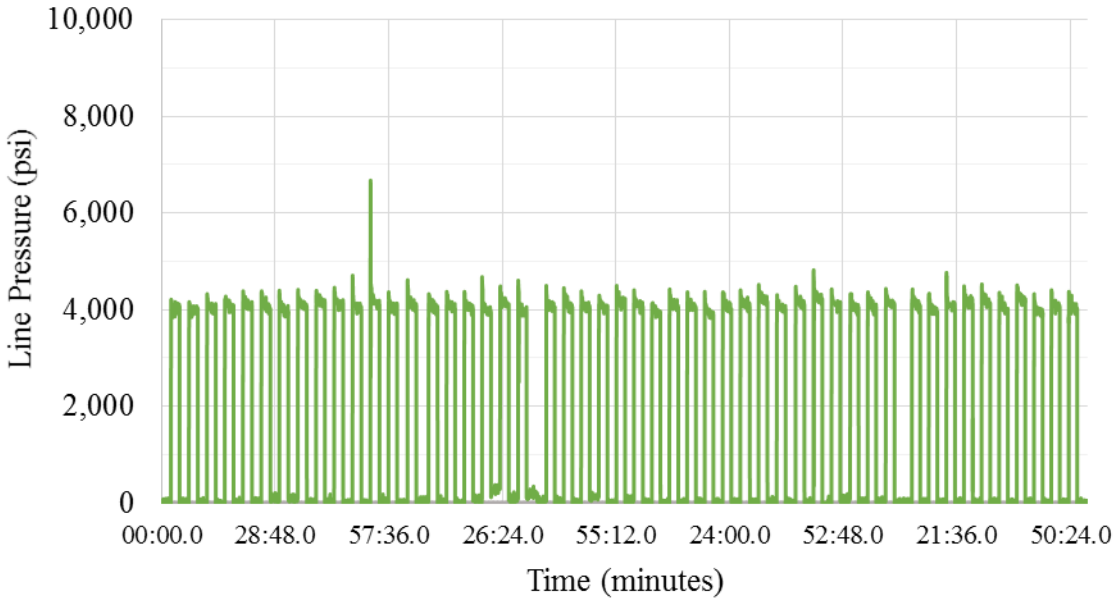

Figure B.38: Cyclic fatigue pressure data for 14.0 ppg SF 4-1 (no confining)

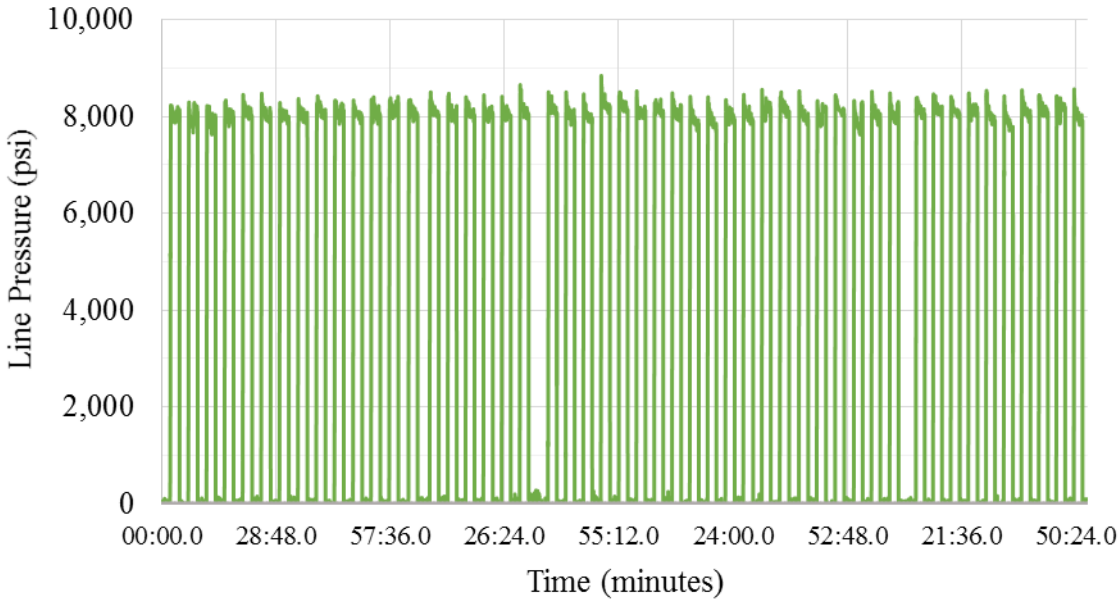

Figure B.39: Cyclic fatigue pressure test data for 14.0 ppg SF 8-1 (no confining)

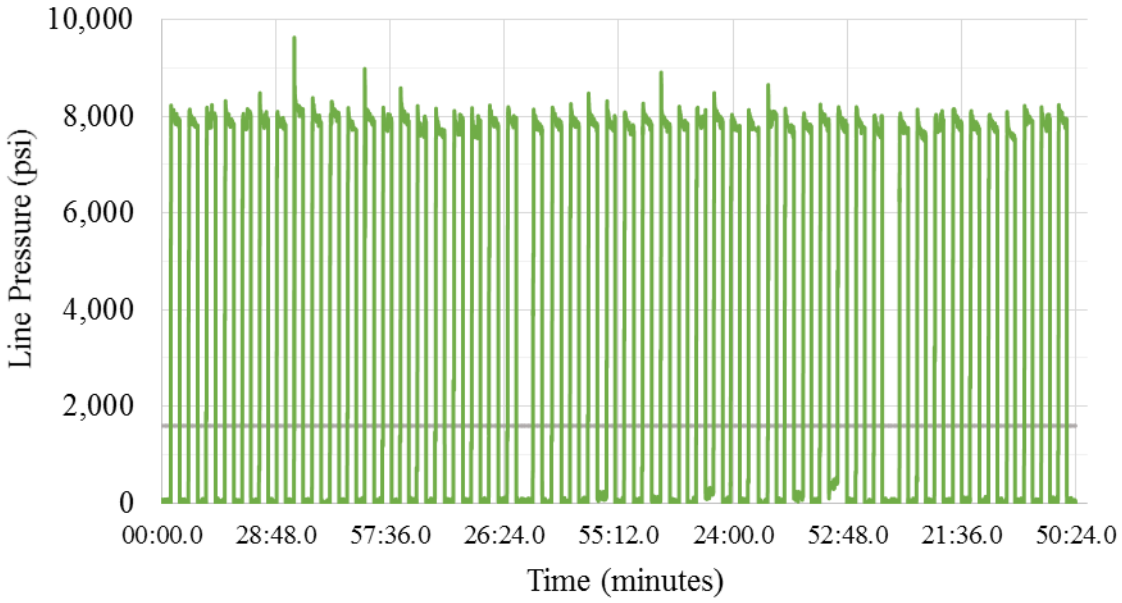

Figure B.40: Cyclic fatigue pressure data for 14.0 ppg SF 6.4-1 (Sch. 80 confining)

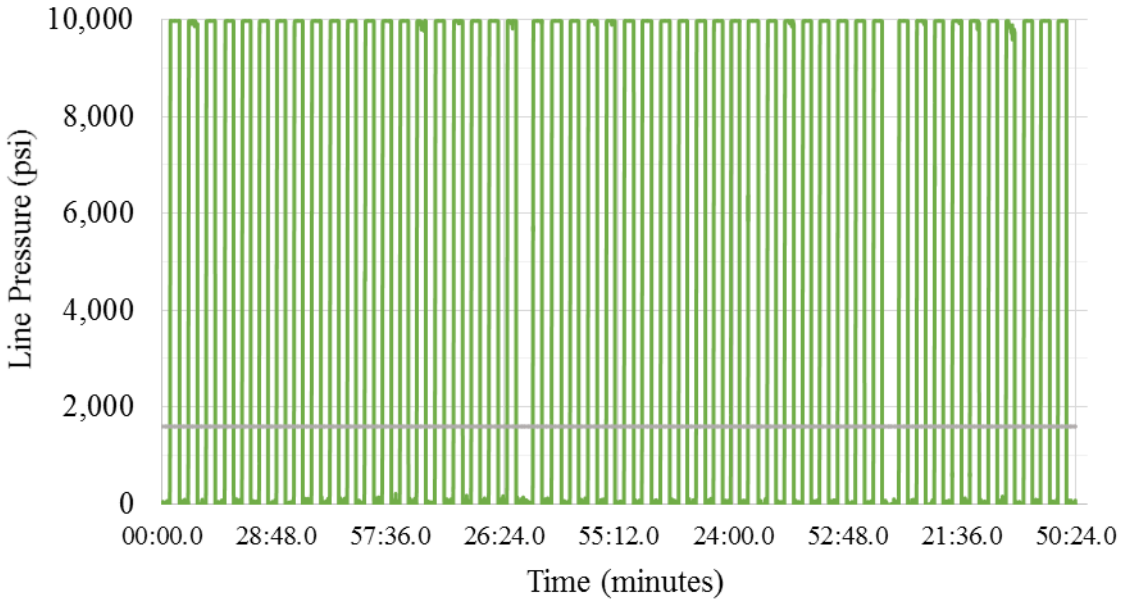

Figure B.41: Cyclic fatigue pressure data for 14.0 ppg SF 8.4-1 (Sch. 80 PVC confining)

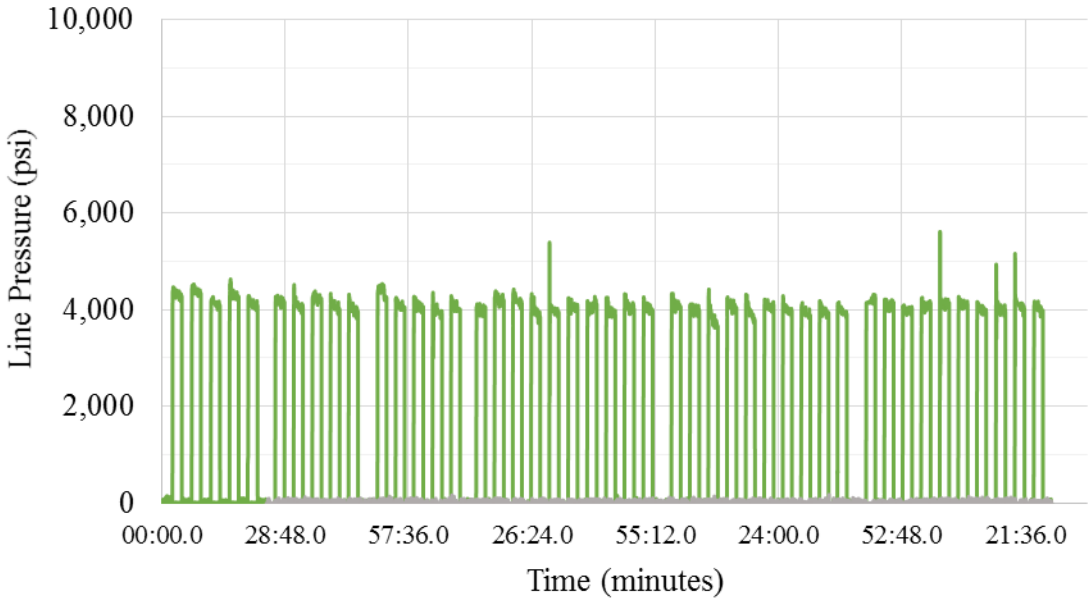

Figure B.42: Cyclic fatigue pressure data for SF 4-1 w/ temperature cycles (no confining)

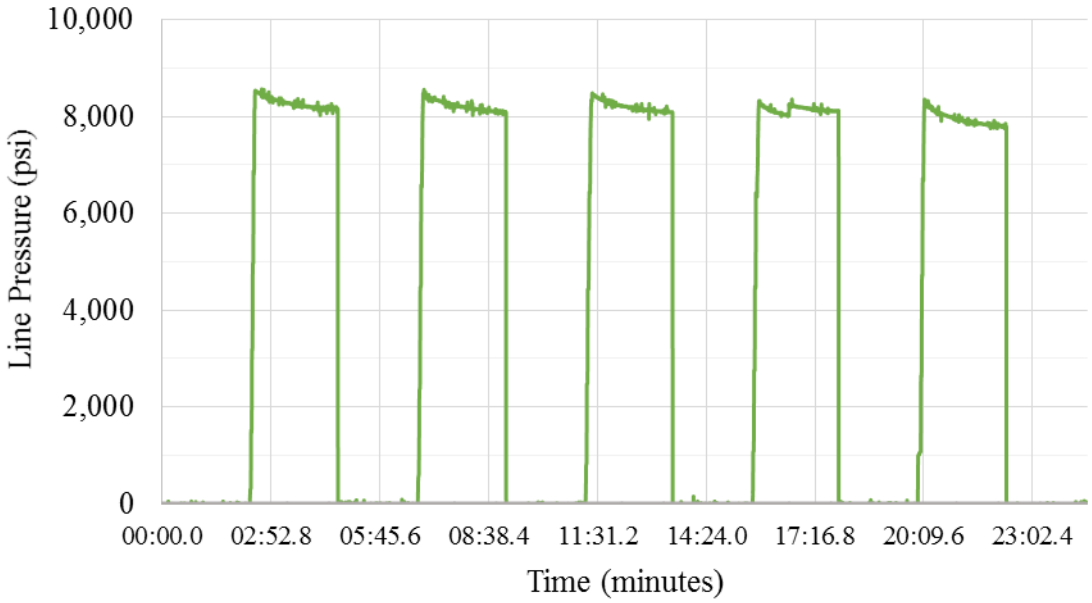

Figure B.43: Cyclic fatigue pressure data for SF 8-1 w/ temperature cycles (no confining)

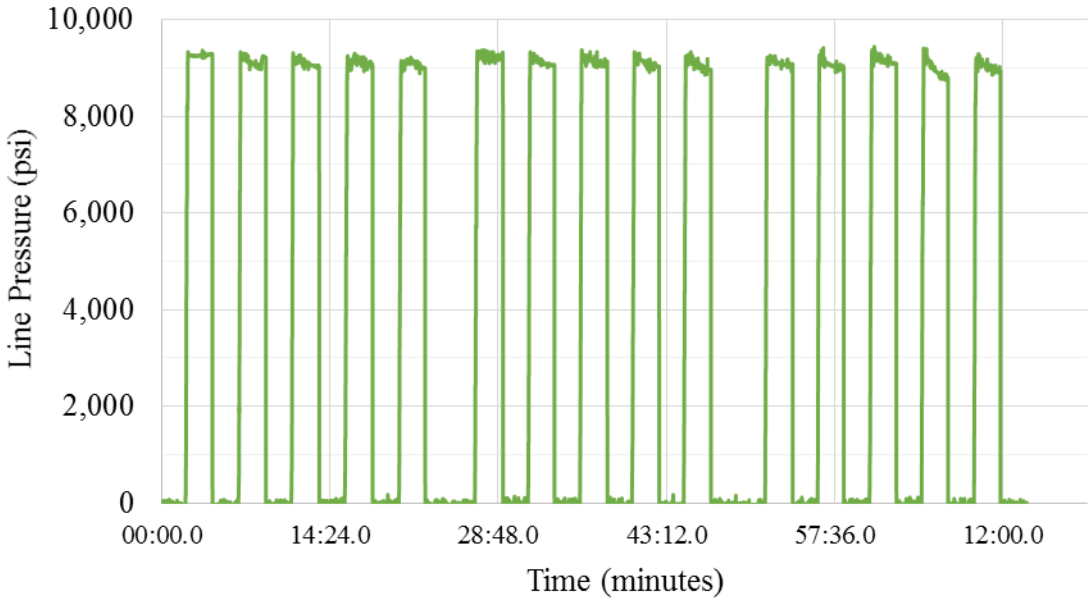

Figure B.44: Cyclic fatigue pressure data for NS 9-1

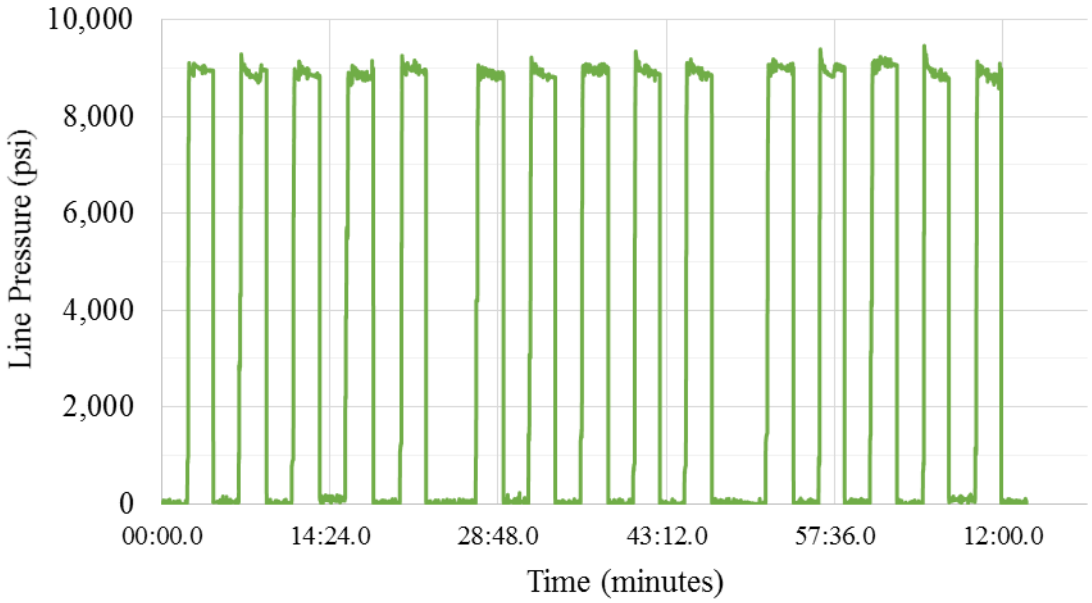

Figure B.45: Cyclic fatigue pressure data for NS 9-2

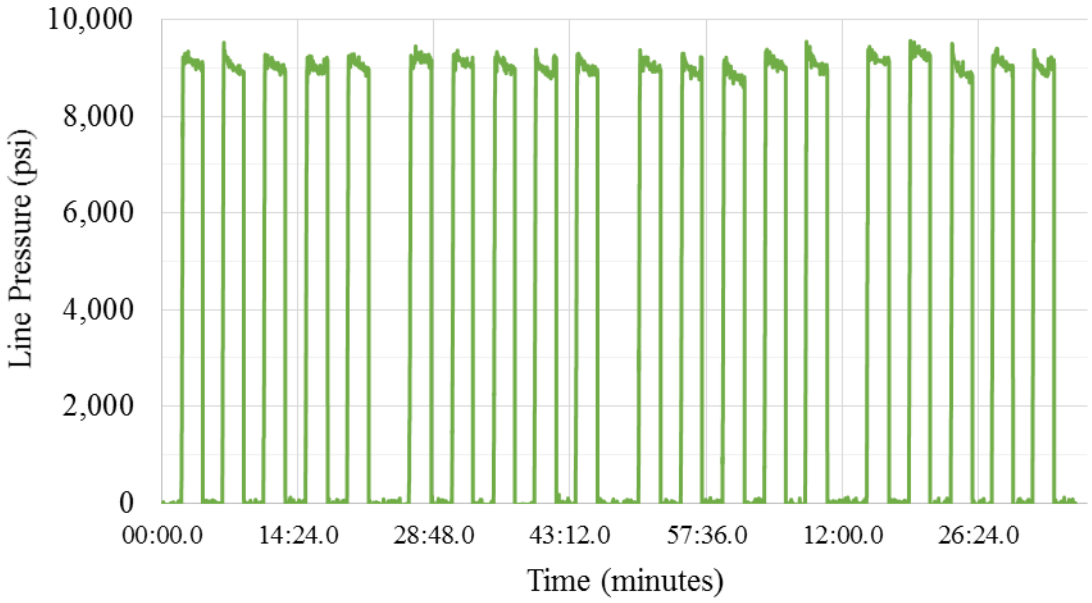

Figure B.46: Cyclic fatigue pressure data for NS 9-3

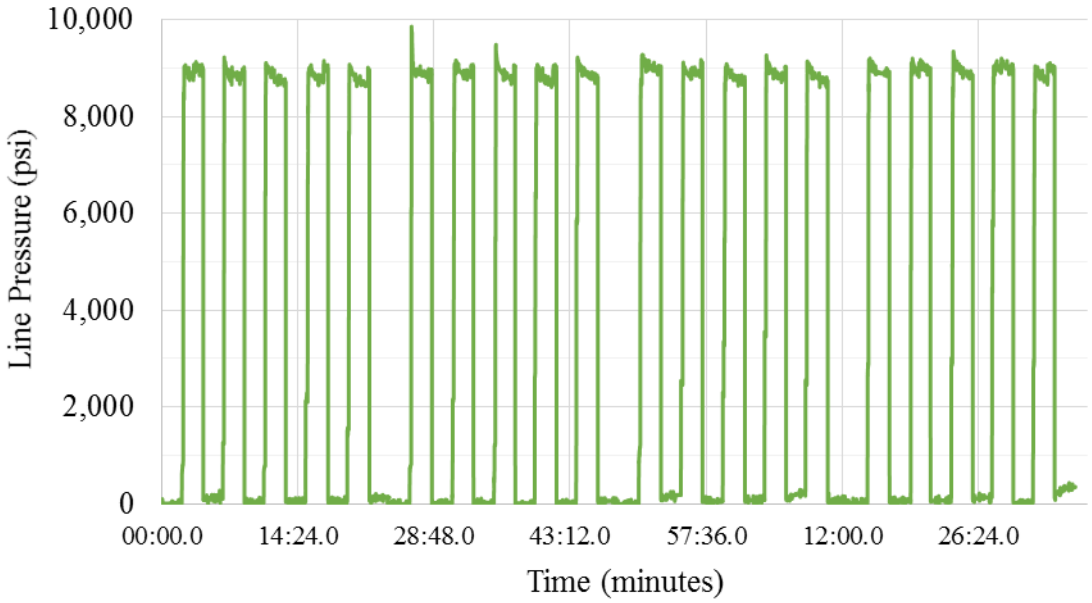

Figure B.47: Cyclic fatigue pressure data for NS 9-4

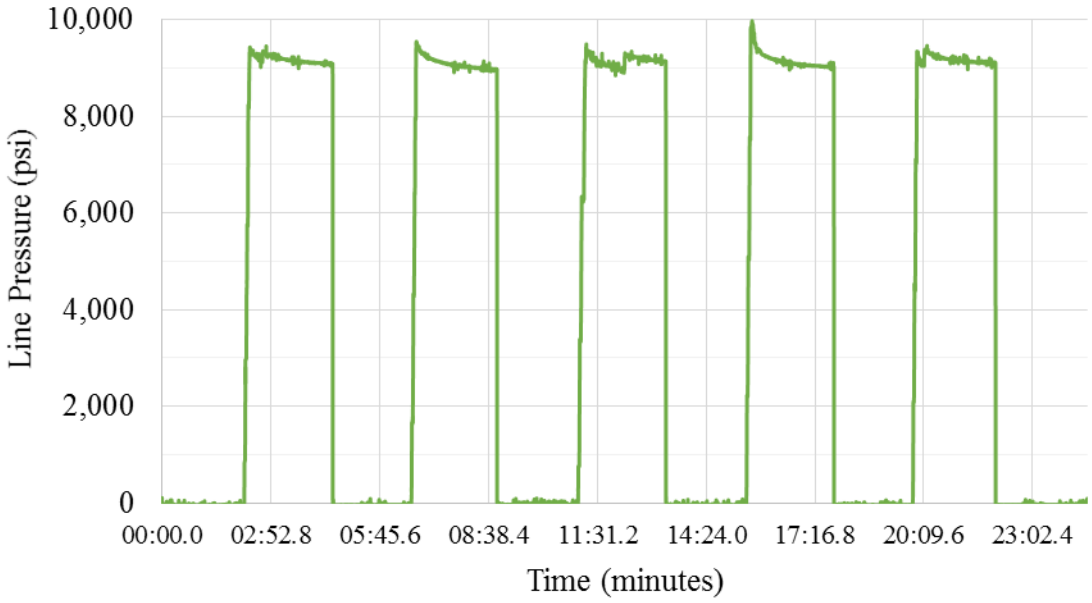

Figure B.48: Cyclic fatigue pressure data for SF 9-1

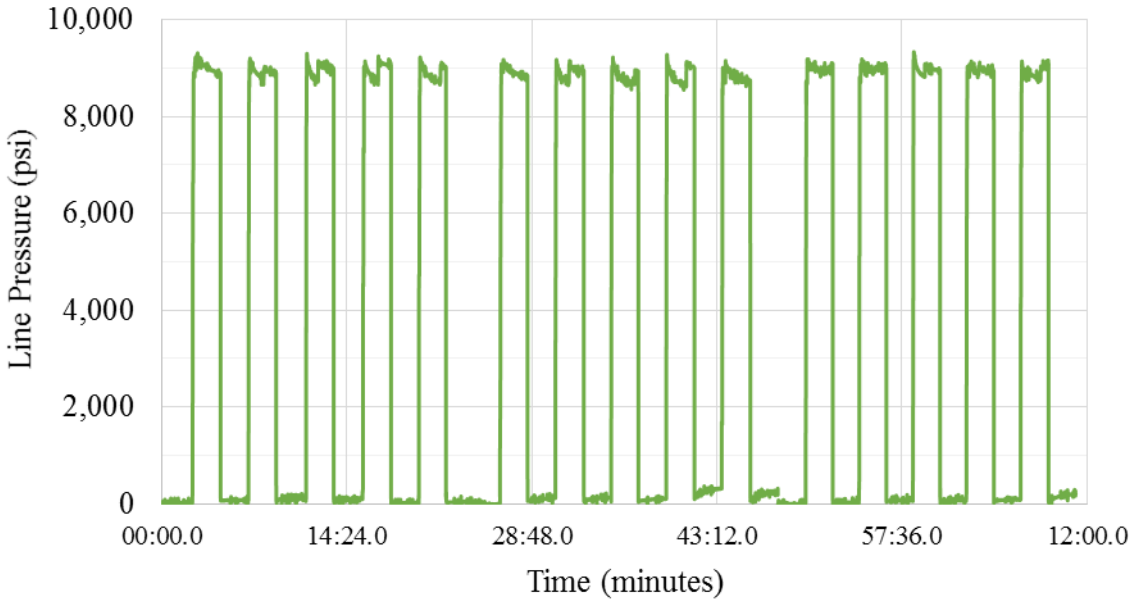

Figure B.49: Cyclic fatigue pressure data for SF 9-2

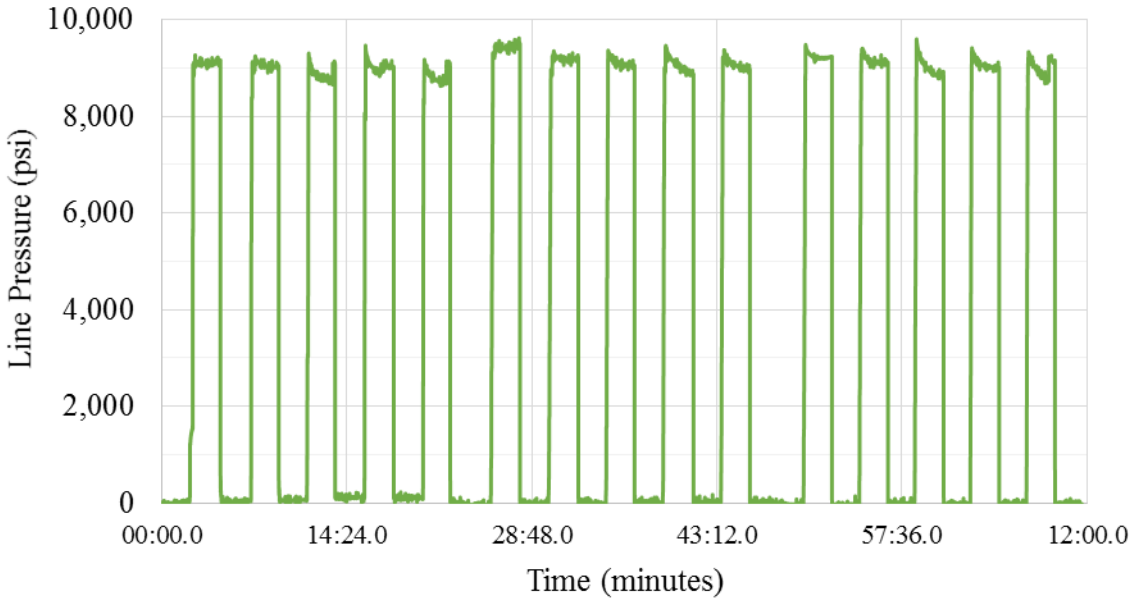

Figure B.50: Cyclic fatigue pressure data for SF 9-3

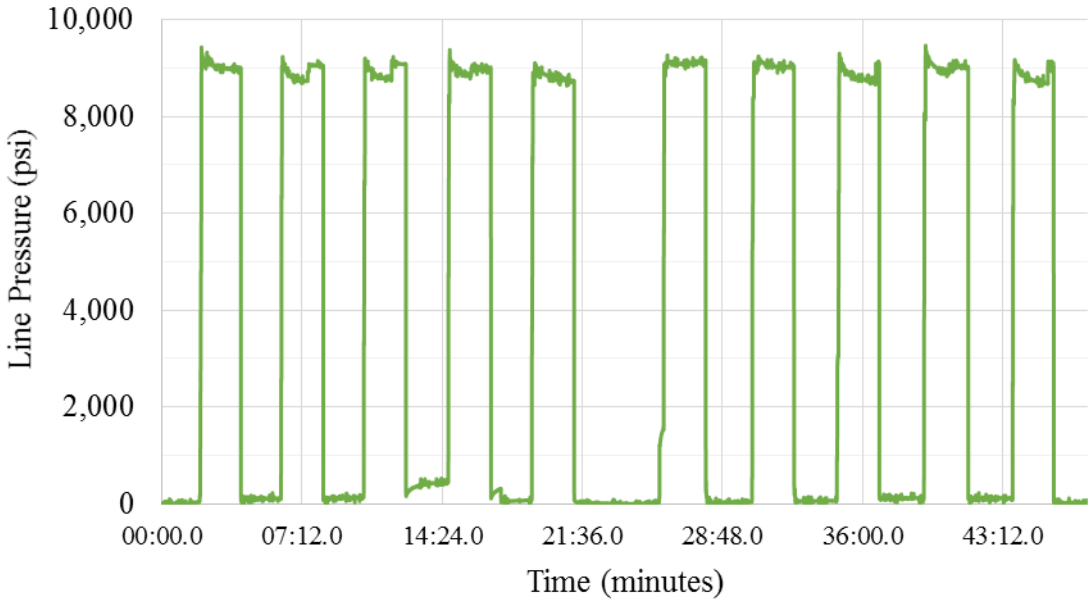

Figure B.51: Cyclic fatigue pressure data for SF 9-4

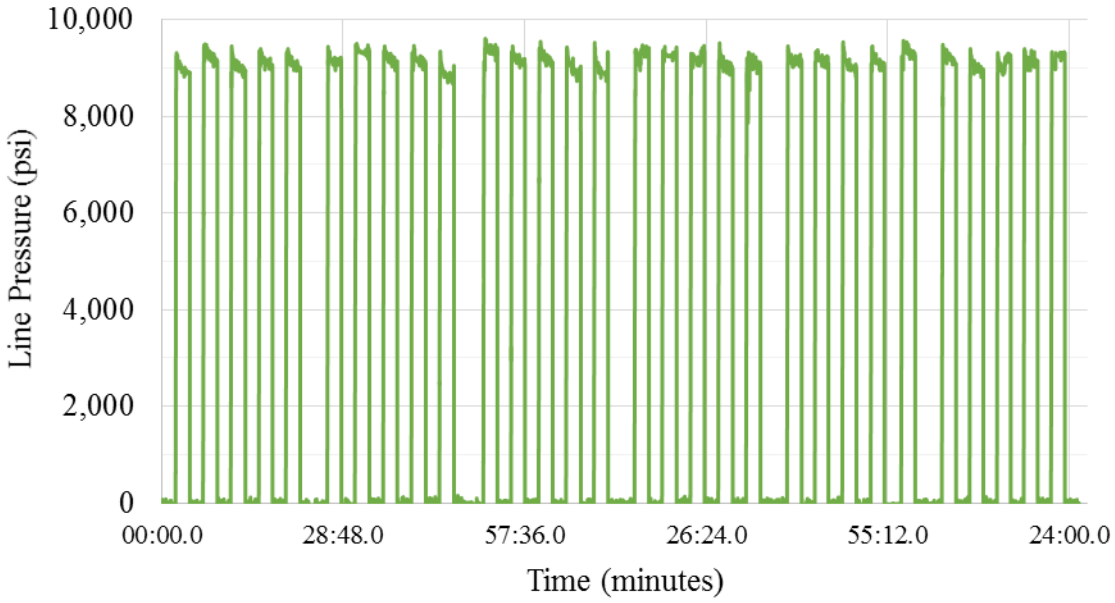

Figure B.52: Cyclic fatigue pressure data for PP 9-1

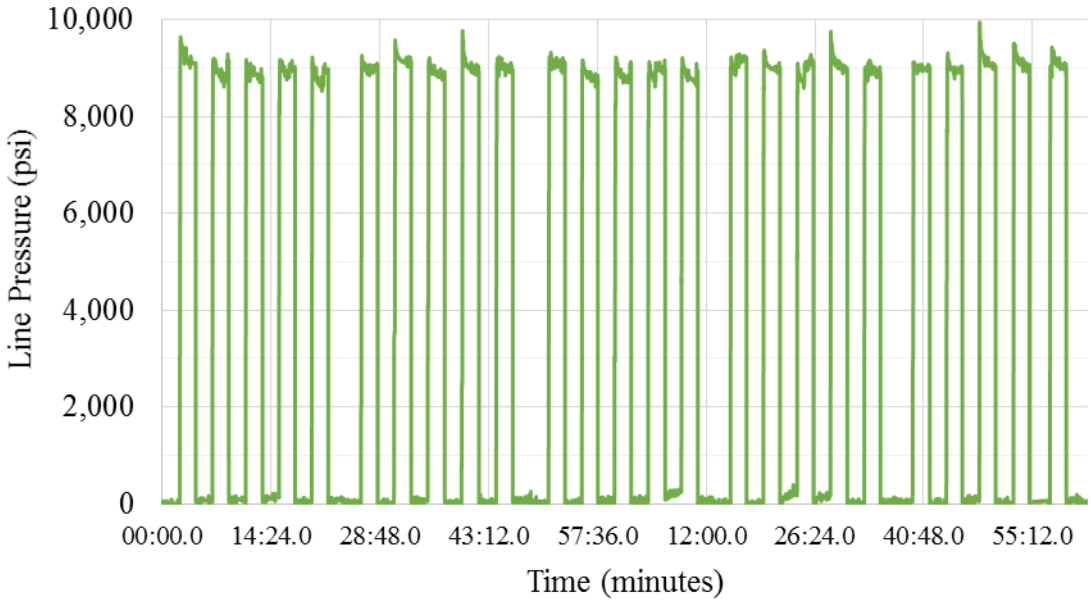

Figure B.53: Cyclic fatigue pressure data for PP 9-2

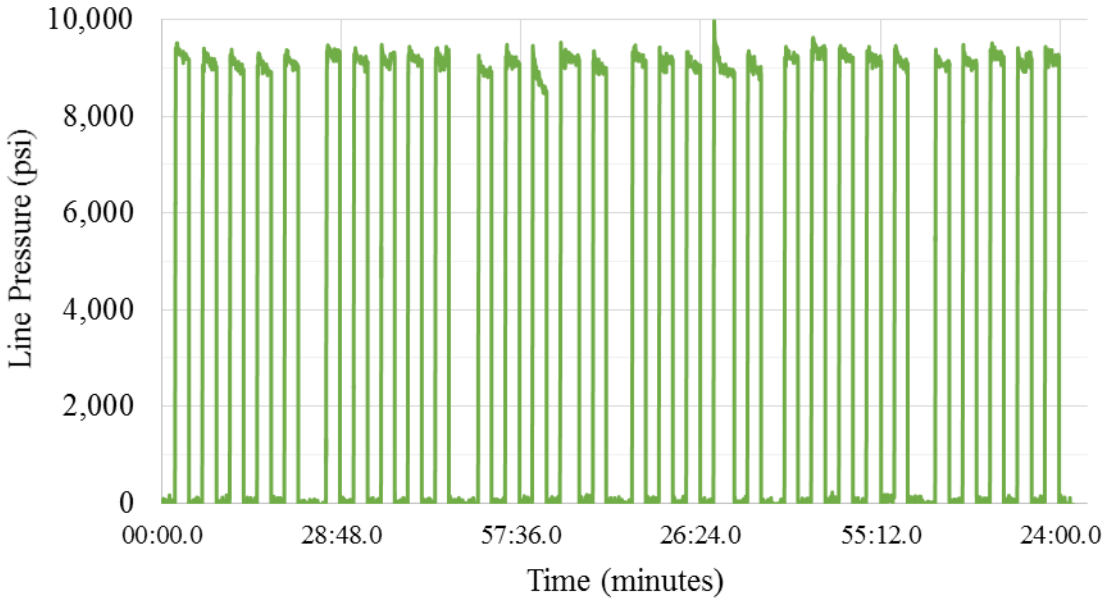

Figure B.54: Cyclic fatigue pressure data for PP 9-3

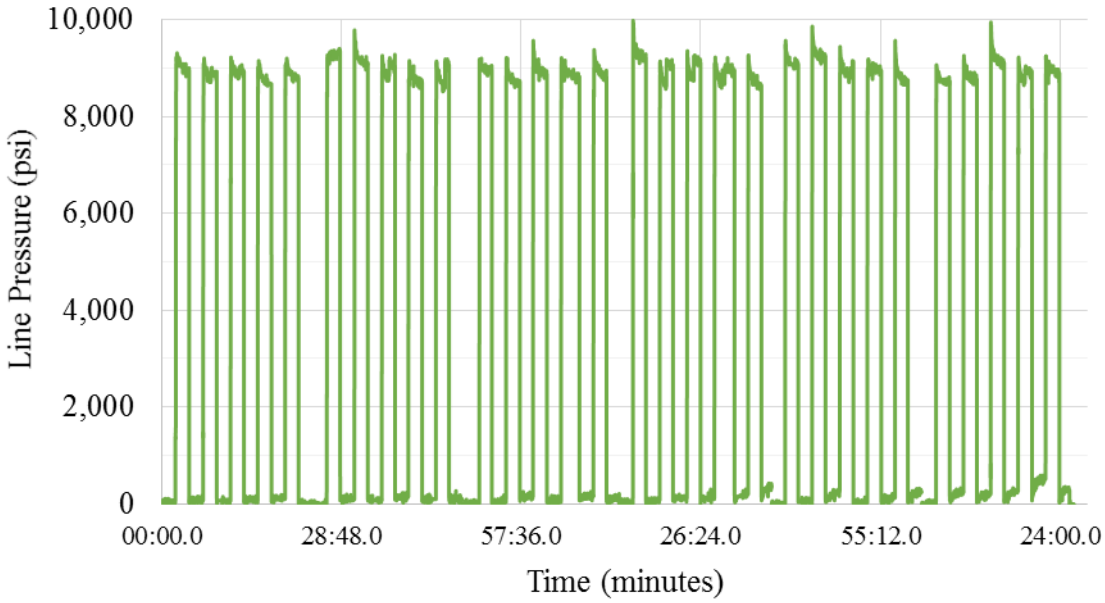

Figure B.55: Cyclic fatigue pressure data for PP 9-4

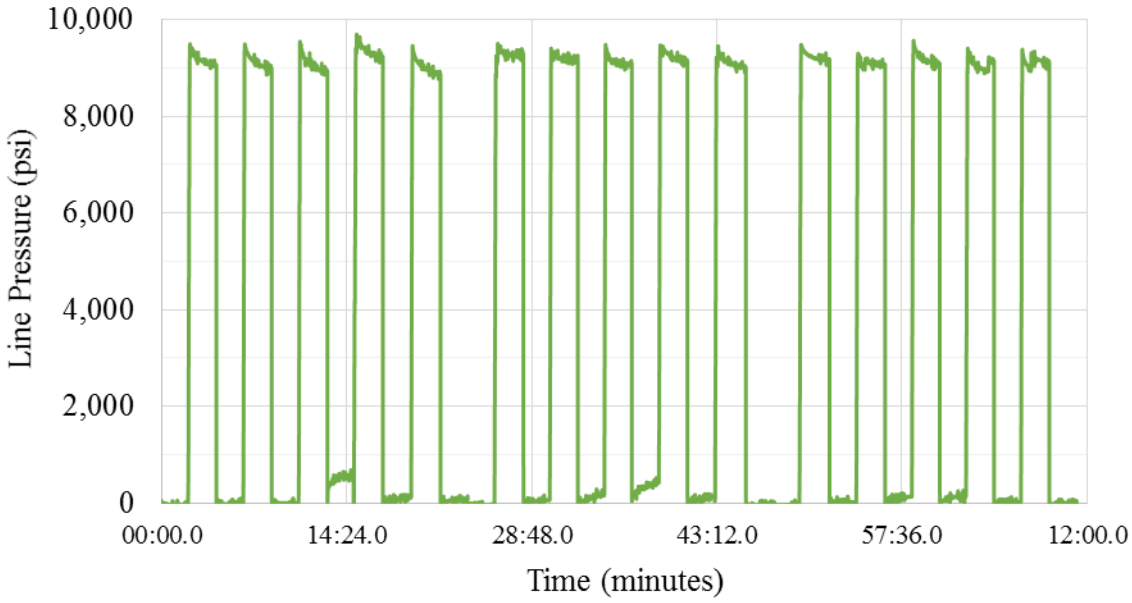

Figure B.56: Cyclic fatigue pressure data for BEN 9-1

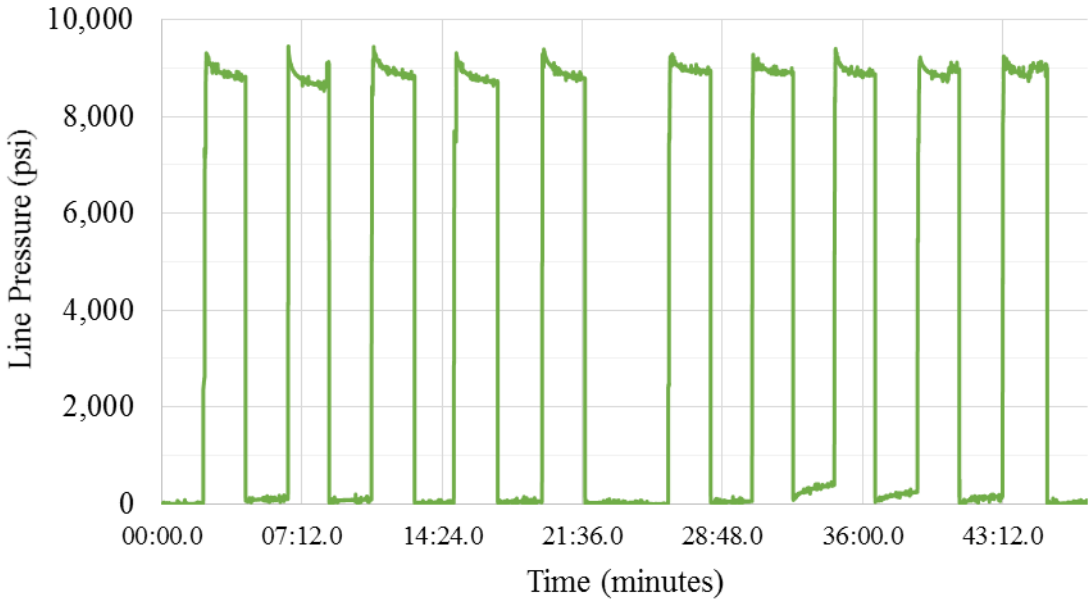

Figure B.57: Cyclic fatigue pressure data for BEN 9-2

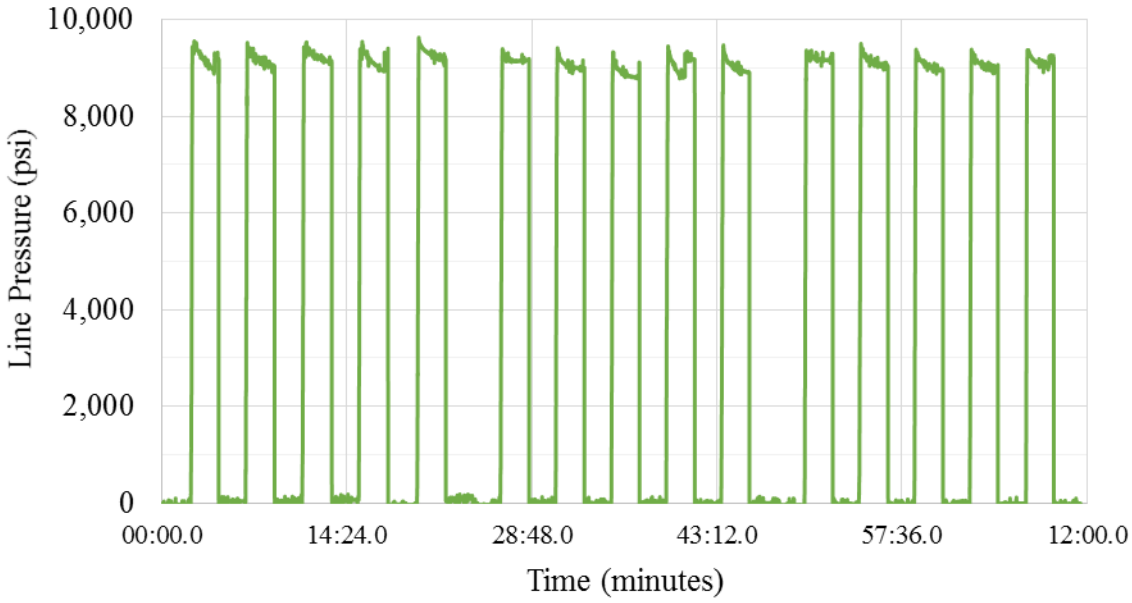

Figure B.58: Cyclic fatigue pressure data for BEN 9-3

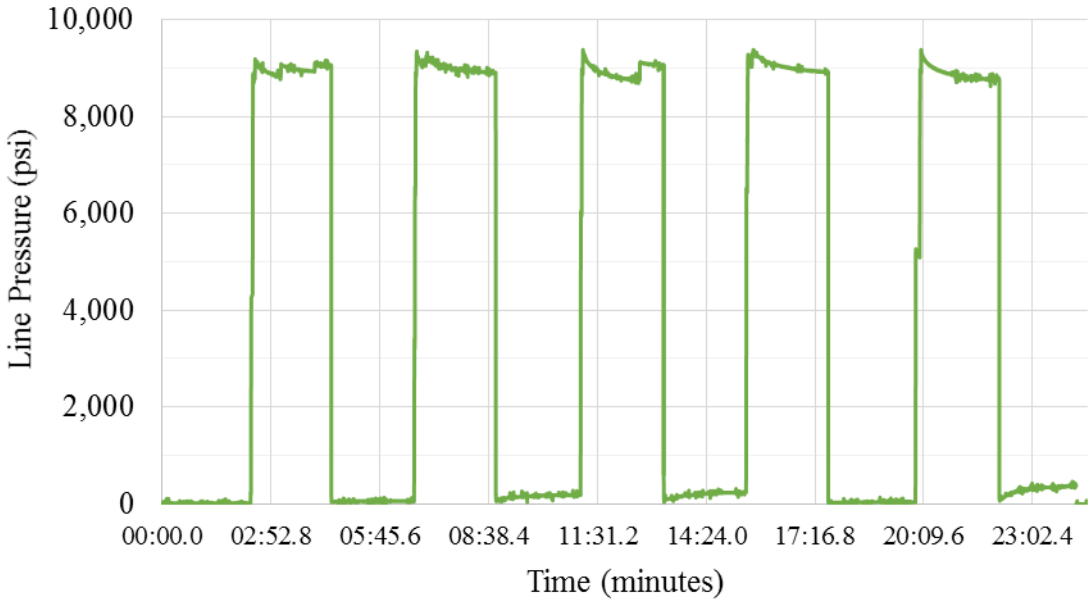

Figure B.59: Cyclic fatigue pressure data for BEN 9-4

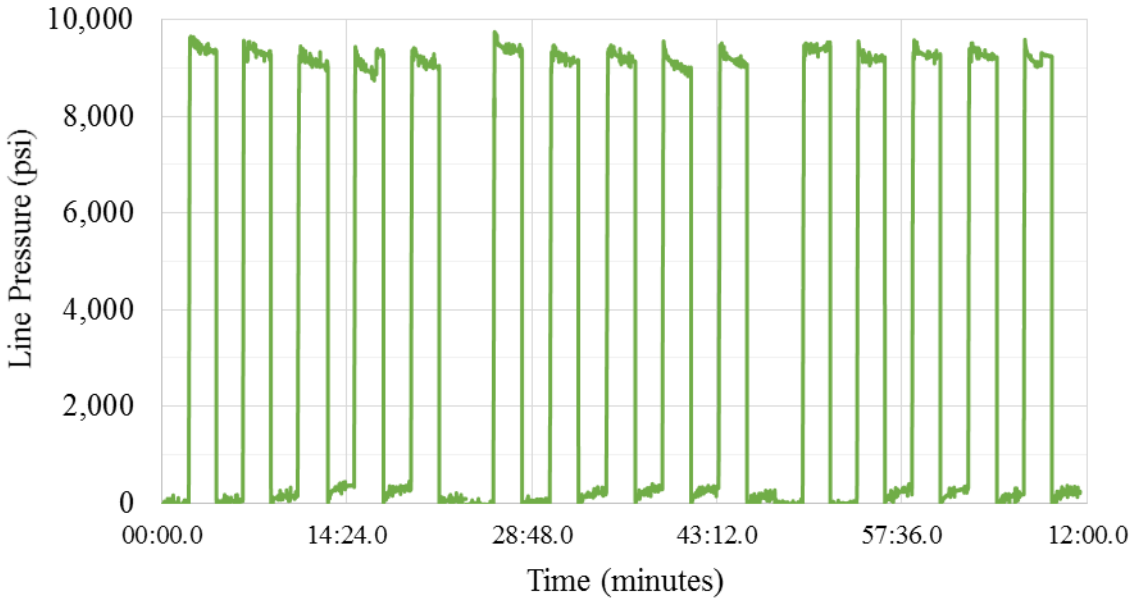

Figure B.60: Cyclic fatigue pressure data for BENPP 9-1

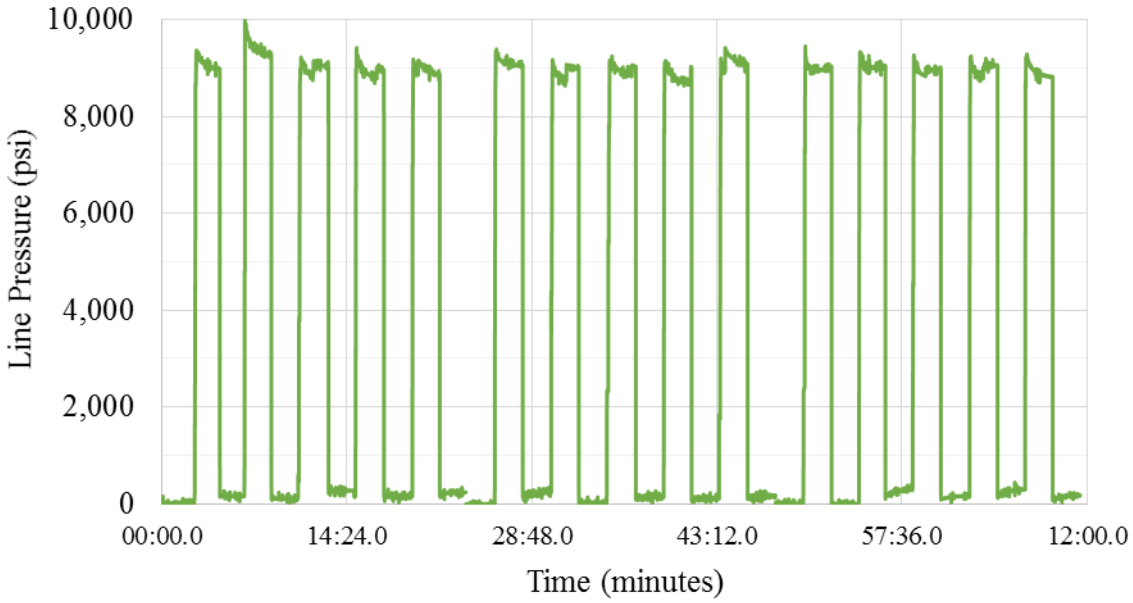

Figure B.61: Cyclic fatigue pressure data for BENPP 9-2

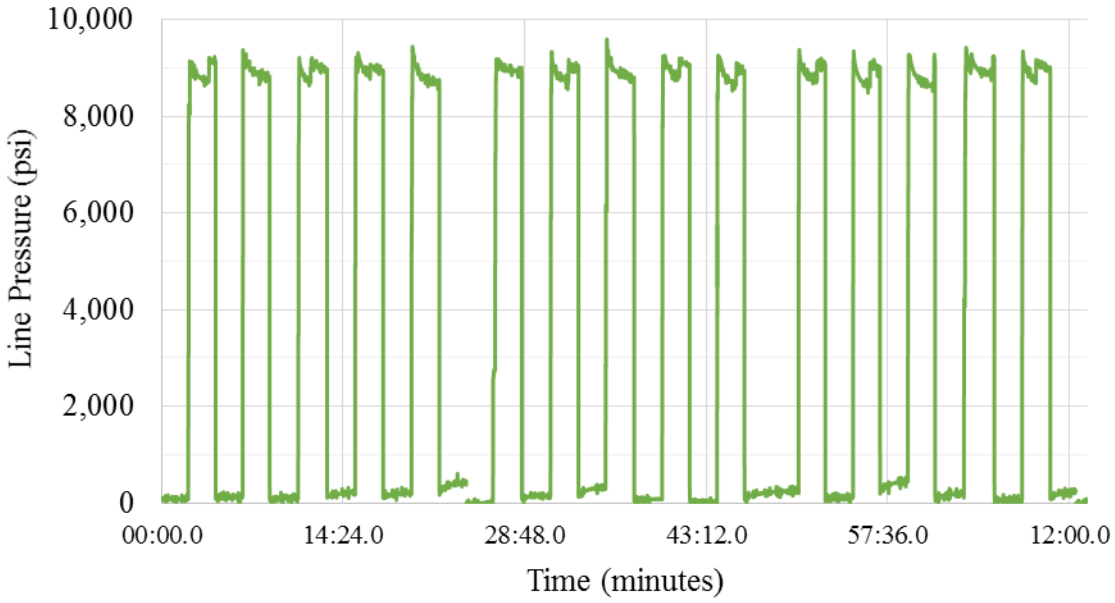

Figure B.62: Cyclic fatigue pressure data for BENPP 9-3

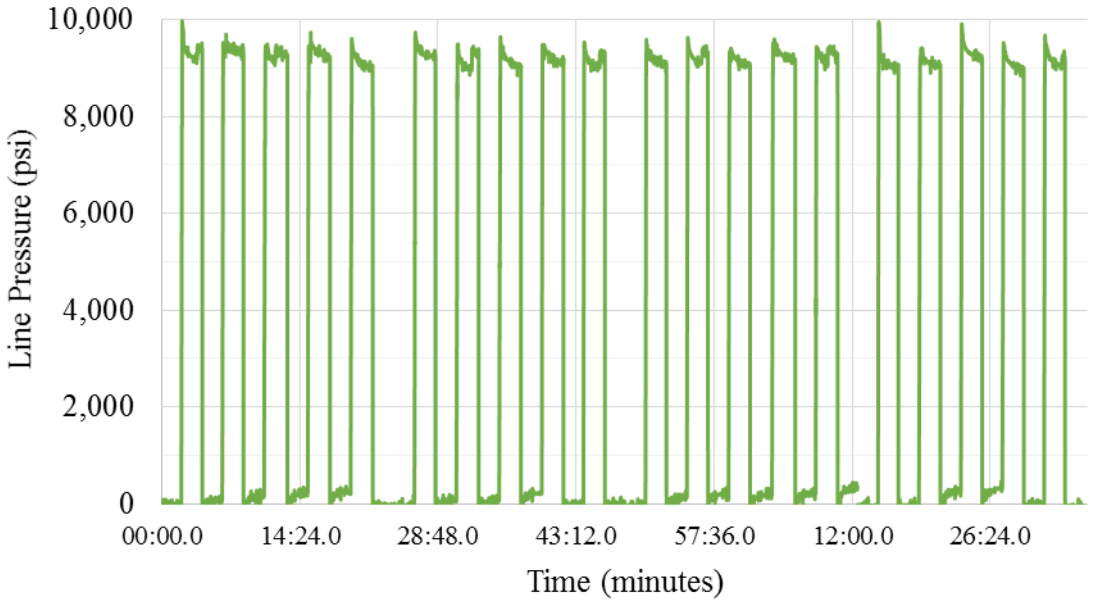

Figure B.63: Cyclic fatigue pressure data for BENPP 9-4

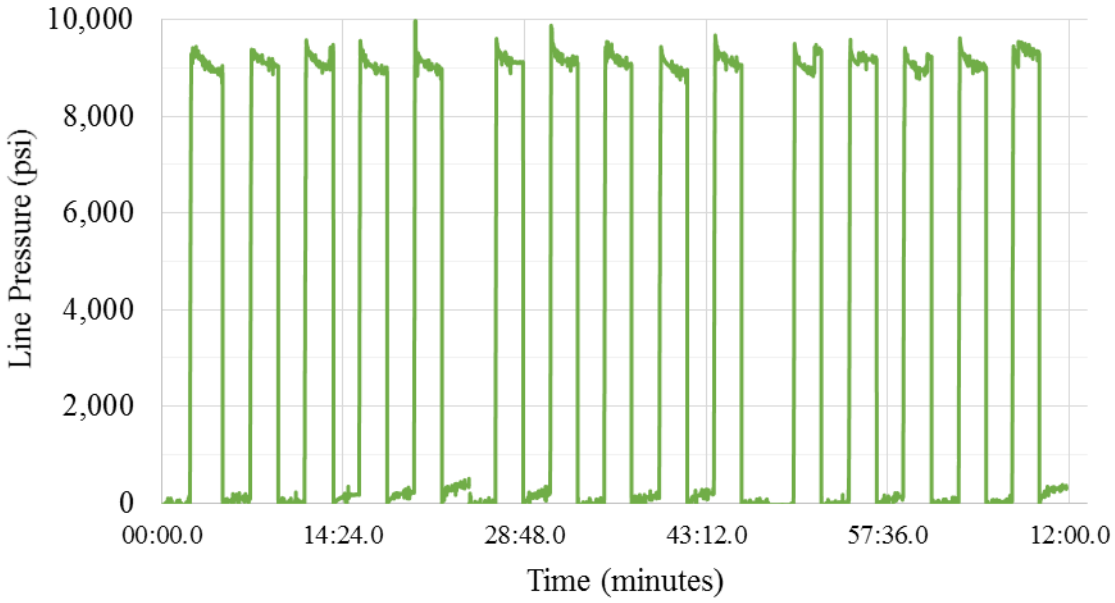

Figure B.64: Cyclic fatigue pressure data for OBM 9-1

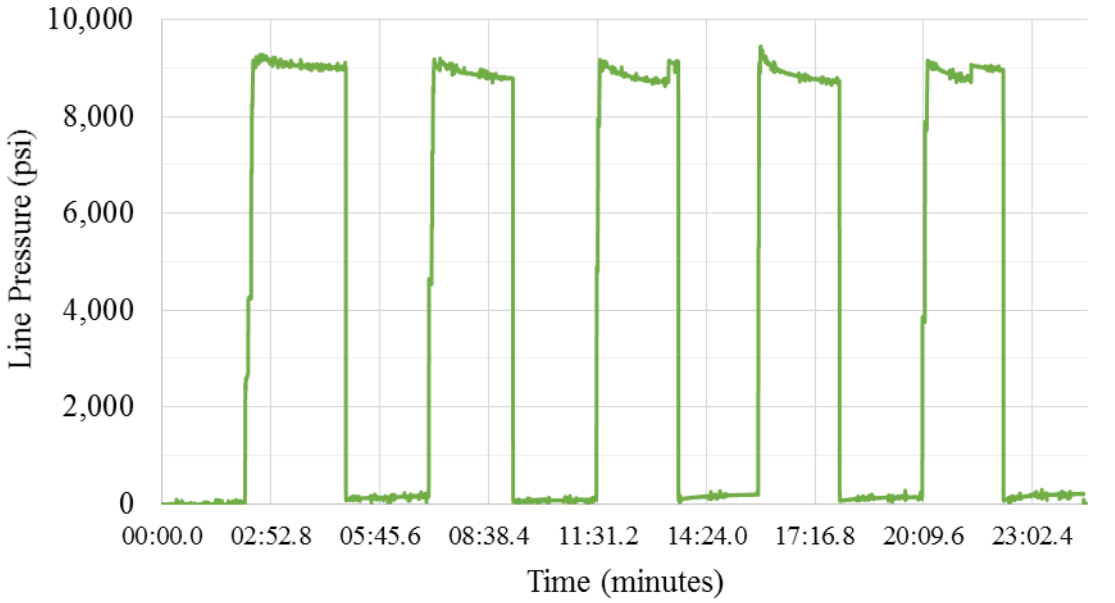

Figure B.65: Cyclic fatigue pressure data for OBM 9-2

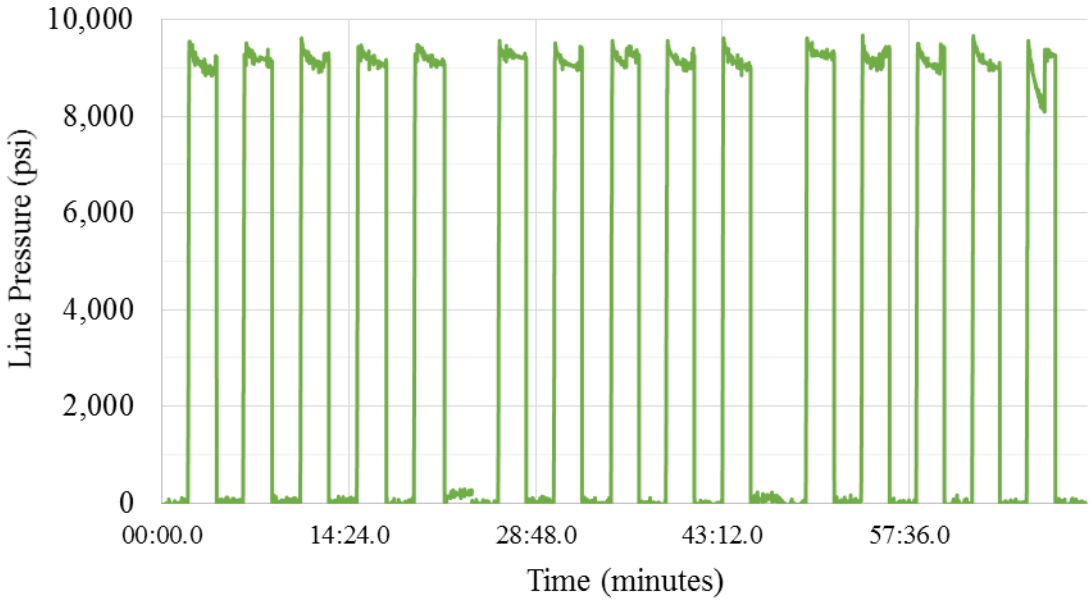

Figure B.66: Cyclic fatigue pressure data for OBM 9-3

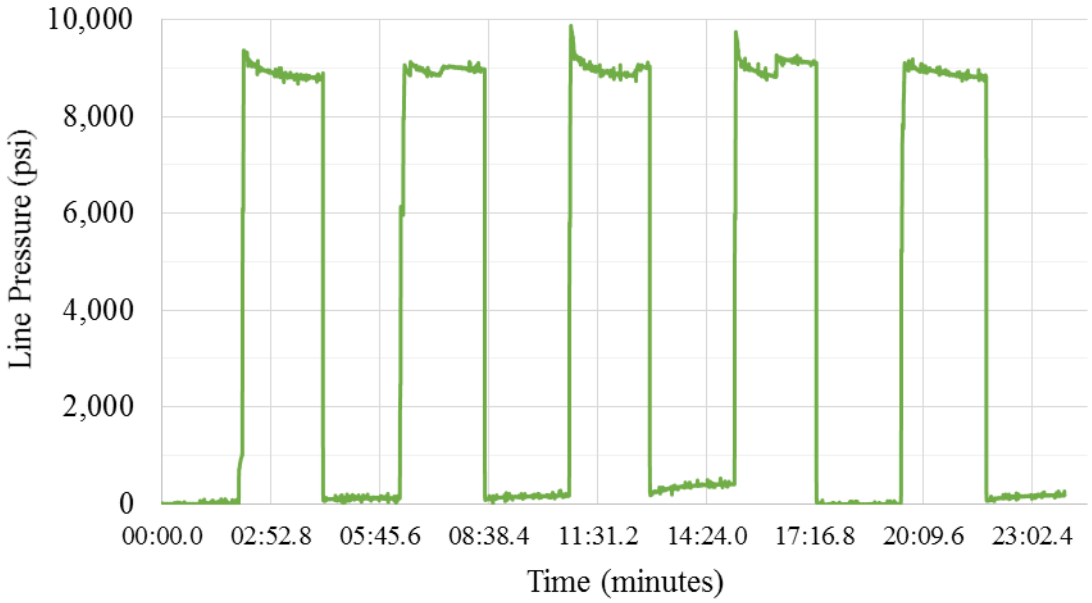

Figure B.67: Cyclic fatigue pressure data for OBM 9-4